Universität Rostock

Traditio et Innovatio

Mechanistic Analysis of Electrochemical Reactions Involving Mediators and Electro-generated Reagents

Cumulative dissertation

for acquisition of the academic degree

doctor rerum naturalium (Dr. rer. nat.)

of the Faculty of Mathematics and Natural Sciences

of the University of Rostock

Presented by

Nayereh Mohebbati

from Tehran-Iran

Rostock, 2023

https://doi.org/10.18453/rosdok_id00004500

Reviewers:

Prof. Dr. Robert Francke, Leibniz Institut für Katalyse e. V.

Prof. Dr. Udo Kragl, Universität Rostock, Institut für Chemie

Prof. Dr. R. Daniel Little, University of California Santa Barbara, Department of Chemistry and Biochemistry

Year of submission: 2023

Year of defence: 2023

The presented work was conducted during the period from November 2018 until April 2023 under the supervision of Prof. Dr. Robert Francke in the Institute of Chemistry at the University of Rostock and Leibniz Institute for Catalysis e. V.

Acknowledgments

At this point I would like to express my appreciation to those who made this thesis possible. First, I would like to acknowledge and thank my supervisor Prof. Dr. Francke for the possibility that I could do this work in his working group as well as his scientific guidance throughout these years. I also would like to thank Prof. Dr. Kragl for providing a working space for me in his laboratory for many of my experiments. I am very happy to have been part of these working groups in the past years as it helped me to expand my knowledge and scientific experience.

I also would like to thank my colleagues. I felt very welcomed from the first day that I joined the working group. Anybody who joins this group benefits from the positive competition, support, and harmonic working atmosphere. My sincere thanks also goes to everybody outside of the working group, especially the analytical department and scientific collaborators who have helped the progress of this work and contributed to it during the past years.

Next, I am very grateful for my wonderful friends who have always been by my side throughout these years. Meeting a group of friends whom you could call your second family is something rare to happen, but I was lucky enough to find it during my time in Rostock.

Finally, a very exceptional appreciation goes to my family, especially my parents. Their hard work in their life has paved the way for me to be at this point today. Their encouragement and emotional support have provided the motivation needed for me to work towards my dreams.

Table of Content

Figures

Schemes

Equations

Symbols

Symbol	Meaning	Unit
Q_i	Passed charge	A s
z_i	Number of transferred electrons per molecule	-
n_i	Moles of substrate *i*	mol
F	Faraday constant	C mol^{-1}
E	Applied potential	V
E_0	Equilibrium potential	V
E_{00}	Standard potential	V
R	Universal gas constant	-
T	Absolute temperature	K
C_{ox}	Concentration of oxidized species	mol L^{-1}
C_{Red}	Concentration of reduced species	mol L^{-1}
C_s	Concentration of substrate	mol L^{-1}
C_p^0	Initial concentration of the analyte	mol L^{-1}
C_p	Concentration of the analyte	mol L^{-1}
η	Overpotential	V
j	Current density	A m^{-2}
j_0	Exchange current density	A m^{-2}
J	Diffusion flux through cross section	mol m^{-2} s^{-1}
J_p	Oxidation peak	A m^{-2}
J_{max}	Plateau current density	A m^{-2}
α	Symmetry factor	-
D	Diffusion coefficient	cm^2 s^{-1}
x	Position relative to the cross section	m
t	Time	s
v	Scan rate	V s^{-1}
k_{obs}	Apparent rate constant	s^{-1}
k_r	Rate constant of the limiting chemical step	s^{-1}
λ	Kinetic factor	-
σ_p^+	Hammett substituent coefficient	-
σ_R	Resonance effect Hammett coefficient	-
σ_F	Inductive effect Hammett coefficient	-

List of Abbreviations

ABNO	9-azabicyclo[3.3.1]nonane *N*-oxyl
ACT	4-acetoxy TEMPO
CCE	Controlled current electrolysis
CE	Counter electrode
CPE	Controlled potential electrolysis
CV	Cyclic voltammetry
ECF	Electrochemical fluorination
ET	Electron transfer
GC	Glassy carbon
HAT	Hydrogen atom transfer
HFIP	1,1,1,3,3,3-Hexafluor-2-propanol
HMF	5-(hydroxymethyl) furfural
IP	Ionization potential
4-MBA	4-methoxybenzyl alcohol
MeCN	Acetonitrile
MeOH	Methanol
NMI	*N*-methylimidazole
PIDA	(diacetoxyiodo)benzene
PIFA	[bis(trifluoroacetoxy)iodo] benzene
PSIB	Poly(styrene)-supported iodobenzene
PTE	Polyeelectrolytes
RAFT	Reversible addition-fragmentation chain-transfer
RE	Reference electrode
SET	Single electron transfer
TEMPO	2,2,6,6-tetramethylpiperidin-1-oxyl
TU	TEMPO units
TPMA	TEMPO-modified polymethacrylate
WE	Working electrode

Part I. Fundamentals of Electrosynthesis

1. Historical overview

Electrosynthesis has been an important but underestimated area of synthetic chemistry. Nowadays, electrosynthesis gains more scientific and social interest due to the unneglectable advantages it brings along. It offers cost reduction, alternative reaction pathways with reduced process waste, and sustainable reaction control.[1] The first electro-organic synthesis was reported by Michael Faraday (1843), who demonstrated the electrolysis of acetic acid, thereby introducing the idea of using electric charge as a replacement for chemical reagents.[2] Later, Hermann Kolbe established the Kolbe electrolysis of valeric, butyric and acetic acid in 1847. He demonstrated that anodic oxidation of aliphatic carboxylic acids can lead to decarboxylative dimerization in aqueous alkaline solutions.[3]

Since the seminal reports by Faraday and Kolbe, electrosynthesis has further evolved and became an important field of synthetic chemistry, not least due to advances in reactor technology and electrical engineering. With these improvements, it became possible to operate at a set working electrode potential (CPE: controlled potential electrolysis) or cell current (CCE: controlled current electrolysis), and to receive more insights about the process at the electrode-electrolyte interface by cyclic voltammetry (CV) and spectroelectrochemical techniques. More electrosynthesis processes were invented in the second half of the 20th century which are up to this day in industrial use.[4]

Nowadays there are many large-scale applications of electrochemical processes in industry. One example is Baizer's process that involves the reductive dimerization of acrylonitrile to adiponitrile, the latter being used to produce Nylon. Simon's process, also known as electrochemical fluorination (ECF), is used for the preparation of perfluorinated hydrocarbons.[5] This is performed by electrolysis of aliphatic compounds in HF/KF electrolyte solutions and nickel as anode material.[6] Other industrial examples are the anodic methoxylation of 4-*tert*-butyltoluene to benzaldehyde dimethylacetal to yield lysmeral after condensation with propanal.[7]

It can be said that after the 60s, the field of electrosynthesis has further picked up pace in evolving. The advancements in organic and (electro)analytical chemistry provide the opportunity to induce highly selective structural changes to gain insights into the reaction mechanisms. Also, the field gained more interest, as it offers substitution of

toxic or expensive reagents by traceless electric current. In addition, due to the increasing importance of sustainable technologies and with the opportunity to utilize power from renewable resources, electrosynthesis experiences a renaissance nowadays.

2. Sustainability and Electrosynthesis

Excessive energy consumption and the resulting pollution has been identified as key problems for our society and economy. Other than using well accessible resources, minimizing the ecological footprint is the focus of innovation in process development. The aim to reduce the pollution, carbon dioxide emission and waste generation reinforces the requirement for renewable energy resources.[8]

The field of synthetic organic chemistry is always challenged to create complex molecules with consideration of atom efficiency, sustainability, and time consumption.[1] As a result, 12 postulates of sustainable ("green") chemistry were established (see Figure 1).[9]

There are many ways in which electrochemistry can relate to these principles and help to preserve the environment.[1, 8-9] In comparison to traditional oxidation and reduction in organic chemistry, electrochemistry offers many interesting features.

First, the electro-organic reactions usually proceed under mild conditions (atmospheric pressure and room temperature). Besides convenient *in-situ* generation of toxic or hazardous reagents or intermediates in a controlled fashion under these mild conditions is a safe and cheap method.[8, 10] Second, redox reagents are replaced by electric current which reduces the amount of generated waste and by this means the cost efficiency is improved as well as environmental compatibility.[10b, 11] Another advantage is the easy control over the reaction's selectivity by the applied potential at the working electrode.[9]

Nevertheless, there are many criteria to assess whether a reaction is green or not and evaluating its environmental impact in comparison to other reactions. Avoiding the use of stochiometric number of reagents alone does not guarantee that electrochemical reactions are sustainable.[12] The full set of principles of sustainable ("green") chemistry needs to be considered together with the green metrics of electrochemistry to evaluate the environmental impact of a chemical reaction in comparison to alternative approaches.[13]

In this context, a few examples will be discussed of how modern electrochemical methodologies offer a more "*green*" option in comparison to traditional alternatives.

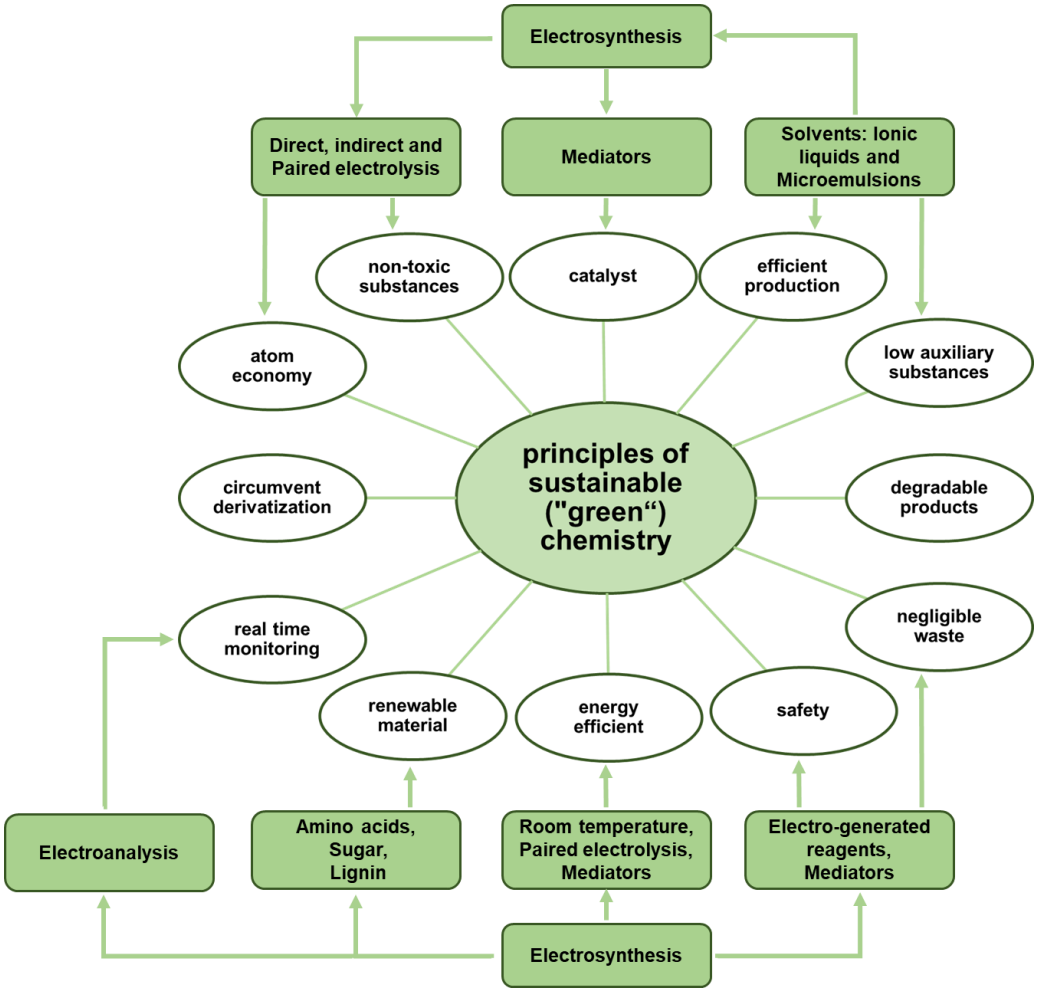

Figure 1. Organic electrosynthesis and its relation to principles of sustainable ("green") chemistry.[9]

An example of this is selective oxidation of primary and secondary alcohol to the respective carbonyl group.[14] Due to their pivotal role in organic synthesis and industrial chemistry, the development of environmentally begin processes is of a great interest. In conventional methods such as Jones oxidation or Collins-reagent, Cr(+VI) salts are used, which are highly toxic.[15] Moreover, more environmentally compatible processes were developed which are based on aerobic oxidation in combination transition metal catalysts (Pd, Ru, Cu and Pt) and further additives.[16] Despite of the selectivity these catalysts provide, the reaction can be hindered if a substrate with a chelating ability bind to the metal. On the other hand, use of metals shows an

environmental impact that needs additional treatment for disposal. With all the above mentioned aspects, electrochemistry can offer a metal-free alternative.[17]

Furthermore, active electrode material can be used for novel electrochemical conversion that gives high-valent metal species.[18] This means an electrically conductive reagent is immobilized on the electrode surface which is regenerated *in-situ*.[19] An example of this immobilized mediator is NiOOH electrode which forms from Ni in alkaline media and has an active and stable surface.[8] This anodic system is applied for example for the selective degradation of bio-based mixtures such as lignin.[20]

It is important to emphasize that electrochemical reactions proceed in pairs, meaning that the desired reaction at the working electrode is coupled to a reaction at the counter electrode (depolarization, often leading to waste generation).[9, 21] In most cases the reaction at the working electrode is the subject of interest.[9] However, one can design electrolysis in which conversions on both working and counter electrode lead to a useful product. This approach is known as paired electrolysis (Scheme 1). By this approach, up to 200% of Faraday efficiency can be obtained, as for each mole of electrons passed through the cell, two beneficial products are produced.[22]

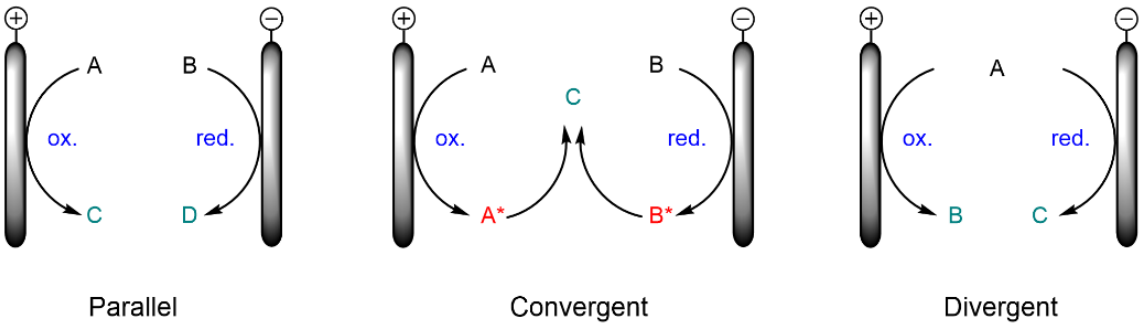

Scheme 1. Variants of paired electrolysis. [22b]

An important example of this method is the combined production of phthalic acid dimethylester and *t*-butylbenzaldehyde dimethylacetal in an undivided cell from the respective starting material shown in scheme 2. This procedure can alone offer 4000 metric tons per year of *t*-butyldimethyl acetal. In this approach, methanol (MeOH) serves both as the solvent and as one of the starting materials for the anodic half-cell reaction. The protons produced at the anode are directly used in the anodic half-cell reaction. This means, both PH and the solvent level are well balanced, as anodically

formed protons are consumed at the cathode and liberated MeOH at the cathode is used for the anodic process.[22a]

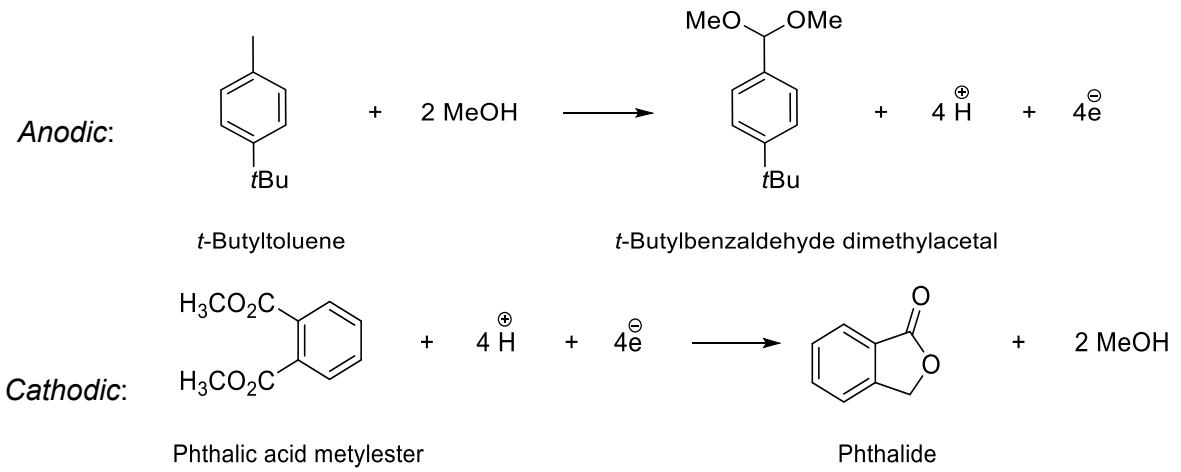

Scheme 2. Paired electrolysis of phthalic acid and 4-tert-butyltoluene.[22a]

Energy efficiency not only ensures sustainability but also enables cost-efficiency. Therefore, changing to a more affordable and renewable source of energy increases the efficiency of a process. Replacement of chemical redox agents by electric current has a significant impact on overall cost and sustainability of a procedure. As mentioned above, the electrochemical reactions are initiated and processed by applied potential instead of merely thermal energy. This enables the operation under ambient conditions. By variation of the current density, optimal operation conditions with minimized heat production (generated by the Ohmic cell resistance) can be achieved. The waste production, safety hazard and extra purification steps can be avoided by replacement of chemical redox agents with electric current.[22c, 23]

It is fair to say that electrochemistry provides many advantages and solves major problems, but the implementation in routine organic synthesis and industry comes with its own challenges. One of these challenges is that charge transport through the cell requires supporting electrolyte. Nevertheless, an ideal supporting electrolyte should provide good conductivity and broad potential range and must be chemically and electrochemically inert under the chosen reaction conditions. Often it is difficult to fulfill all these criteria for a single medium.[9] Aside from the supporting electrolyte issue, electrodes may be prone to corrosion and deactivation by formation of coatings. Some of these issues can be avoided by indirect electrolysis (see part I, section 4). These constitutes to extra purification steps, waste generation and raise of capital costs.[10a]

It is noteworthy that most of the research has been done for the anodic conversion and there is still significant demand for research about cathodic transformations.[11]

3. Physiochemical Background

In an electrochemical transformation, the conversion is directly proportional to the amount of charge transferred. This was established by M. Faraday, reported in 1833, and became later known as Faraday's Law (eq. (1)),

$$Q = n_i z_i F \tag{1}$$

whereby F is the Faraday constant and Q_i the amount of charge passed in Coulombs (C) to convert n_i moles of substrate i. In this conversion, z_i is the number of transferred electrons per molecule. The Faraday constant equals to 96485 C mol^{-1}. In electrosynthesis, the parameter is frequently used as a charge equivalent that indicates how much electricity is needed to perform the full conversion of one mole of a compound in a single electron transfer ("F per mole of substrate").[2]

From thermodynamic perspective, electron transfer is enabled by application of an equilibrium potential (E_0) followed by the concentration ratio of the corresponding oxidized (C_{Ox}) and reduced (C_{Red}) form of redox pair. This correlation is defined by the Nernst equation where E_{00} is the standard potential of the redox pair, R the universal gas constant and T is the temperature (eq. (2)).

$$E_0 = E_{00} + \frac{RT}{nF} ln \frac{C_{Ox}}{C_{Red}} \tag{2}$$

The relationship between the measured current density and the applied overpotential η (difference between the equilibrium potential E_0 and the potential E applied to the working electrode) is described for the kinetically controlled region by the Butler - Volmer equation (eq. 3). It shows the influence of the exchange current density j_0 and the symmetry factor α on the resulting electrode current density j.[24]

$$j = j_0 \left(e^{\frac{\alpha z F}{RT} \eta} - e^{-\frac{(1-\alpha) z F}{RT} \eta} \right) \tag{3}$$

The exchange current density j_0 is the amount of current flowing in both directions at $E = E_0$. The symmetry factor α is between zero and one and determines the rate difference between anodic and cathodic current. If α is 0.5, both oxidation and reduction are on equal terms, whereas values between 0.5 and 1.0 indicate that the anodic current rises much faster than the cathodic one upon deviation from equilibrium (and *vice versa* for values between 0 to 0.5).[24-25]

In an electrosynthesis reaction there will be lower reactant concentration at the electrode surface than in the bulk solution. Similarly, there is a higher concentration of product at the electrode surface in comparison to the bulk solution. This causes a diffusive flux to the gradient of the concentration which is significant for mass transport process in an electrochemical cell. This is mathematically described by Fick's law. The first law (eq. (4)) relates the diffusion flux through cross section (*J*) to concentration (*c*) gradient and diffusion constant (*D*).

$$J = -D\frac{dc}{dx} \tag{4}$$

Fick's second law (eq. (5)) describes the change of concentration as a function of time. In this case *x* is the position relative to the cross section and *t* is time.[24-25]

$$\frac{\partial c}{\partial t} = D\frac{\partial^2 c}{\partial x^2} \tag{5}$$

4. Indirect Electrosynthesis

Bulk organo-electrosynthesis can be performed directly or indirectly. Direct electrosynthesis refers to direct transformation of substrate molecules at the electrode-electrolyte interface. Thus, for the electron transfer (ET), it is necessary to have direct contact between the electrode surface and the substrate. Direct electrolysis frequently comes with challenges such as low selectivity and kinetic inhibition of the heterogenous electron transfer.[26] In addition, the electrode could be passivated due to the formation of non-conductive polymer films on the electrode surface .[23] In this context, indirect electrosynthesis is an approach that provides many advantages in comparison to direct electrosynthesis (Scheme 3). Indirect electrosynthesis can be considered as a hybrid between direct electrochemical conversion and homogenous redox reaction. The direct ET between the electrode and the substrate is replaced by a homogenous redox reaction in the solution. A redox mediator acts as an electron transfer-shuttle between the electrode surface and the dissolved substrate.[21, 26a]

The application of indirect electrolysis might result in additional costs, waste, and separation issues, but it provides many advantages as well. The use of a mediator renders the possibility for circumventing electrode passivation and offers ways to tune the selectivity. In addition, lower potential is needed, which leads to milder reaction

conditions and the presence of a mediator may also help to overcome kinetic inhibitions associated with the direct ET.[21, 23, 26a, 27]

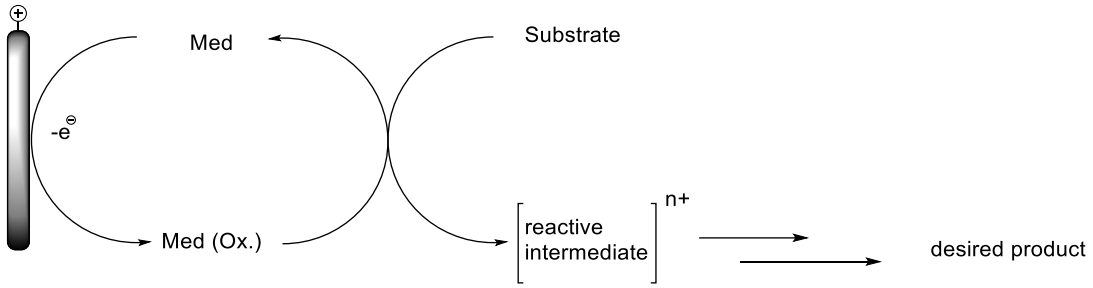

Scheme 3. Indirect elecrosynthesis.

A mediator can be used in two different fashions, as so-called *in-cell* or *ex-cell* mediators (Scheme 4). *In-cell* mediation means that the mediator activation and the consecutive reaction takes place simultaneously inside the same vessel. After electron exchange with the substrate, the mediator returns to its original state and is available for further oxidation or reduction cycles. As it is possible to reactivate the mediator within the same cell, it can be used in sub-stochiometric amounts. This results in less waste production, more economical and ecological advantage, and easier work up. Nevertheless, stable active species can also be used for *in-cell* processes, for example oxoammonium in TEMPO oxidations.

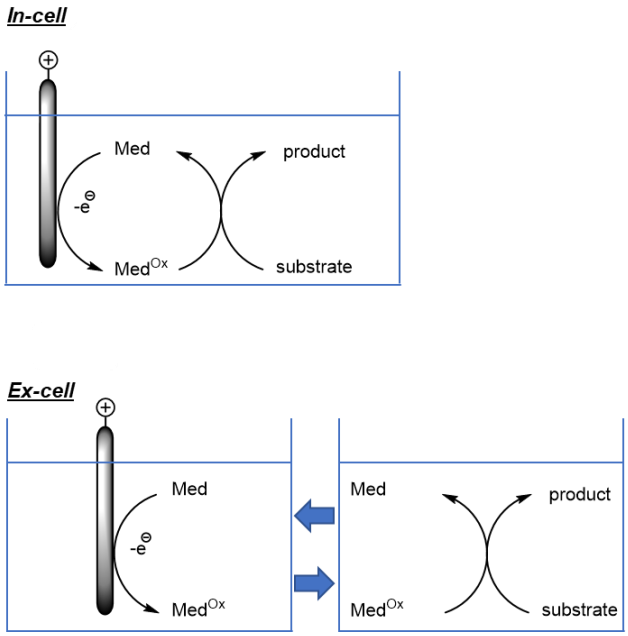

Scheme 4. Comparison between in-cell and ex-cell mediation.

An *ex-cell* procedure refers to an electrolysis where the mediator is activated in one vessel and transferred to a different vessel to react with the chosen substrate. This requires the mediator to be very stable in its activated form for being able to be

transferred to a new cell for the next step. *Ex-cell* mediators cannot be reactivated *in-situ*, therefore they need to be used in stochiometric or over-stochiometric amounts. In general, *ex-cell* mediators offer two advantages. First, they can be used even if the redox potential of the substrate is below the one of the mediators. Second, they provide the opportunity to study and optimize the electrochemical step and the chemical reaction independently from each other.[28]

The ET between the mediator and the substrate can progress in two distinct mechanisms, namely via inner-sphere or outer-sphere ET (Scheme 5). During an inner-sphere ET, a chemical bond is formed between the mediator and the substrate, which is cleaved after the ET and the mediator reverts to its inactive form. In outer-sphere ETs, the exchange occurs directly between the mediator and the substrate, without any bond-forming event.[28]

A careful choice of the mediator is very important for a successful application of indirect electrosynthesis. Therefore, the mediator needs to fulfill certain criteria. First, the redox potential of the mediator should be less positive than the one of the substrates in case of oxidation and less negative in case of reduction. Fast and reversible ET between the electrode and mediator is required and the produced active intermediate should be inert towards all the processes in the reaction mixture except for the desired ET to avoid side reactions. For an indirect electrolysis, the mediator should be soluble in the chosen medium both in oxidized and reduced form.[21]

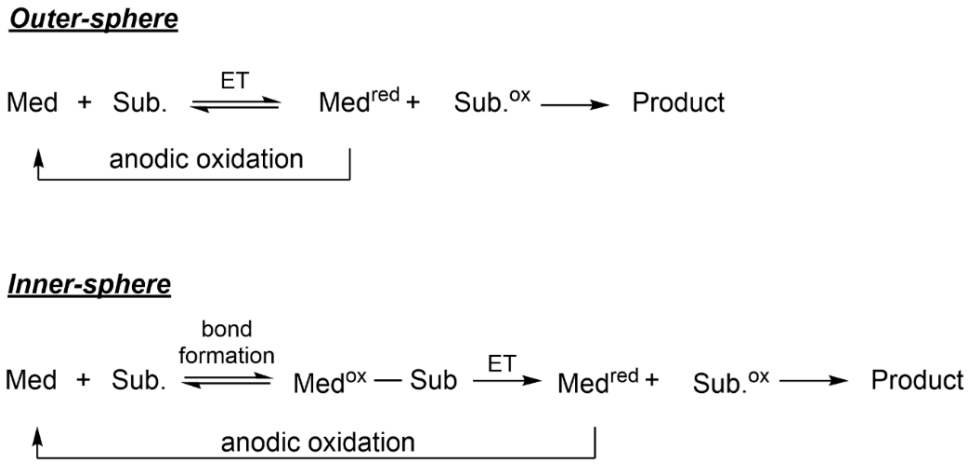

Scheme 5. Top: Mechanism of an outer-sphere ET. Bottom: Mechanism of an inner-sphere ET.

5. Cyclovoltammetric Analysis of Mediated Processes

Under non-catalytic conditions for a reversible electron transfer, both an oxidation peak (maximum current density) and a reduction peak (minimum current density) are visible

in the cyclic voltammogram (CV) of a redox couple. The current peaks are caused by diffusion limitation upon increasing potential (driving force) and a time-dependent progression of the diffusion profile (non-stationary conditions). Under catalytic conditions (here: anodic reaction), the intensity of the oxidation peak increase and the shape of the CV changes with respect to the experimental parameters as shown in the kinetic zone diagram (see Figure 2). The higher peak arises because the oxidized form of the mediator undergoes a chemical step that restores the non-oxidized form. In non-catalytic measurements, the intensity of the oxidation peak (j_p) is given by the Randles-Sevcik equation (eq. (6)).

$$j_p = 0.4463\, zFC_p^0 \sqrt{\frac{zF\nu D}{RT}} \tag{6}$$

With D for the diffusion coefficient, $C_p{}^0$ for the initial concentration of the analyte, z for the electrons required per formula unit. The peak current j_p therefore increases with the square root of the scan rate v. By taking measurements at different v values, one can determine the diffusion coefficient D from this equation by plotting j_p against v.

It can be expected in certain catalytic measurements that if the scan rate is sufficiently high, there will no longer be an increase in the peak current. Thus, a plateau is reached with current density j_{max}, that is defined by:

$$j_{max} = zFC_p^0\sqrt{Dnk_{obs}} \tag{7}$$

and,

$$k_{obs} = k_r \cdot C_s \tag{8}$$

Where k_r, is the rate constant of the limiting chemical step, k_{obs} is the apparent (pseudo-first order) rate constant, and C_s is the concentration of the substrate and D is the diffusion coefficient of the catalyst.[29] Figure 2 shows a zone diagram with possible CV shapes under catalytic and non-catalytic conditions. Here, γ is the so-called excess factor defined as the ratio between substrate and mediator concentration, $C_A{}^0$, and $C_P{}^0$, while λ is defined by $\lambda = \frac{RTF}{k_{obs}C_p^0\nu}$ (the “kinetic factor”).

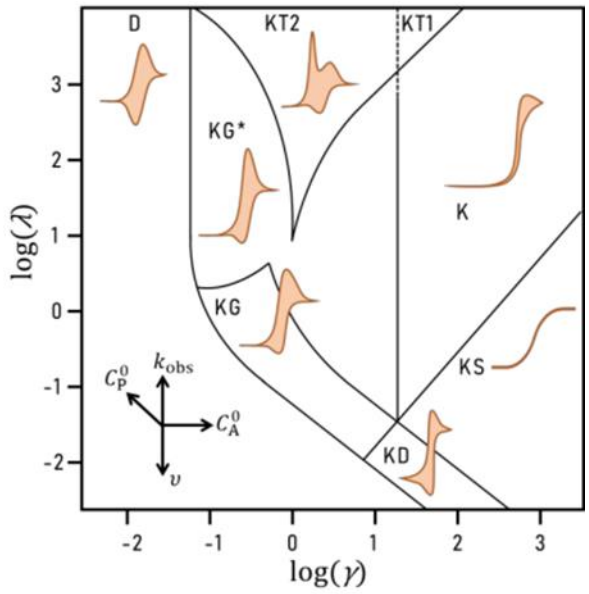

Figure 2. Kinetic zone diagram for homogeneously electrocatalyzed processes.

6. State of the Art in Anodic TEMPO-mediated Alcohol Oxidations

Cyclic nitroxides are mainly known from TEMPO (2,2 6,6-tetramethylpiperidine-1-oxyl) and their respective derivatives. Due to its unique properties, TEMPO derivatives are used in a broad range of processes. Some of the most important applications are the following[30]:

I. Organic radical batteries and TEMPO-modified polymers for energy storage (i.e. redox flow batteries).[31]
II. Functional group transformation in synthesis such as alcohol and amine oxidation, C-H and C-N bond formation and natural product synthesis.[32]
III. Stabilizer, radical trap, polymerization and antioxidant.[33]
IV. Nitroxide-mediated polymerization (NMP) for synthesis of well-defined functional polymers with tailored properties.[32a, 34]
V. Spin labelling in EPR spectroscopy.[35]

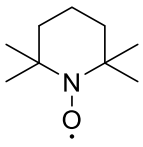

TEMPO

Scheme 6. Structure of 2,2,6,6-tetramethylpiperidin-1-oxyl (TEMPO)

In this thesis we focus more on the TEMPO mediated experiments in homogenous electrocatalysis.

Catalytic oxidation of alcohols to aldehydes or ketones using the organocatalyst TEMPO or its derivatives is widely used in the production of fine chemicals and pharmaceutical ingredients.[31a, 32a] This highly selective metal-free method was first developed by Lebedev and Kazarnowskii in 1960.[36] Another method was developed in 1990 by Anelli and Montanari, in which aqueous NaOCl was used as an oxidant under alkaline buffered conditions.[37] In 1983 Semmelhack et al. demonstrated an efficient electrochemical route for TEMPO-mediated oxidation in which electric current replaces an oxidant (see Scheme 7). This approach leads to prevention of undesired waste formation and renders aldehydes and ketones which can serve as drug precursors, fragrances, and aromas.[32c] As mentioned earlier in part I, section 4, such reactions normally require stochiometric amounts of oxidants. Besides that, commonly used reagents for alcohol oxidation (chromium or ruthenium reagents) are highly toxic and harmful for the environment.[32c] With the method suggested by Semmelhack et al, these challenges can be tackled. Scheme 6 demonstrates the catalytic cycle of anodic alcohol oxidation mediated by TEMPO.

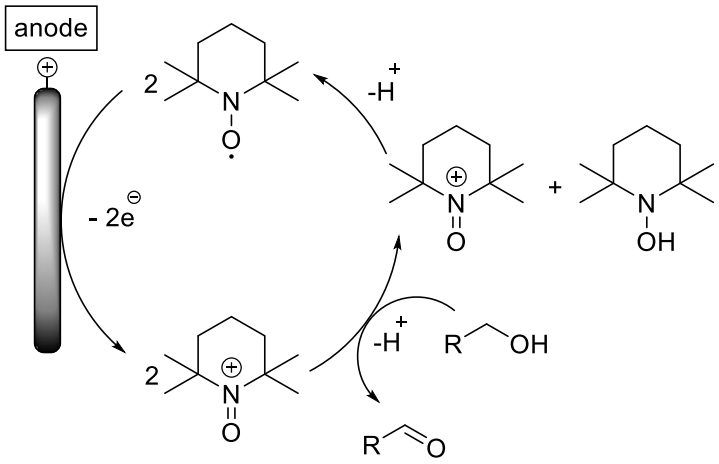

Scheme 7. Catalytic cycle of the TEMPO-mediated alcohol oxidation.

Furthermore, employment of TEMPO for amine oxidation was reported for the first time by Semmelhack and Schmidt in 1983. Depending on the reaction medium, different products can be obtained from oxidation of primary, secondary, or tertiary amines.[38] [39]

Xu and coworkers reported in 2017 a TEMPO-mediated oxidative C-S coupling reactions.[40] *N*-arylthioamides and amino-pyridine thioamides can undergo electrooxidation to yield respectively the corresponding benzothiazole and thiazolopyridine. Furthermore, it has been shown that TEMPO-catalyzed

electrooxidation is useful for oxidation of carbohydrates and other polyols. This approach exhibits minimum over-oxidation and high selectivity under mild conditions.[38c, 41] [42].

7. Recycling of Mediators and Supporting Electrolytes

Despite all the advantages that mediators in indirect electrolysis provide, they are usually associated with separation issues, since they typically have similar size and polarity as the electrolysis products. Additionally, they constitute an extra source of waste unless they are recovered and reused. To overcome these challenges, researchers have focused their efforts mainly on the use of homogeneous mediators which can be conveniently filtered off after completed electrolysis. The reported cases include poly(styrene)-supported iodobenzene (PSIB) and TEMPO immobilized on silica gel. The PSIB system was developed by Fuchigami et al. for anodic fluorodesulfurization of benzophenone dithioacetals, which was performed in $Et_3 \cdot 5HF$ ionic liquid (Figure 3, top left).[43] TEMPO-modified silica gel was developed for electrosynthesis by Tanaka et al. and used for anodic oxidation of alcohols in aqueous electrolyte (Figure 3, top right). Due to low solubility in the aqueous electrolyte, the starting material needed to be adsorbed on the silica gel prior to the electrolysis.[44] Due to poor kinetics of the ET between electrode and redox-active particle, a halide salt additive is crucial to activate the mediator units in PSIB as well as in the modified silica gel particles. The halide salt serves as a co-mediator and requires an additional separation step after completion of electrolysis. A third approach was developed by Schille, Francke et al. for homogeneously catalyzed electrochemical conversion using recyclable polymediators in combination with membrane separation processes for recovery of polymers (Figure 3, bottom).[14] A modified polymer synthesis from Schubert et al. was employed to gain a polymethacrylate backbone with TEMPO moieties attached to it.[36] In the seminal study, it was shown that TEMPO-modified polymethacrylates (TPMA) are well soluble, easy to synthesize and can be recycled easily by the end of the electrolysis.[45]

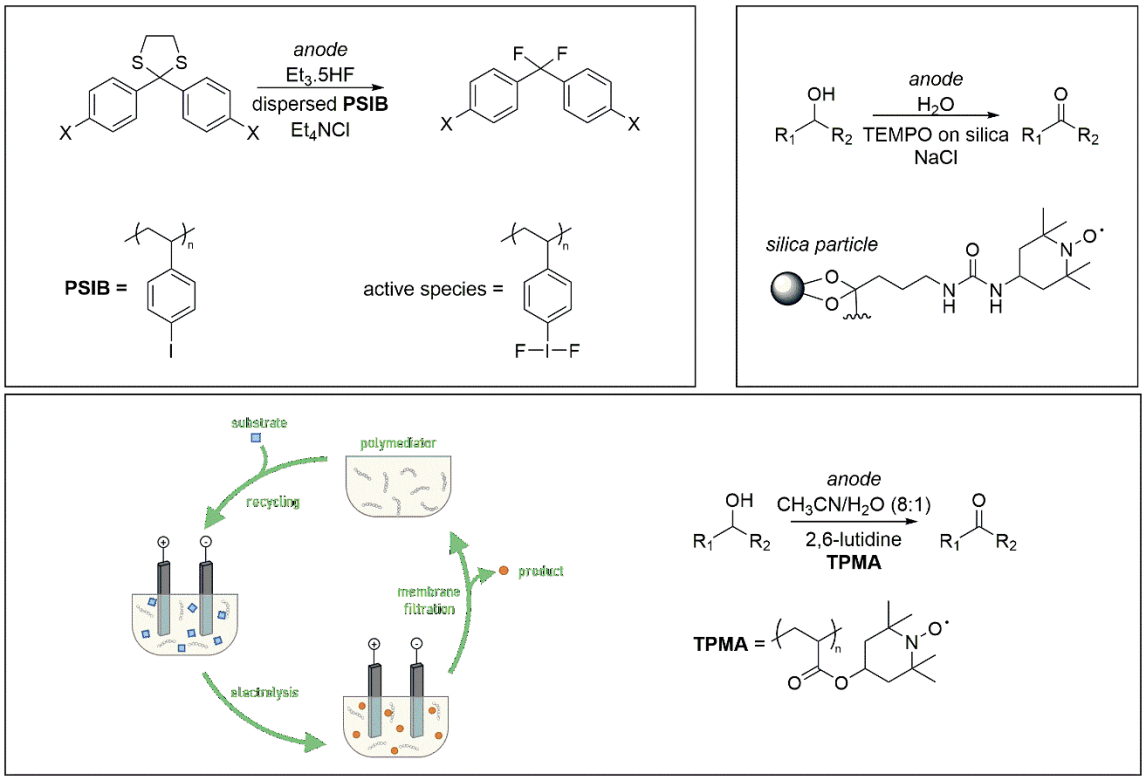

Figure 3. Strategies for immobilization of mediators to enable recovery by filtration techniques.

TPMA offers homogeneously catalyzed electrochemical conversion using recyclable polymediators in combination with membrane separation process for recovery of the polymers.

As mentioned earlier, indirect electrolysis using redox mediators is a frequently used approach toward controlling selectivity and reducing energy consumption of electro-organic transformations.[46] Although the benefits of mediators are undisputed, they may be offset by more difficult separation procedures, increasing waste generation, and additional expenses, which is why concepts to facilitate separation and recycling deserve more attention.[47] The main challenge in recovering mediators from reaction mixtures is the similarity to the product in terms of polarity and molecular size. For example, column chromatography is required for separation of organic mediators such as iodoarenes or TEMPO. To overcome this challenge, the installment of mediators on soluble polymer backbones is an interesting alternative, since the resulting polymediators can act as classic homogeneous electrocatalysts that are activated at the electrode surface and react with the substrates in solution. Simultaneously, the increased molecular size allows the use of size exclusion membrane processes for mediator recovery (i.e., dialysis and ultrafiltration). Based on the TEMPO-catalyzed anodic alcohol oxidation, Schille, Francke, et al. have shown for the first time that

indirect electro-organic reactions can efficiently be coupled to dialysis and ultrafiltration when polymediators are employed (Figure 4).[45b]

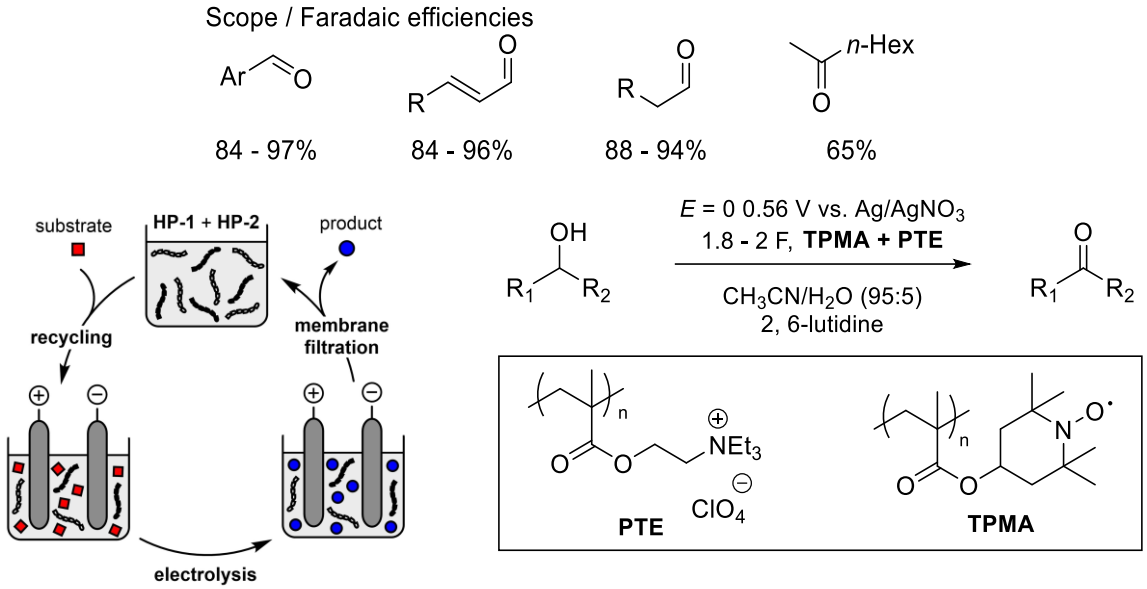

Figure 4. Top: Top: Scope and Faradaic efficiencies of TPMA-mediated electrooxidation. Bottom left: Schematic illustration of the electrolysis and recycling process. Bottom right: Preparative-scale anodic oxidation of alcohols using polymediators (TPMA) and polyelectrolytes (PTE).

8. State of the Art in the Field of Hypervalent Bromine(III) Compounds

Hypervalency refers to a situation in which a main group element has more than eight electrons in its valence shell. The *λ* notation is given to the compounds with non-standard bonding numbers according to IUPAC rules. The hypervalent bond is highly polarized, longer, and weaker than a regular covalent bond. The hypervalent bonding leads to distinctive structural features and reactivity pattern on the compound..[48] This provides the opportunity for development of new chemical reagents and specially in the field of hypervalent halogen compounds. A number of research publications can be found in literature that exclusively focuses on this topic.[22c, 48b, 49]

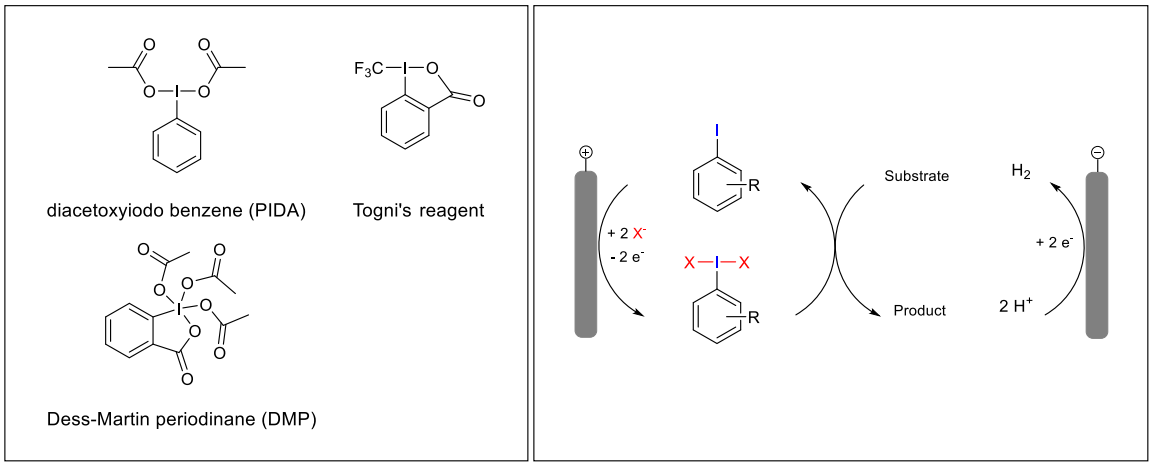

Scheme 8. Left: Common hypervalent iodine compounds. Right: electrochemical generation of iodine(III) species for indirect electrosynthesis.

Hypervalent halogen compounds have attracted great attention in organic chemistry which has been ascribed to their unique properties as reagents and catalysts.[48b, 50] Most of this attention and research has been attributed to hypervalent iodine compounds in recent years, which has led to many novel reactions and new reagents.[48a, 51] They are a mild, non-toxic, easy to handle, and environmentally benign class of reagents. The reactivity pattern of hypervalent iodine is similar to heavy transition metals and are applied in diverse forms of reactions as a non-toxic reagent.[48b] The nature of these reactions includes oxidative couplings, halogenations, arylations, oxidative rearrangements, trifluoromethylation, and C-H functionalization.[48a] Additionally, electrochemically generated iodine(III) derivatives have been frequently utilized as *ex-cell* mediators in organic electrosynthesis.[52]

Among the most prominent hypervalent iodine reagents in conventional organic synthesis are Dess-Martin periodinane, [bis(trifluoroacetoxy)iodo]benzene (PIFA), (diacetoxyiodo)benzene (PIDA) and diaryliodonium-type compounds (Scheme 8, left).[53] The corresponding isoelectronic hypervalent bromin(III) species feature superior reactivity to that of iodine(III) counterparts. Hypervalent bromine(III) compounds have higher oxidizing ability, stronger electrophilicity and better nucleofugality.[54] Despite these remarkable properties, the chemistry of λ^3-bromanes has been rarely investigated. This is mainly due to lack of efficient and user-friendly preparation methods. Much of the challenge is based on the thermodynamic barrier to oxidation of Br(I) arising from the properties of the element bromine, namely its great electronegativity (Br: 2.96 > I: 2.66) and its large ionization potential (IP); e.g. PhBr (IP: 8.98 eV) > PhI (IP: 8.69 eV).[55]

The superior reactivity has enabled the development of useful synthetic transformations such as Bayer-Villiger-type oxidations of open-chain aliphatic aldehydes, metal-free C-O and C-N couplings, oxidative coupling of alkynes and 1° alcohols, metal-free amination of inactivated alkanes, and thermal solvolysis of cyclopent-1-enyl- λ^3-bromaness for generation of vinyl cations.[51, 54] Undoubtedly, the development of a convenient synthetic approach to λ^3-bromanes is the most challenging part to initiate the rapid development of hypervalent bromine(III) chemistry. Herein, the development of investigated methods is described.

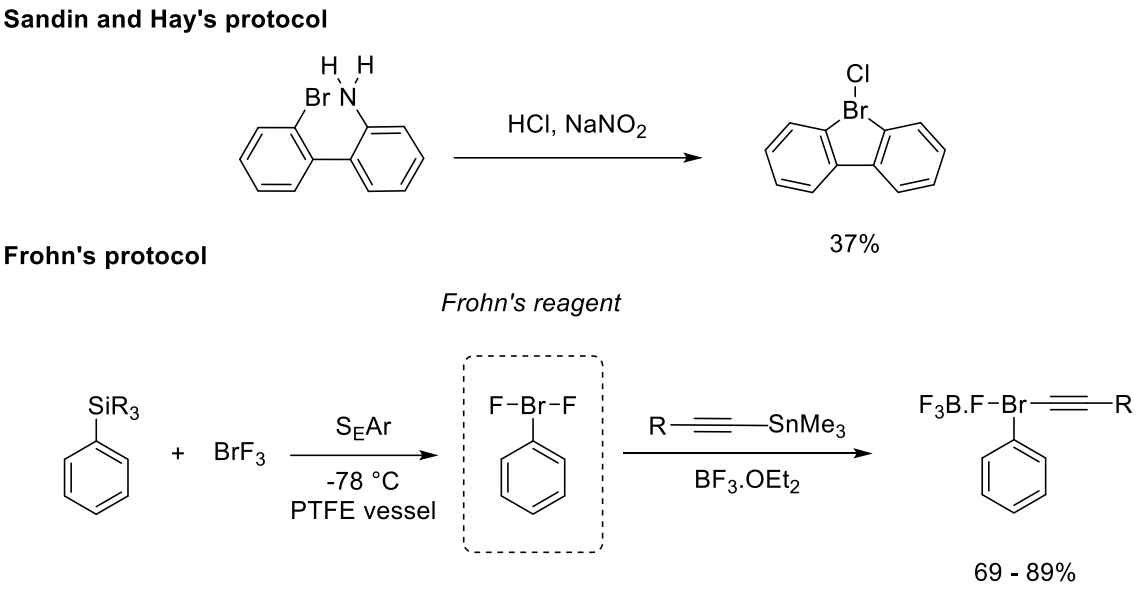

Scheme 9. Different protocols for synthesis of hypervalent bromine compounds.

The first hypervalent bromonium compound was synthesized by Sandin and Hay in 1952 (Scheme 9). They reported the formation a bromonium salt by intramolecular nucleophilic bromine attack on an aryldiazonium salt.[56] As promising as this synthesis seems, the addition of aryl cations to aryl bromides, regardless of their precursors and generation methods, leads to poor yields. [57] Another method of synthesis of hypervalent bromine compounds is ligand-exchange reactions of bromine trifluoride. The ligand exchange proceeds at low temperature in a rapid addition-elimination process. Bromine trifluoride, a highly toxic and reactive liquid, reacts with arylstannanes, arylmercury, or arylboron compounds to produce (difluoro)-λ^3–bromanes (Frohn's reagent). Furthermore, Frohn and Giesen developed the use of alkynylstannanes for ligand exchange on bromine trifuoride to produce aryl (alkynyl)-λ^3–bromanes (Scheme 9).[58]

Martin's protocol

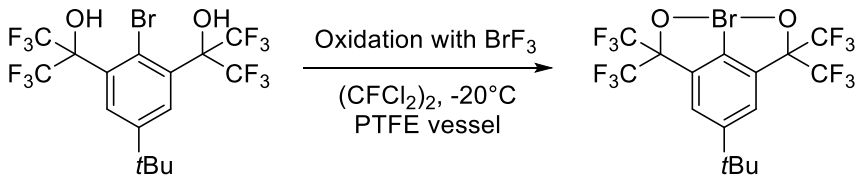

Current work

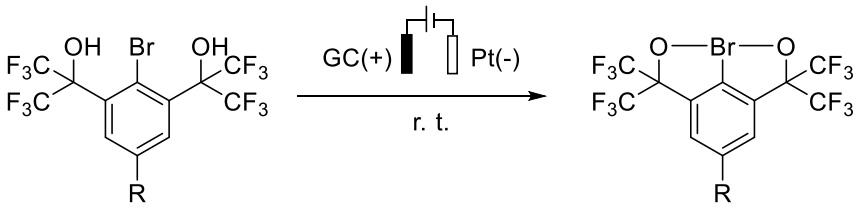

Scheme 10. Martin's protocol for the synthesis of chelation-stabilized bromanes in comparison to current work.

In 1986, Nguyen and Martin have introduced the bench-top stable chelation-stabilized aryl λ^3-bromanes using bromine trifluoride as precursor for synthesis.[59] The approach is, however, not ideal in terms of practicality. BrF_3 is a highly toxic and extremely reactive liquid, which is an important limitation of this method. It is required to use specific experimental techniques, equipment such as PTFE vessels, and very low temperature to handle this reagent properly and safely. In addition, aryl bromides have high oxidation potentials (e.g. 2.0 V vs. Ag/0.01 M $AgNO_3$ for PhBr in CH_3CN. All these circumstances complicate a two-electron oxidation by a non-electrochemical conversion.[59-60] Possibilities for electrochemical synthesis of Martin's bromane were explored in this work and are discussed in part III, section 2.

Part II. Goals of the Thesis

In this work, the goal is to generate a better mechanistic understanding of electrochemical processes involving polymediators and electro-generated bromane reagents.

The first goal is to develop a comprehensive understanding of reactions mediated by TEMPO-modified polymethacrylates (TPMA, case studies I and II). One of the key-questions is whether mass transfer occurs as a regular diffusion-type process or via electron hopping between redox-active units. Furthermore, it is important to determine whether electrocatalysis with TPMA is a homogenous or a heterogenous process, i.e., whether adsorption of TPMA on electrode surface plays a role. Next, the influence of the molecular weight on redox-properties and catalytic activity of TPMA is to be established, enabling an understanding of the relationship between mediator structure and kinetics of the catalytic process.

The second major goal is to reveal the mechanisms that are involved in the formation of hypervalent bromine(III) compounds and in the reagent applications. For this purpose, it is necessary to conduct detailed electroanalytical studies, which are complemented by control experiments and quantum chemical calculations. Another interesting feature to analyze is the dependency of the oxidizability (half-peak potential) of λ^3-bromanes from the electron withdrawing/donating ability of the substituents. Furthermore, the properties of chelation-stabilized λ^3-bromanes as chemical oxidants are to be evaluated, including a mechanistic analysis their activation for synthesis.

Part III. Results and Discussion of the Publications

1. Polymediators in Organic Electrosynthesis

Based on previous studies, it is shown that the TEMPO-modified polymethacrylates (TPMA) is an efficient and recyclable mediator for anodic alcohol oxidation.[45b] A comparative mechanistic study is needed between TMPA and TEMPO with lower molecular weight. This study can also be extended to TMPA from low to high chain-length.

In the approach by Schille et. al., free-radical polymerization was employed on 2,2,6,6-tetramethylpiperidin-4-ylmethacrylate (**1**) to obtain precursor polymer **2a** (Scheme 11, route 1)**.** 2-Mercaptoethanol was used as a modifier to achieve low molecular mass and to guarantee solubility for further electrochemical studies. Subsequently, **2a** was oxidized in two steps with H_2O_2/Na_2WO_4 and MCPA. This yielded the desired TEMPO-modified polymer (**HP-2**) with number average molecular weight (M_n) of 2.9 kDa. This straightforward procedure has also enabled easy scale-up. However, this method lacks control over chain growth, which is expressed by the high polydispersity ($Đ$ = 1.89).[45b] In the present study, the focus is on development of a polymerization protocol that provides proper control over chain length growth and narrow molecular weight distribution. Furthermore, it continues by investigating the electrochemical and electro-catalytical properties of the produced polymer in different molecular weight and respective comparison with low-molecular model compounds. The goal was achieved by reversible addition – fragmentation chain transfer (RAFT) polymerization. of hydrochloride **1·HCl** using dithioester **3** as a chain transfer reagent (Scheme 11, route 2).

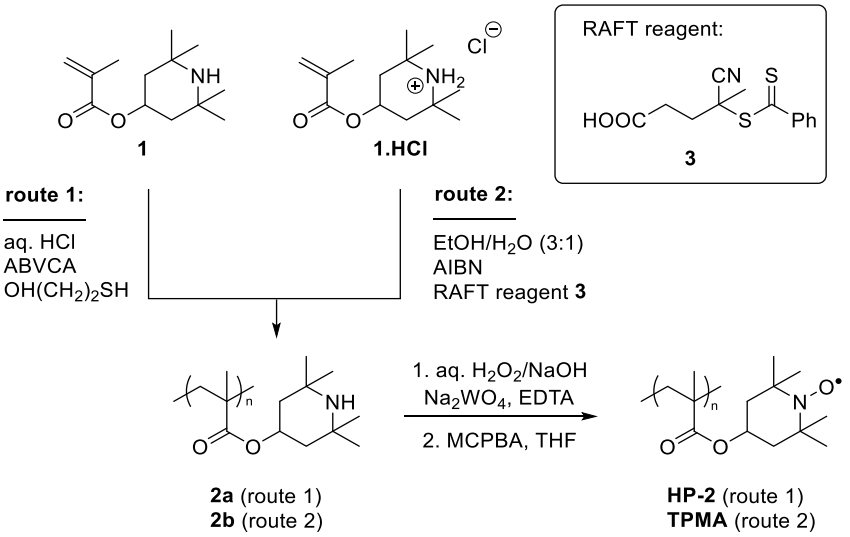

Scheme 11. Comparison of synthesis of TPMA by free-radical polymerization with RAFT polymerization.

RAFT polymerization is followed by oxidation of intermediate **2b** using the abovementioned two-step protocol, and purification of the TPMA by dialysis. In total, 15 samples with narrow molecular weight distributions were prepared using this method (see Figure 5), with number average molecular masses between 3.5 to 126.0 kDa, the polydispersity (*Đ*) ranging from 1.16 to 1.45, and with isolated yields between 48% to 94%. The molar mass was adjusted by varying the ratio between monomer and chain transfer agent. All the samples exhibit a monomodal molecular weight distribution. Increased dispersity is observed at higher molecular weight because less control over radical polymerization is possible with lower concentrations of RAFT reagent.[61]

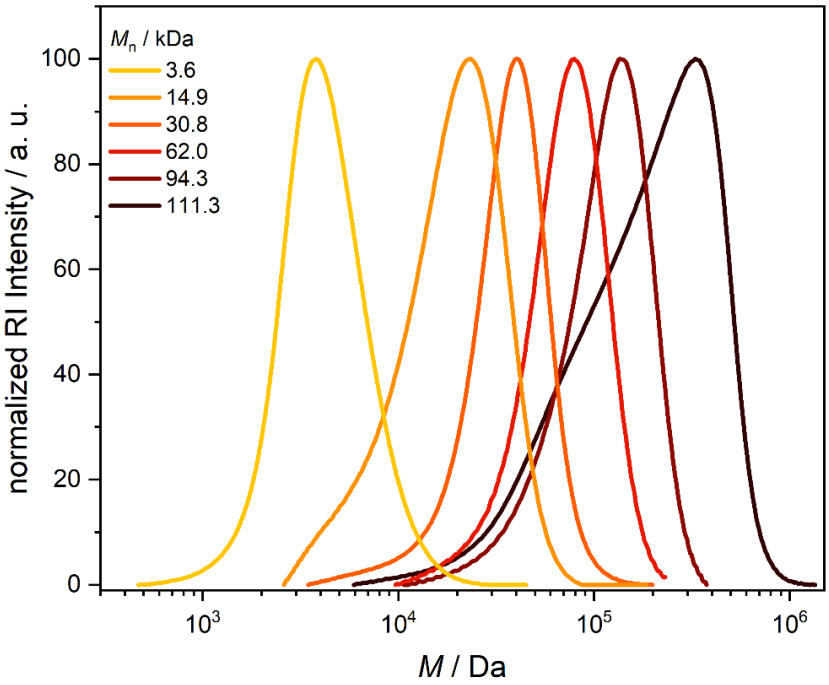

Figure 5. Molecular weight distributions of representative TPMAs.

For the electrochemical characterization of the TPMAs, cyclic voltammetry (CV) was carried out in 0.1 M solutions of NBu_4ClO_4 in CH_3CN/H_2O (8 :1 vol/vol) using a glassy carbon working electrode (WE) and a Ag/0.01 M $AgNO_3$ reference electrode (RE) (E_0 = 87 mV vs. Fc/Fc^+ couple). Detailed mechanistic studies were first carried out using 3.6-TPMA, a polymer sample with a M_n value of 3.6 kDa. TEMPO and 4-acetoxy TEMPO (ACT) were selected for comparison. Some exemplary CVs recorded at v = 100 mV s^{-1} are shown in figure 6. For each species, a single reversible redox couple ($R_2N\ O^{\bullet}/R_2N{=}O^+$) with a typical diffusive profile is visible. Consequently, there is no significant electronic coupling between the TEMPO moieties across the polymer

chain and the redox characteristics at 100 mV s^{-1} are essentially the same as those shown by the monomer. For TPMA (blue line), the redox couple is centered around E_0 = 0.42 V with an anodic shift of 120 mV compared to free TEMPO (green line). The shift can be ascribed to the presence of the acyloxy linker, which is confirmed by comparison to the CV of structurally similar ACT (red line, E_0 = 0.40 V).[62]

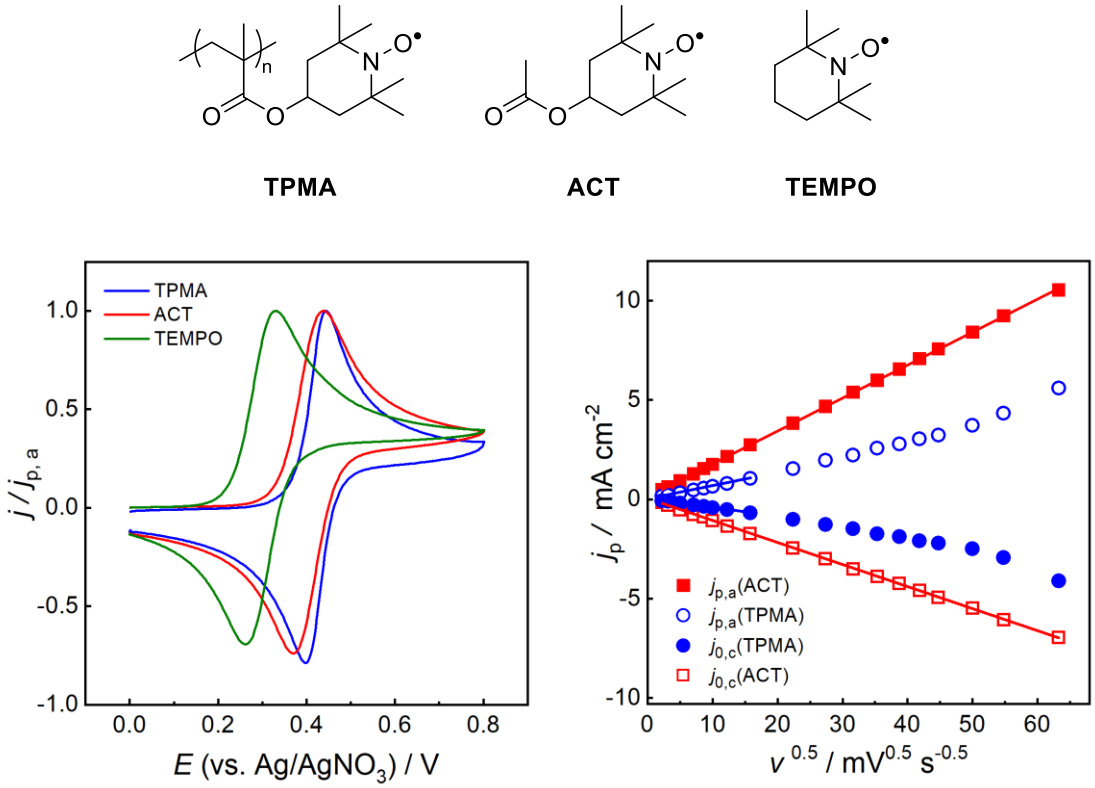

Figure 6. Top: Structures of the investigated mediators. Bottom left: Background-corrected CV of TEMPO, ACT and TPMA normalized vs. the anodic peak current density $j_{p,a}$. Conditions: 0.1 M NBu_4ClO_4 in acetonitrile/water (8 : 1), c_{TU} = 5 mM, v = 100 mVs^{-1}. Bottom right: Comparison between peak current densities (j_p) of ACT and TMPA with respect to square root of scan rate (v).

However, TPMA shows deviation from the linear dependency for scan rates above 250 mV s^{-1}. This effect is due to superposition of adsorptive and diffusive processes, which means that charge transfer occurs to both dissolved and adsorbed polymer chains. The linear dependency indicates that at lower scan rates, most of the charge is transferred via diffusive process. The adsorptive fraction of j_P increases at higher v, since for adsorbed redox-active species, j_P increases linearly with v.[63] Furthermore, the diffusion coefficients (D) were calculated from the slope of j_p versus $v^{0.5}$ from Eq. 6. (as explained in part I, section 4). D_{TPMA} is one order of magnitude smaller than D_{TEMPO} and D_{ACT}. This aligns with the Stokes-Einstein's equation, which relates the diffusion coefficient of a molecule to its molecular size. This same effect is observed by increasing the c_{TU} (TU:TEMPO units).

Adsorption of TPMA was confirmed by additional CV measurements at c_{TU} = 1 mM, followed by careful rinsing of the glassy carbon electrode with acetonitrile. Then the electrode was transferred to a blank electrolyte solution, where cycling was repeated. At 100 mV s^{-1}, the redox couple appears with weaker intensity and without peak-to-peak separation, which confirms irreversible adsorption of TPMA on the electrode surface. By increasing *v*, well-defined and nearly symmetric CVs were observed that centered around 0.43 V, which is characteristic for identical and independent redox-active species that are attached to the electrode surface.

Table 1.Summary of slopes of linear fits of Figure 6 and the corresponding diffusion coefficients.

Compound	Slope [mA $s^{0.5}$ cm^{-2} $mV^{-0.5}$]	D [cm^2 s^{-1}]
TEMPO	0.202	2.26 x 10^{-5}
ACT	0.166	1.53 x 10^{-5}
TPMA	0.065	2.35 x 10^{-6}

Additionally, the electrocatalytic behavior of TPMA was investigated. It was found that the polymer solutions exhibit a high electrocatalytic activity toward oxidation of various alcohols. A comparison is shown for TPMA, ACT and TEMPO at 100 mV s^{-1} in absence and presence of 4-methoxybenzyl alcohol (4-MBA). *N*-methylimidazole (NMI) was added as a proton scavenger and TBAPC was used as supporting electrolyte.

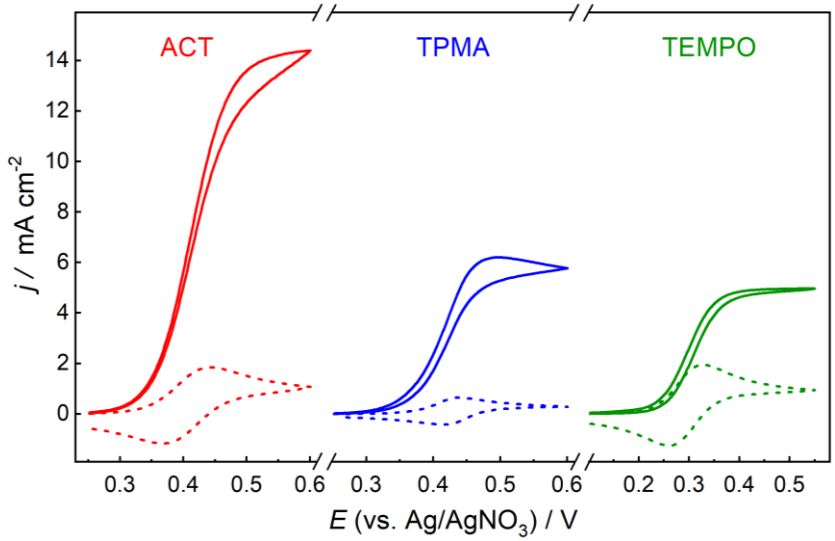

Figure 7. Comparison between background-corrected CVs of ACT (left), TPMA (middle), and TEMPO (right) under non-catalytic and catalytic conditions (c_{TU} = 5 mM, v = 100 mVs^{-1}). Electrolyte: 0.1 M NBu_4ClO_4 in acetonitrile/water (8:1). Substrate: 0.1 M 4-methoxybenzyl alcohol (4-MBA). Base: 0.45 M NMI.

The catalytic peak current density (j_{cat}) of TPMA is slightly higher than the one of TEMPO and lower than the one of ACT. This is due to the electron-withdrawing acyloxy linker in position 4 of the piperidinyl ring and the curbed mass transfer. The electronic influence of the acyloxy group results in the increased redox potential of ACT and TPMA (visible in Figure 7), which adds driving force for alcohol oxidation and thereby enhances homogeneous kinetics.[62] On the other hand, the increased molecular weight of TPMA leads to a decrease in activity compared to ACT, as the catalyst moves slower in the reaction diffusion layer (compare eq 6). It is worthy to mention that in absence of mediator the direct alcohol oxidation does not proceed within the same potential window.

The scan rate was increased to achieve S-shaped voltametric profiles where it is a pure kinetic condition (no substrate consumption), which is a prerequisite for the quantitative treatment of the kinetics of the catalytic process.[64] More detailed information on this matter can be found in publication I.[47b]The homogenous rate constant k_{cat} was extracted from these measurements. The calculated homogeneous rate constant k_{cat} for the oxidation of 4-methoxybenzyl alcohol is 397 L L^{-1} s^{-1} for TPMA, 330 L mol^{-1} s^{-1} for ACT, and 24 L mol^{-1} s^{-1}. (Figure 8)

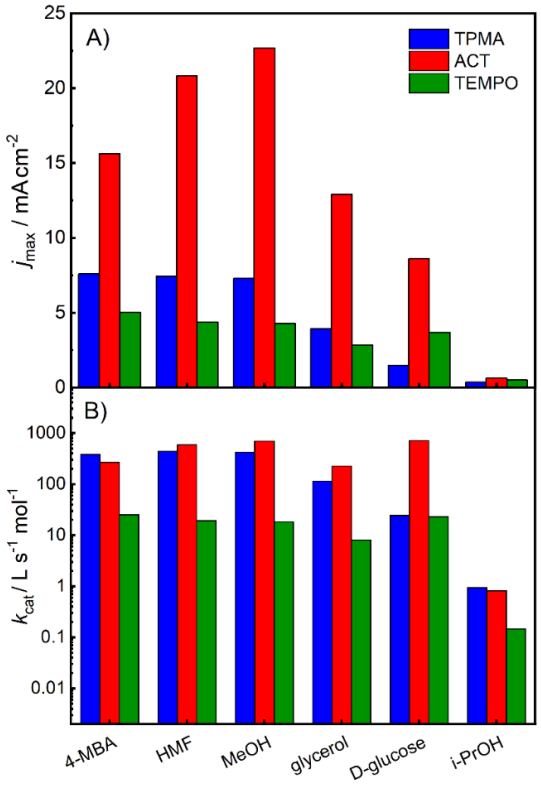

Figure 8. Comparison between the catalytic activities of TPMA, ACT and TEMPO for various substrates. Top: Plateau current densities (j_{max}) achieved under "no substrate consumption – pure kinetic conditions" (c_{TU} = 5 mM, c_{sub} = 0.1 M). Bottom: Rate constants k_{cat} calculated from the j_{max} values.

The relatively small k_{cat} for TEMPO confirms that the homogenous rate of alcohol oxidation is determined by redox potential of TEMPO unit rather than by its attachment to the polymer backbone. This catalytic study was extended to 5 - (hydroxymethyl)furfural (HMF), glycerol, methanol and propan-2-ol. In all cases, TPMA and ACT exhibit similar rate constants, while TEMPO exhibits distinctively lower k_{cat} values. Consequently, the TEMPO units on the polymer seem well accessible to the substrate and available for catalysis. The similarity between the results of ACT and TPMA confirms that the homogenous kinetics are not strongly affected by the attachment of the TEMPO units to the polymeric backbone.

The main difference within the TPMA is observed between the redox current. At higher molecular weight the diffusion rate is decreased. This means low-chain TPMA is more rapidly charged, hence higher currents are observed. This is in agreement with the Stokes-Einstein equation.[61]

2. Electrochemistry of Hypervalent Bromine(III) Compounds

Hypervalent bromine(III) chemistry appears to be underdeveloped in comparison to that of the iodine(III) counterparts. This notable disparity has been ascribed to two unfavorable factors. First, bromine(III) reagents exhibit poor stability and high oxidizing power, which has led to the general perception of difficult-to-control reactivity and poor compatibility with functional groups.[50, 65] Second, conventional routes to λ^3-bromane reagents rely eventually on the use of BrF_3, a highly toxic and extremely reactive liquid that demands for specific equipment and experimental techniques for its safe handling.[66] Based on previous work by Francke, et. al. in the electrochemical generation of hypervalent iodine compounds, it was hypothesized that the electrochemical oxidation would also be possible for the synthesis of aryl-λ^3-bromanes, provided that they are compatible with anodic oxidation conditions.[26b] For this purpose, Martin's bromane was chosen as a model system which is stabilized by chelation through the *ortho* substituents. This compound is moisture and air stable which brings another important advantage. The published conditions for anodic oxidation of iodoarenes to λ^3-iodane were used as the foundation for investigation for preparation of λ^3-bromane **5**. The detailed synthesis of compound **4** is also explained in publication III. to the optimized conditions successfully afforded compound **5a** (72% on a 10 mmol scale) using glassy carbon (GC) as WE, platinum foil as CE in a TBA-BF_4/HFIP electrolyte at 10 mA cm^{-2}. The structure of **5a** was confirmed with single crystal X-ray analysis (Scheme 12, right).

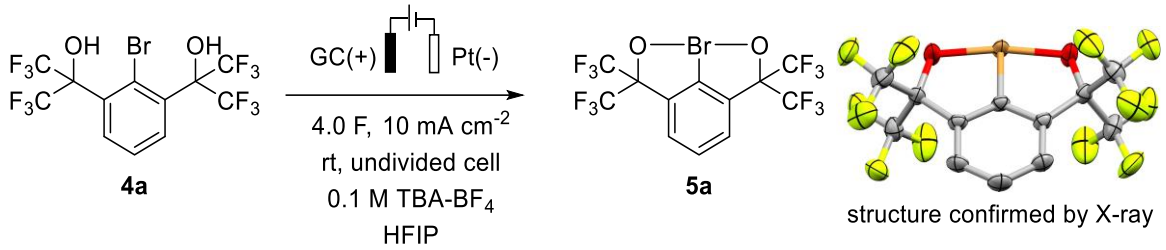

Scheme 12. Electrochemical generation of a hypervalent bromine(III) compound.

The optimized conditions were used to prepare six additional products of type **5** with different substituents in *para* position to create a reagent variety with tunable activity and electrochemical properties. Detailed information about the optimization and other compounds of type **5** are found in publication III.

As mentioned before, Martine's bromane exhibits high stability. This permits straightforward electrosynthesis and purification, easy handling, and long storage time. However, the synthetic application of bromanes requires activation to unlock the

intrinsic reactivity. To this end, oxidative biaryl coupling and C(sp^3)-H amidation of anilines were chosen as model reactions to study the reactivity profile of the bromane.[67] On the other hand, chelation-stabilized λ^3-bromanes seem to possess comparable SET oxidizing ability to that of hypervalent iodine(III) reagents. This requires activation by Lewis acid to effect SET oxidation in, for example, oxidative biaryl coupling[68], whereas strong Brønsted acids such as TfOH turned out to be most efficient for activation of Martin-type λ^3-bromanes (Scheme 13).[69]

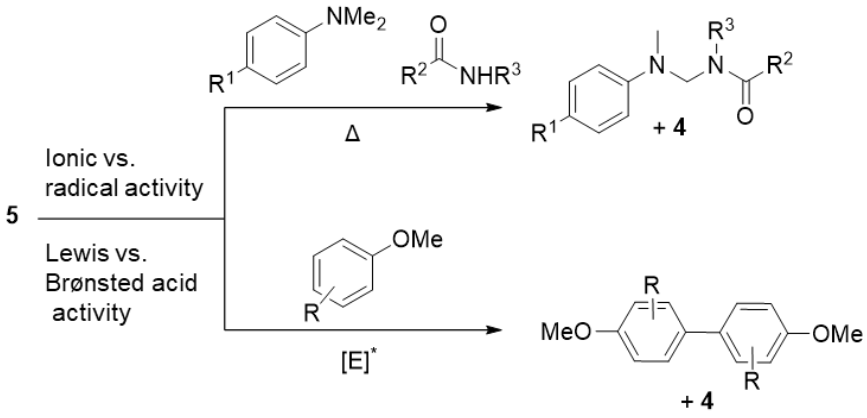

Scheme 13. Reactivity and activation of aryl-λ^3-bromanes.

To understand and characterize the electrochemical properties of the obtained λ^3-bromanes redox couples, the synthesized bromides **4a** – **g** were studied by CV.

*Table 2. Summary of the half-peak potentials ($E_{P/2}$, determined at v = 10 mV s^{-1}) and slopes of the j_p vs. $v^{0.5}$ plots for the anodic oxidation of **4** in HFIP.*

Compound	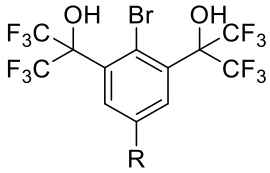	**$E_{p/2}$ / [V]**	**Slope j_p vs. $v^{0.5}$ [mA $s^{0.5}$ $mV^{-0.5}$ cm^{-2}]**
4a	R = H	2.27	0.156
4b	R = F	2.26	0.161
4c	R = Cl	2.22	0.194
4d	R = *t*Bu	2.13	0.168
4e	R = OMe	1.86	0.088
4f	R = CF_3	2.54	0.150
4g	R = NO_2	2.60	0.140

Thus, voltametric analysis of **4** at 10 mV s^{-1} between 0 and 2.7 V versus Ag/0.01 M $AgNO_3$ (E_{ref} = 87 mV vs. Fc/Fc^+ couple) using an electrolyte consisting of 0.1 M NBu_4BF_4 in HFIP showed that each of the bromoarenes exhibits a single irreversible

anodic feature. The half-peak potentials are positioned between 1.86 V (**4e**, R = OMe) and 2.60 V (**4g**, R = NO_2). A linear correlation between $E_{1/2}$ and the Hammett substituent coefficient (σ^+_p) shows that oxidizability is strongly dependent on the electron donating or withdrawing nature of the R substituent and shows a predictable behavior.

To understand the mechanism of formation of **5**, the scan rate was increased stepwise from 10 to 1000 mV s^{-1}. The voltametric response of **4a** – **4d**, **4f** and **4g** are characteristic with a signal shape indicating one or more chemical steps associated to the electron transfer (chemical irreversibility, Figure 9). In the other case, **4e** (R = OMe) shows an exceptional behavior. At low scan rates, it displays irreversible behavior which is followed by gradual change to a fully reversible CV profile. Besides that, the anodic peak current density j_p of **4e** is significantly smaller. This resulted in having the slope of the linear fit of j_p versus $v^{0.5}$ approximately half as high as other compounds. One-electron oxidation of **4e** and two-electron oxidation of the rest of the substituents is the cause of this effect. More precisely, the majority of the bromoarenes undergoes a two-electron oxidation in which the second ET is energetically more favorable than the first one and where a fast chemical reaction is interposed between the two electrochemical steps.[70]

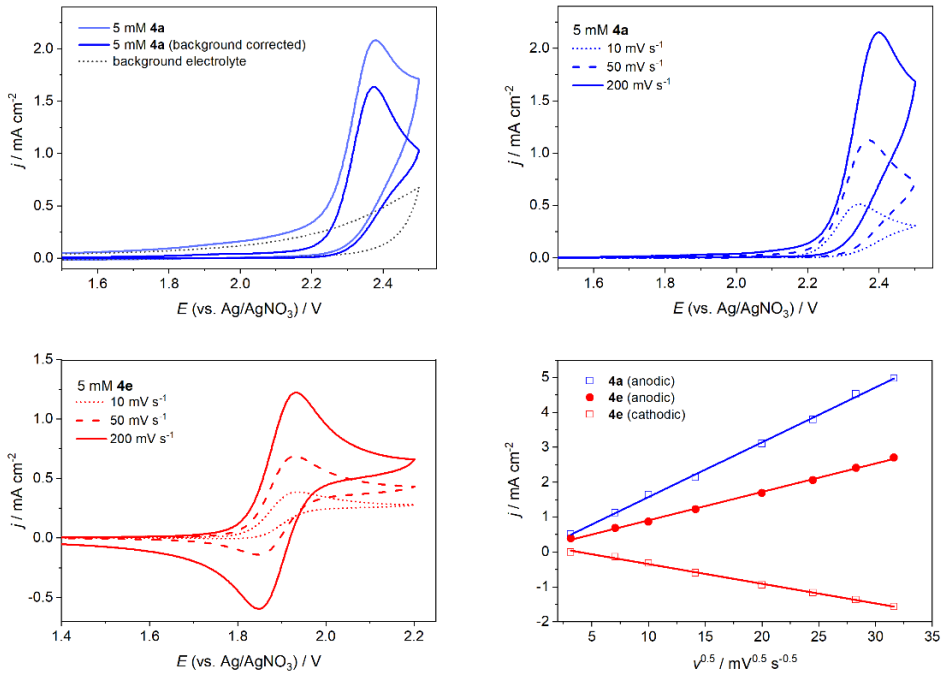

*Figure 9. Background and iR drop-corrected CVs of 5 mM **4a** and 5 mM **4e** at different scan rates (solvent: HFIP, working electrode: glassy carbon, supporting electrolyte: 0.1 M Bu_4NBF_4). Bottom right: Plot of the peak current densities (j_P) vs. $v^{0.5}$.*

Based on the above-mentioned analysis a mechanism for anodic oxidation of compound **5** was proposed. The bromanes are formed by a two-electron oxidation via an ECEC pathway (Figure 10). This contains initial one electron abstraction, deprotonation, second electron transfer which is continued by a second deprotonation (producing **4**$^{\bullet+}$, **4**$^{\bullet}$, **5**$^{+}$, **5**). Competitive homogeneous disproportionation of **4**$^{\bullet}$ (or between **1**$^{\bullet+}$ and **1**$^{\bullet}$) within the diffusion layer would also be in agreement with the diagnostic criteria (ECE_{disp} pathway).[71] Nevertheless, if the deprotonation step **4**$^{\bullet+}$ to 1$^{\bullet}$ is slow caused by stabilization of **4**$^{\bullet+}$, the radical cation wins enough time to diffuse into the bulk solution from the electrode surface. In this case, disproportionation leads to formation of **5** and **4**. The delayed deprotonation explains the distinctive behaviors of **4e** in CV and formation of **5e** in preparative scale electrolysis despite the voltammetry indicating a one electron oxidation. The electron-donating character of the methoxy substituent is responsible for the prolonged lifetime of **4e**$^{\bullet+}$. Further confirmation of the mechanism was achieved by quantum chemical calculations which are discussed in detail in publication IV.

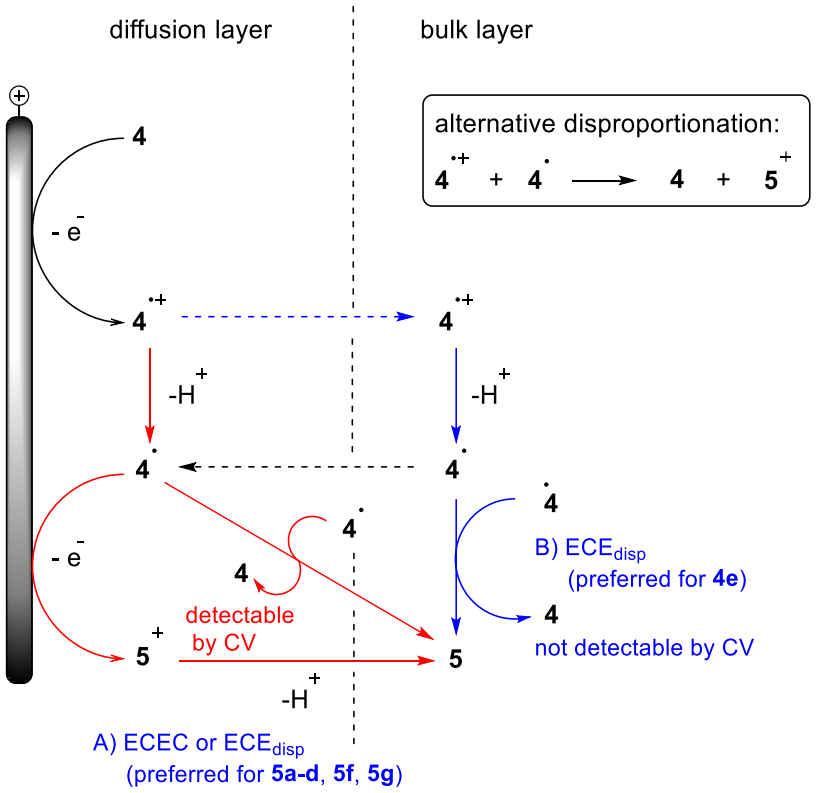

Figure 10. Proposed mechanism for anodic bromane formation.

Furthermore, electroanalytical experiments were conducted on the bromane compounds. Knowledge of their cathodic behavior is important, as it provides

information about the properties of compounds **5** as chemical oxidants. The electroanalytical studies were performed using the same solvent as in the synthetic applications (acetonitrile for C – H amidations and dichloromethane for arene – arene homocouplings).[60] CV studies of the cathodic reduction were thus carried out in each of these solvents using a glassy carbon working electrode and NBu_4BF_4 as the supporting electrolyte, whereby both the shape of the profiles and the half-peak potentials are quite similar between all of the studied bromanes.

Each of the bromanes exhibits an irreversible one electron reduction preak. The corresponding $E_{P/2}$ values are situated in the range between -0.35 V (**5g**, R = NO_2) and -0.53 V (**5e**, R = OMe) in acetonitrile. A good match was found between the experimental half-peak potentials and $E_{P/2}$ values predicted on the basis of a two-parameter correlation with σ_F and σ_R substituent constants, the latter two explicitly accounting for inductive (σ_F) and resonance effects (σ_R) (Figure 11).[72] Similar to bromoarenes, a linear correlation can be seen here.

compound	$E_{P/2}$ (obs.) [V]	$E_{P/2}$ (pre.) [V]
5a (R = H)	-0.50	-0.49
5b (R = F)	-0.41	-0.42
5c (R = Cl)	-0.39	-0.42
5d (R = *t*Bu)	-0.49	-0.50
5e (R = OMe)	-0.53	-0.49
5f (R = CF_3)	-0.37	0.38
5g (R = NO_2)	-.0.35	0.33

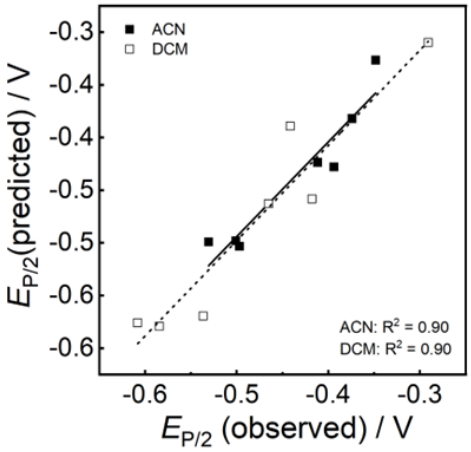

*Figure 11. Left: Half-peak potentials $E_{P/2}$(obs.) measured in CH_3CN and the values predicted using σ_R and σ_F substituent constants, $E_{P/2}$(pred.). Right: Correlation between $E_{P/2}$(obs.) and $E_{P/2}$(pred.) for **5** in CH_2Cl_2 and CH_3CN.*

To further analyze the reduction mechanism, controlled potential electrolysis was performed on **5a** (CPE, scheme 14). In acetonitrile, bromoarene **4a** could be isolated in 74 % yield after passing 1.0 F at 0.78 V versus Ag/0.01 M $AgNO_3$ (11% recovered **5a**). This result confirms the one-electron transfer observation that was obtained from the CV studies. A mechanism that explains this peculiarity is shown in Scheme 14. Initially, the radical anion **5a**$^{\bullet-}$ is formed which is followed by hydrogen atom transfer (HAT) from the from the solvent molecule that leads to formation of **4a**.[73] Further protonation can happen during the workup or by anodically generated acid.

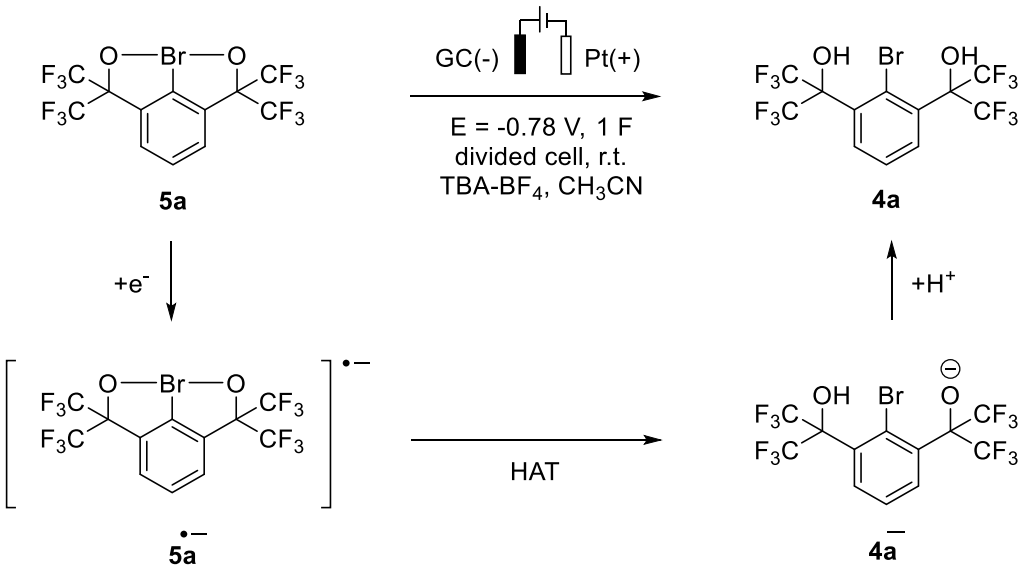

*Scheme 14. Result of preparative-scale cathodic reduction of **5a** in CH_3CN.*

More detailed information on oxidation of **4** and reduction of **5** are presented in publication III and IV.

Part IV. Summary

Four case studies on polymediators and electro-generated hypervalent bromine compounds were presented, significantly improving the mechanistic understanding and showing promising results for further development of these topics in the future.

In publications I and II, the electrocatalytic properties of TEMPO-modified polymethacrylates (TPMA) were investigated in view of anodic alcohol oxidation. These properties were brought in the focus by a comparison with 4-acetoxy TEMPO (ACT) and TEMPO. All three species exhibited a single reversible redox couple upon CV analysis. This indicates that all three redox couples show similar characteristics such as equilibrium potential, chemical reversibility, and diffusive character (at low scan rates). For TPMA, it could be clearly established that there is no electronic coupling between the TEMPO moieties along the polymer chain. A lower diffusion coefficient was estimated for TPMA, which is explained by the Stokes-Einstein equation in which the diffusion is decreased by increasing hydrodynamic radius of diffusing species.

To establish the relationship between the TPMA chain length and the electrochemical properties, a series of TPMA was synthesized with number average molecular weight (M_n) between 2.5 kDa to 126.0 kDa. The diffusion coefficients were estimated by cyclic voltammetry (CV), and it was observed that with higher molecular weights, lower diffusion coefficients are obtained. In terms of scaling theory, the observed behavior is in good agreement with a random coil conformation of the polymers surrounded by a "good solvent".[74]

Additionally, it became evident that the polymer tends to irreversibly adsorb on glassy carbon which forms a redox active layer on the surface of the electrode. These layers have significant effect on voltametric profiles under typical electroanalytical conditions (low polymediator concentrations). However, in preparative-scale electrolysis at high polymediator concentrations, alcohol conversion is mainly a homogeneously electro-catalyzed process.

Overall, short chain-length polymediators showed useful reaction rates for alcohol oxidation, while the longer chain TPMAs exhibit only poor catalytic activity. Preliminary recycling studies using dialysis to recover the polymediators gave promising results. In contrast, pressure-driven ultrafiltration did not provide the same results, as the short-

chain TPMAs were not properly retained. Therefore, nanofiltration with dense membranes appears to be a promising alternative to investigate.

The second study focused upon the mechanistic analysis of electrochemical generation of λ^3-bromane using cyclic voltammetry and controlled potential electrolysis. A series of arylbromides with oxidation potentials ranging between 1.86 V to 2.60 V were converted into the corresponding λ^3-bromanes. A good correlation was observed between the oxidation half-peak potential and Hammett substituent coefficient. Similar observation was obtained for the reduction half-peak potential of λ^3-bromane compounds. This indicated that the half-peak potential is dependent on the electron donating / withdrawing ability of the substituent.

These studies also showed that the anodic oxidation of parent bromoarenes proceeds via parallel ECEC and ECE_{disp} sequences, whereby the initially formed cation radical intermediate could be detected in the case of the *para*-methoxy-substituted bromoarene by UV-Vis spectroelectrochemistry. In contrast, the cathodic conversion of λ^3-bromane to the parent boromoarene occurs via single electron transfer reduction that is followed by hydrogen atom abstraction from the solvent and protonation.

The reactivity of these λ^3-bromanes can be unlocked by strong Brønsted acids for application in biaryl coupling. On the other hand, the oxidative amidation of anilines apparently proceeds through an ionic mechanism.

The case studies show how thorough investigations using combined methods can reveal mechanistic details of electrochemical conversions, thereby enabling knowledge-based optimization of the system. At this point, the properties of TPMA as a mediator and λ^3-bromane as an electrochemical reagent are much better understood, on the basis of which future developments can build.

Part V. Outlook

Both case studies of polymediators in organic electrosynthesis and electrochemistry of hypevanelnt bromine(III) compounds show great potential for further research.

In the topic of polymediators, more studies are required on the recycling and recovery of TPMA. This follows by development of industrial conditions for the application of TPMA. This can be achieved by when a cross-flow membrane filtration is coupled with an electrochemical flow reactor.

In the topic of hypervalent bromine(III) compounds, there needs to be more studies and investigation done on the mechanistic studies of electrochemical properties and reactivities of these compounds. First, λ^3-bromanes with one chelating moiety can be synthesized instead of two and its effect on stability and activity as oxidant can be investigated. Furthermore, the effect on electrochemical generation of λ^3-bromane can be analyzed. Consequently, this can cause a shift on oxidation potential of bromoarenes and reduction potential of bromanes. Furthermore, the influence of the substituent on para position on reaction rate can be investigated and tuned properties can be introduced to this oxidant.

Part VI. Publications

Part of this thesis:

I. **N. Mohebbati**, A. Prudlik, A. Scherkus, A. Gudkova, R. Francke. TEMPO-Modified Polymethacrylates as Mediators in Electrosynthesis – Redox Behavior and Electrocatalytic Activity towards Alcohol Substrates. *ChemElectroChem* **2021**, *8*, 3837. DOI: 10.1002/celc.202100768.

II. A. Prudlik, **N. Mohebbati**, L. Hildebrandt, A. Heck, L. Nuhn, R. Francke. TEMPO-Modified Polymethacrylates as Mediators in Electrosynthesis: Influence of the Molecular Weight on Redox Properties and Electrocatalytic Activity. *Chem. Eur. J.* **2023**, e202202730. DOI: 10.1002/chem.202202730

III. I. Skolovs, **N. Mohebbati**, R. Francke, E. Suna. Electrochemical Generation of Hypervalent Bromine(III) compounds. *Angew. Chem. Int. Ed.* **2021**, *60*, 15832. DOI: 10.1002/anie.202104677.

IV. **N. Mohebbati**, I. Sokolovs, P. Woite, M. Lõkov, E. Parman, M. Ugandi, I. Leito, M. Roemelt, E. Suna, R. Francke. Electrochemistry and Reactivity of Chelation-stabilized Hypervalent Bromine(III) Compounds. *Chem. Eur. J.* **2022**, *28*, e202200974. DOI: 10.1002/chem.202200974

Publication I

TEMPO-Modified Polymethacrylates as Mediators in Electrosynthesis – Redox Behavior and Electrocatalytic Activity toward Alcohol Substrates

Nayereh Mohebbati (60%), Adrian Prudlik (20%), Anton Scherkus (5%), Aija Gudkova (5%), and Robert Francke (10%).

DOI: 10.1002/celc.202100768.

Abstract: Homogeneous catalysts (“mediators”) are useful for tuning selectivity in organic electrosynthesis. However, they can have a negative impact on the overall mass and energy balance if used only once or recycled inefficiently. In a previous work, we introduced the polymediator concept, in which soluble redoxactive polymers catalyze the electrochemical reaction, allowing for recovery by dialysis or pressure-driven membrane filtration. Using anodic alcohol oxidation as a test case, it was shown that TEMPO-modified polymethacrylates (TPMA) can serve as efficient and reusable mediators. In the present study, the properties of a TPMA sample with well-defined molecular weight distribution were studied using cyclic voltammetry and compared to low-molecular TEMPO species. The non-catalytic profiles of TPMA are shaped by diffusive and adsorptiveprocesses, whereby the latter only become pronounced at low mediator concentrations and high scan rates. Electrocatalytic studies suggest that under the applied conditions, TPMA catalyzed alcohol oxidation is a predominantly homogeneous process. The homogeneous kinetics are determined rather by the mediator potential than by steric influences of the polymer backbone.

My Contribution (60%):

I carried out the synthesis and electrochemical analysis of TPMA, ACT and TEMPO in cooperation with A. Gudkova (5%) as the assigned master student. A. Prudlik (20%) carried out adsorption analysis together with A. Scherkus (5%) as the assigned master student. R. Francke (10%) had the initial idea, guided the project, and wrote the manuscript.

Special Collection

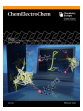

TEMPO-Modified Polymethacrylates as Mediators in Electrosynthesis – Redox Behavior and Electrocatalytic Activity toward Alcohol Substrates

Nayereh Mohebbati,[a, b] Adrian Prudlik,[a, b] Anton Scherkus,[b] Aija Gudkova,[b] and Robert Francke*[a, b]

Dedicated to the memory of *Jean-Michel Savéant*.

Homogeneous catalysts ("mediators") are useful for tuning selectivity in organic electrosynthesis. However, they can have a negative impact on the overall mass and energy balance if used only once or recycled inefficiently. In a previous work, we introduced the polymediator concept, in which soluble redox-active polymers catalyze the electrochemical reaction, allowing for recovery by dialysis or pressure-driven membrane filtration. Using anodic alcohol oxidation as a test case, it was shown that TEMPO-modified polymethacrylates (TPMA) can serve as efficient and reusable mediators. In the present study, the properties of a TPMA sample with well-defined molecular weight distribution were studied using cyclic voltammetry and compared to low-molecular TEMPO species. The non-catalytic profiles of TPMA are shaped by diffusive and adsorptive processes, whereby the latter only become pronounced at low mediator concentrations and high scan rates. Electrocatalytic studies suggest that under the applied conditions, TPMA-catalyzed alcohol oxidation is a predominantly homogeneous process. The homogeneous kinetics are determined rather by the mediator potential than by steric influences of the polymer backbone.

In organic electrochemistry, indirect electrolysis using homogeneous catalysts ("mediators") is a useful tool for shaping the course of the reaction and for reducing the energy consumption.[1] Consequently, mediators are widely used and find application both in *in-cell* processes (homogeneous electrocatalysis) and in *ex-cell* protocols (transformations with electrogenerated reagents).[2] Another key advantage is that a variety of synthetic challenges can be addressed with a broad range of well-established mediators including organometallic compounds,[3] halide salts,[4] triarylamines,[5] iodoarenes,[6] and *N*-oxyl radicals.[7] However, these positive features may be offset by additional costs, a more complex separation procedure, and increased waste generation, which is why concepts to improve separability and recyclability deserve more attention.[8]

The main cause of separation problems in indirect electrosynthesis is the similarity between mediator and product in terms of polarity and molecular size. For example, column chromatography is necessary in protocols involving organomediators such as iodoarenes or 2,2,6,6-tetramethylpiperidinyl-1-oxyl (TEMPO). While this is not a particular problem on a laboratory scale, more straightforward methods such as extraction and filtration are required when scaling up. In this context, tuning of the mediator polarity by attaching charged groups ("ionic tags") has turned out as a promising approach, facilitating recovery by extraction while eliminating the need for supporting electrolyte additives.[9] In further studies, mediator immobilization on suspended particles was attempted. Using poly(styrene)-supported phenyl iodide[10] and TEMPO attached to silica gel,[11] a straightforward recovery via simple filtration was achieved. However, the use of halide salts as co-mediators was necessary for activation of the immobilized mediator units, which is symptomatic for poor kinetics of the electron exchange between electrode and immobilized phenyl iodide units.

Compared to the dispersed-phase strategy, the attachment of a mediator to soluble polymer backbones (polymediators) leading to homogeneous electrolyte systems represents a promising approach. Such systems do not require a co-mediator and allow for recovery via size exclusion membrane processes (ultra-/ nanofiltration and dialysis).[12] Using the example of TEMPO-catalyzed alcohol oxidation as a test case, we have demonstrated for the first time that indirect electrosynthesis can be efficiently coupled to dialysis and ultrafiltration using polyelectrolyte HP-1 and polymediator HP-2 (see Figure 1). The polymer solutions are sufficiently conductive and exhibit a high electrocatalytic activity toward oxidation of various alcohols. Electrolysis on the preparative scale showed that various

[a] *N. Mohebbati, A. Prudlik, Dr. R. Francke*
Leibniz Institute for Catalysis
Albert-Einstein-Str. 29a, 18059 Rostock, Germany
E-mail: robert.francke@catalysis.de
[b] *N. Mohebbati, A. Prudlik, A. Scherkus, A. Gudkova, Dr. R. Francke*
Institute of Chemistry
Rostock University
Albert-Einstein-Str. 3a, 18059 Rostock, Germany

Supporting information for this article is available on the WWW under https://doi.org/10.1002/celc.202100768

An invited contribution to a joint Special Collection in memory of Prof. Jean-Michel Savéant.

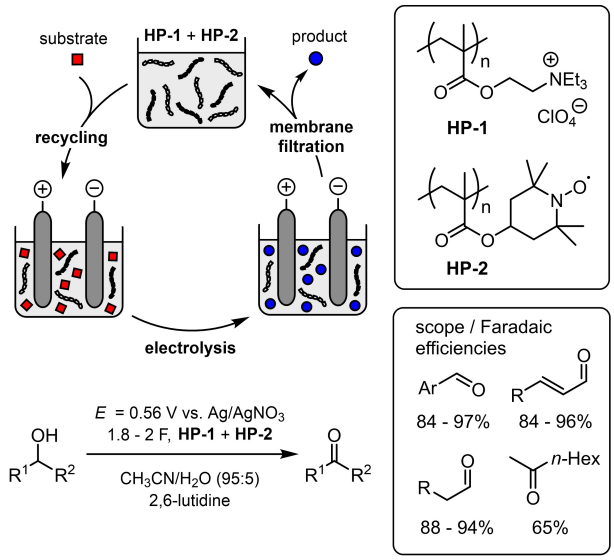

Figure 1. Summary of our previous study on the use of soluble polymediators and polyelectrolytes using the TEMPO-catalyzed oxidation of alcohols as a test case (Faradaic efficiencies determined after passing 1.8–2.0 charge equivalents).[12]

benzylic, allylic and aliphatic alcohols can be selectively converted to the corresponding carbonyl compounds, and that the electrolyte solution can be reused multiple times.

Initial cyclic voltammetry (CV) studies on a glassy carbon electrode showed that compared to "regular" TEMPO, the peak currents obtained for HP-2 under non-catalytic conditions are smaller, whereas the catalytic currents are significantly higher. Furthermore, the voltammetric response of the polymer exhibited some distinctive features, such as a peak-to-peak separation ($\triangle E_p$) of 35 mV (at a scan rate of $v = 50$ mV s^{-1}), which is atypical both for adsorptive and diffusive behavior.[13] We believe that a better understanding of the voltammetry of polymediators is of high importance for future developments in the area of polymediated electrosynthesis. We have therefore carried out a detailed electroanalytical study on redox behavior and electrocatalytic properties of TEMPO-modified polymethacrylates, the results of which are presented herein.

1. Results and Discussion

1.1. Polymer Synthesis

In our previous work[12] we employed a free radical polymerization of commercially available 2,2,6,6-tetramethylpiperidin-4-yl-methacrylate (**1**) for the synthesis of precursor polymer **2a** (see Scheme 1, route 1).[14] 2-Mercaptoethanol was used as a modifier to lower the molar mass, to reduce the dispersity, and ultimately to guarantee sufficient solubility for electrochemical studies. A subsequent two-step oxidation with H_2O_2/Na_2WO_4 (step 1) and MCPBA (step 2) yielded the desired TEMPO-modified polymer HP-2 with a mass average molecular weight (M_w) of 2.74 kDa.[15] A simple experimental procedure and good

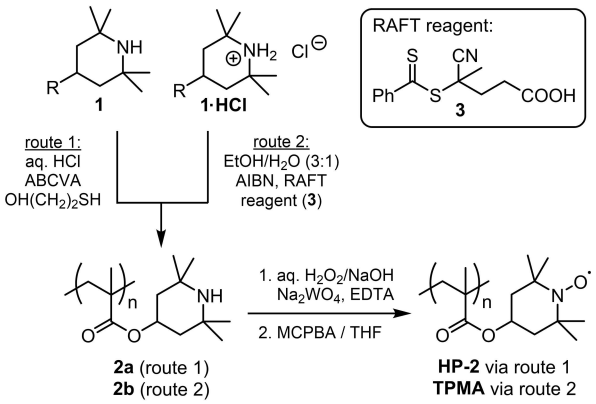

Scheme 1. Preparation of **HP-1** and **TPMA** from monomer **1** (R = methacryloxy).

scalability are among the advantages of the method. However, the method features only a limited control over the length of the polymer chain, which is reflected by a relatively high dispersity ($Đ = 1.89$).

For the present study, we intended to reduce the dispersity to exclude possible influences of large molar mass differences. We achieved this goal by RAFT polymerization[16] of hydrochloride **1·HCl** using dithioester **3** as a chain transfer reagent (route 2). This approach, followed by oxidation of intermediate **2b** using the abovementioned two-step protocol, rendered the TEMPO-modified polymethacrylate (TPMA) in 87% yield with a higher molecular weight ($M_w = 4.67$ kDa) compared to HP-2 and to our delight, a much smaller dispersity ($Đ = 1.29$).[17] UV vis spectroscopic analysis indicates that intermediate **2b** contains intact thiobenzoylthio end groups, which are removed during conversion to TPMA. Cleavage under these reaction conditions is also in agreement with literature reports on the stability of thiobenzoylthio moieties.[18] Further details regarding synthesis and characterization are summarized in the supporting information (SI).

1.2. Redox Behavior Under Non-Catalytic Conditions

For the electrochemical characterization of TPMA, cyclic voltammetry (CV) was carried out in a 0.1 M solution of NBu_4ClO_4 in CH_3CN/H_2O (8:1 vol/vol) using a glassy carbon working electrode and a Ag/0.01 M $AgNO_3$ reference electrode ($E_0 = -87$ mV vs. Fc/Fc^+ couple).[19] The polymer content was adjusted to a concentration of TEMPO units (c_{TU}) of 5 mM.[20] To contrast the voltammetric behavior of TPMA against other *N*-oxyl radicals, we chose TEMPO as well as 4-acetoxy-TEMPO (ACT, Figure 2, top) for our studies. The CVs recorded at $v = 100$ mV s^{-1} are shown in Figure 2 (bottom, for extracted parameters see Table 1). For each species, the scan reveals a single reversible redox couple ($R_2N{-}O^{\bullet}/R_2N{=}O^+$) with a typical diffusive profile. With respect to TPMA, this is well worth mentioning, as it suggests that there is no significant electronic coupling between the TEMPO motifs across the polymer chain,

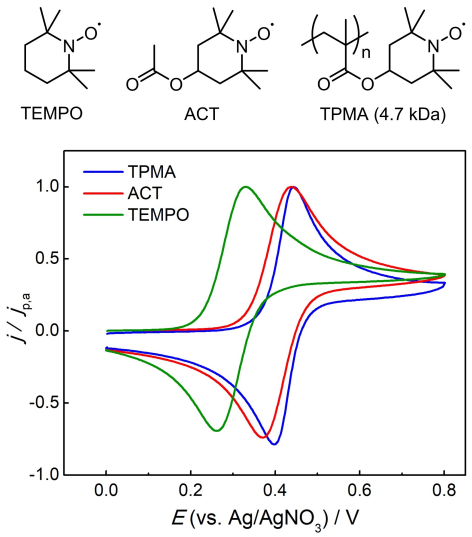

Figure 2. Top: Structures of the investigated mediators. Bottom: Background-corrected cyclic voltammetry (CV) of TEMPO, 4-acetoxy-TEMPO (ACT) and TEMPO-modified polymethacrylate (TPMA) normalized vs. the anodic peak current density $j_{p,a}$. Conditions: 0.1 M NBu_4ClO_4 in acetonitrile/water (8:1), c_{TU} = 5 mM, v = 100 mV s^{-1}.

Table 1. Summary of equilibrium redox potentials E_0, peak-to-peak separations ΔE_p, anodic peak current densities $j_{p,a}$, and peak current ratios $|j_{p,c}/j_{p,a}|$ obtained from the CVs shown in Figure 2 (bottom).

Compound	E_0 [V]	ΔE_p [mV]	$j_{p,a}$ [mA cm^{-2}]	$\lvert j_{p,c}/j_{p,a}\rvert$
TEMPO	0.30	69	1.94	1.0
ACT	0.40	67	1.73	1.0
TPMA	0.42	46	0.74	1.0

and that the redox characteristics at 100 mV s^{-1} are essentially the same as those displayed by the monomer.[21]

For TPMA (blue line), the redox couple is centered around E_0 = 0.42 V with an anodic shift of 120 mV compared to free TEMPO (green line). The shift can be assigned to the presence of the acyloxy linker,[22] which is confirmed by comparison to the CV of structurally similar ACT (red line, E_0 = 0.40 V). There are also significant differences between the peak intensities: While ACT and TEMPO show comparable anodic peak current densities ($j_{p,a}$), TPMA achieves only about 40% of these values. The latter indicates that the availability of TEMPO units at the electrode surface is lower, which may be attributed to slower mass transfer (*vide infra*). Full chemical reversibility on the voltammetry timescale is confirmed for TPMA, ACT and TEMPO by calculation of the ratio between the cathodic and the anodic peak current density $|j_{p,c}/j_{p,a}|$ according to the method reported by Nicholson and Shain (for details see the SI).[23]

For TPMA, the presence of only one redox couple and the magnitude of the j_p values suggest that each polymer chain can be oxidized multiple times at the same potential, which is confirmed by a controlled potential coulometry experiment carried out at E = 0.6 V in a divided cell (for details see the SI). The results show that at least 89% of the available TEMPO units are oxidized before the current drops from the initial value of 1.6 mA to the baseline.[24]

Further differences between TPMA and ACT become apparent upon variation of v (Figure 3A and Figure 3B). While ACT exhibits a good linear correlation between $j_{p,a}$ and $v^{0.5}$ in the entire range, indicating a diffusive process,[25] for TPMA this is only the case between 5 and approx. 250 mV s^{-1} (Figure 3E). A possible explanation for the deviation of TPMA above 250 mV s^{-1} is a superposition of adsorptive and diffusive processes, i.e., charge transfer to both dissolved and adsorbed polymer chains. Thus, the square root dependency of j_p at low scan rates would indicate that at long time scales, the majority of the charge is transferred via diffusive processes. As the scan rate increases, the adsorptive fraction of j_p that increases linearly with v[13] would become more pronounced. At this point, the v range dominated by the diffusive process is evaluated first to allow a comparison between the transport properties of the different *N*-oxyl species, while the unusual behavior of TPMA at high v will be discussed in detail below. The diffusion coefficients D were calculated from the slope of j_p versus $v^{0.5}$ from Eq. 1,[25]

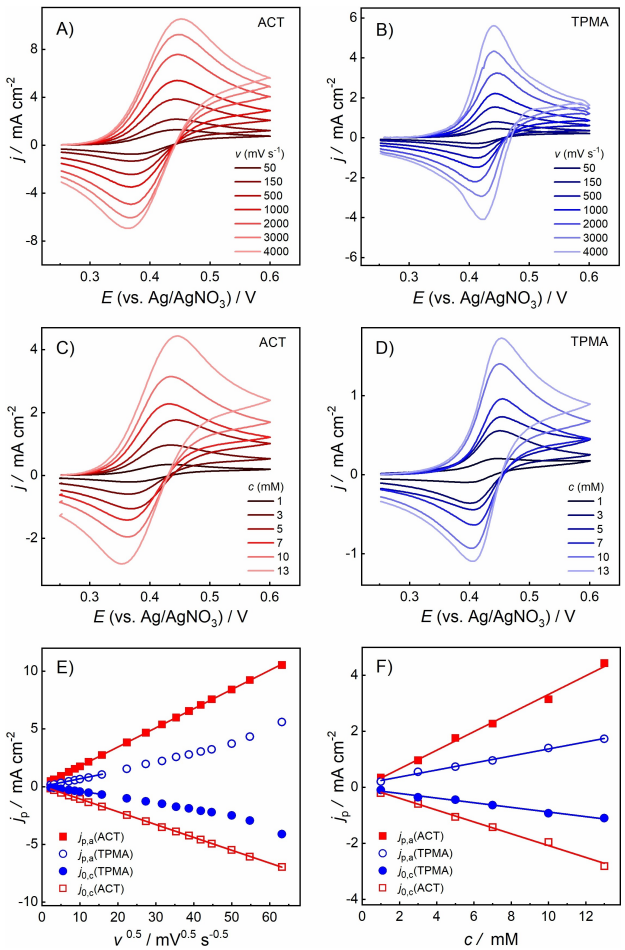

Figure 3. Top: Background-corrected voltammetry of ACT (A) and TPMA (B) at c_{TU} = 5 mM and varying v. Middle: Background-corrected CVs of ACT (C) and TPMA (D) at 100 mV s^{-1} and varying c. Bottom: Comparison between the peak current densities (j_p) of ACT and TPMA at varying v (E) and c_{TU} (F). Electrolyte: 0.1 M NBu_4ClO_4 in acetonitrile/water (8:1).

$$j_P = 0.4463zFc_{TU}\sqrt{\frac{zFvD}{RT}} \quad (1)$$

where z is the number of transferred electrons ($z=1$), F the Faraday constant, R the gas constant, and T the temperature (the other parameters are defined above). The results are summarized in Table 2 and more details are provided in the SI.

For TPMA, only the range between 5 and 250 mV s^{-1} was analyzed, whereas the full range was used for ACT and TEMPO. With $2.35\cdot10^{-6}$ cm^2 s^{-1}, D_{TPMA} is one order of magnitude lower than D_{TEMPO} and approximately seven times smaller than D_{ACT}. The decrease in D follows the pattern predicted by the Stokes-Einstein equation in the sense that diffusion is curbed with increasing molecular size. The same effect is observed upon increasing c_{TU} (Figure 3C and Figure 3D), which also leads to a slower increase of j_p for TPMA as compared to ACT (Figure 3F).

To verify the assumption that adsorption of TPMA causes a deviation of j_p from the square root dependency, another experiment was performed in which CVs were first recorded at $c_{TU}=1$ mM (see Figure 4A, dashed blue line), followed by careful rinsing of the glassy carbon electrode with acetonitrile, transfer to a blank electrolyte solution, and repeated cycling (Figure 4A, solid blue line). At 100 mV s^{-1}, the appearance of a redox couple with weak intensity and without peak-to-peak separation confirms irreversible adsorption of TPMA on the electrode surface. Increasing v leads to well-defined and nearly symmetric features centered around 0.43 V with very small splitting between the oxidative and the reductive peak ($\triangle E_p \leq 10$ mV), which is characteristic for identical and independent redox-active species attached to the electrode surface (Figure 4B).[25] At constant scan rate, the profiles do not significantly change over ten cycles (see Figure S7), indicating a good stability of the TPMA film on the voltammetry time scale. A control experiment in which the electrode was immersed into the TPMA-containing solution without applying a potential, followed by transfer to a blank electrolyte and cycling, gave similar results. This indicates that the adsorption process is not electrochemically induced but more likely due to a mixture of physisorption and low solubility of the polymer. Similar adsorption behavior was previously observed for other soluble redox-active polymers tested for energy storage applications.[26]

Table 2. Summary of the slopes of the linear fits in Figure 3E and the calculated diffusion coefficients D (for analysis of TEMPO see the SI).

Compound	slope [mA s$^{0.5}$ cm^{-2} mV$^{-0.5}$]	D [cm^2 s^{-1}]
TEMPO	0.202	$2.26\cdot10^{-5}$
ACT	0.166	$1.53\cdot10^{-5}$
TPMA	0.065	$2.35\cdot10^{-6}$

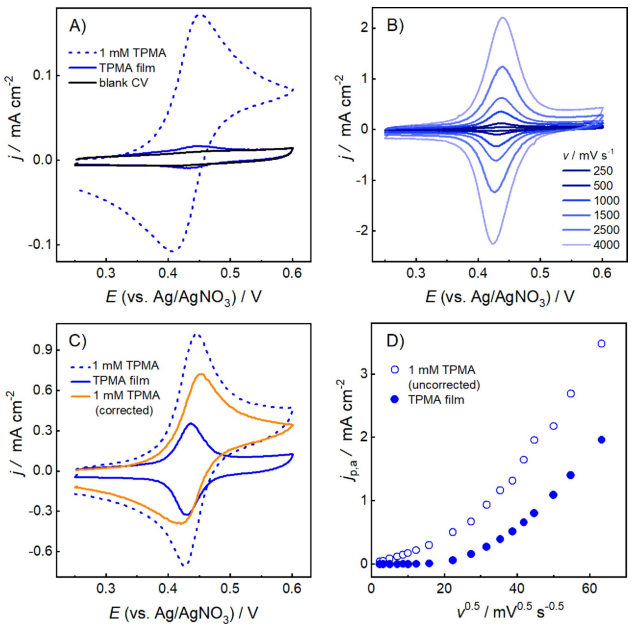

Figure 4. A) CV of 1 mM TPMA (dashed blue line) recorded at 100 mV s^{-1}, repeated scan after replacing the solution with blank electrolyte (solid blue line), and repeated scan after polishing the electrode (solid black line). B) CV of the TPMA film at various scan rates. C) CV of 1 mM TPMA recorded at 1 V s^{-1} (dashed blue line), repeated scan in blank electrolyte (solid blue line), and CV of 1 mM TPMA after subtraction of adsorption contributions (solid orange line). D) Plot of j_p vs. $v^{0.5}$ for 1 mM TPMA (hollow circles) and the TPMA film (filled circles). Electrolyte: 0.1 M NBu_4ClO_4 in acetonitrile/water (8:1).

A comparison between the CVs of 1 mM TPMA and of the TPMA film at 1 V s^{-1} confirms that at higher scan rates, the contribution of the TPMA film to the overall current response becomes more pronounced (Figure 4C), thus underlining the abovementioned responsibility of the adsorptive process for the deviations from the square root dependency. As expected, the deviation also increases with decreasing c_{TU} (compare $c_{TU}=$ 1 mM in Figure 4D with $c_{TU}=5$ mM in Figure 3E).

The key parameters extracted from the film CV recorded at 1 V s^{-1} are summarized in Table 3. Both analysis of the anodic and cathodic peak charges (q_a and q_c) and calculation of the peak current ratio indicates a high chemical reversibility of the adsorbed redox couple ($q_c/q_a=1.03$, $j_{p,c}/j_{p,a}=0.94$). The apparent surface concentration of TEMPO units calculated from q_a corresponds to $\Gamma_{TU}=1.44\cdot10^{-10}$ mol cm^{-2}, which is in the same order of magnitude but well below sterically limited Γ values reported for monolayers of other redox-active molecules (e.g. ferrocene) covalently attached to smooth surfaces.[27] The peak widths at half of the maximum heights ($W_{1/2}$) are significantly smaller than the ideal value of 90 mV.[25]

By subtracting the film voltammogram from the one measured in TPMA solution, a correction for adsorption contributions was attempted (Figure 4C, orange line). The resulting profile exhibits a $\triangle E_p$ of 34 mV. This value is significantly higher than the $\triangle E_p$ of the uncorrected CV (20 mV), but still well below the 57 mV expected for a purely diffusive process. Considering that for other redox-active polymers, e.g.

Table 3. Analysis of the TPMA film CV recorded at $v=1$ V s^{-1} (see Figure 4C).

Peak	E_p [V]	q [10^{-7} C]	j_p [mA cm^{-2}]	$W_{1/2}$ [mV]
anodic	0.44	2.79	0.35	46
cathodic	0.43	2.86	0.33	49

linear chains carrying ferrocene, anthraquinone, or tris (dialkylamino)cyclopropenium units, $\triangle E_p$ values of 60 mV and higher have been reported,[28] the behavior of TPMA is quite unusual. While investigations of the unusual peak-to-peak separation are ongoing, it can already be concluded from the results presented in this section that i) the high molecular weight of TPMA reduces the diffusion-controlled current compared to TEMPO and ACT, ii) TPMA forms a redox-active film by irreversible adsorption on the glassy carbon surface, iii) the voltammetric profiles of TPMA are shaped both by diffusive and adsorptive processes, and iv) the influence of adsorbed TPMA becomes negligible at low v and high c_{TU}.

1.3. Electrocatalytic Studies

We continued our investigations by characterizing the electrocatalytic behavior of TPMA. A comparison between the voltammetric profiles of TPMA, ACT, and TEMPO recorded at 100 mV s^{-1} in the absence and presence of 4-methoxybenzyl alcohol (4-MBA) is depicted in Figure 5. To facilitate alcohol oxidation, *N*-methylimidazole (NMI) was added as a proton scavenger. A separate CV recorded in absence of any mediator confirmed that direct alcohol oxidation does not proceed in the studied potential regime (see Figure S24). Interestingly, the catalytic peak current density (j_{cat}) for TPMA is slightly higher than for TEMPO, but well below the value of ACT. Moreover, the ratio j_{cat}/j_p that reflects the rate of the homogeneous reaction, is significantly higher for TPMA (9.6) as compared to TEMPO (2.5). In our previous work,[12] we attributed this observation to the electron-withdrawing acyloxy linker in position 4 of the piperidinyl ring, the resulting increase of the redox potential and thereby to a higher driving force for alcohol oxidation. This conjecture is supported by the similar magnitude of the j_{cat}/j_p values of TPMA and ACT (9.6 and 7.8), which would also be in line with a previous report by Rafiee, Stahl et al. that highlights the strong influence of the redox potential on the electrocatalytic activity of *N*-oxyl radicals.[22]

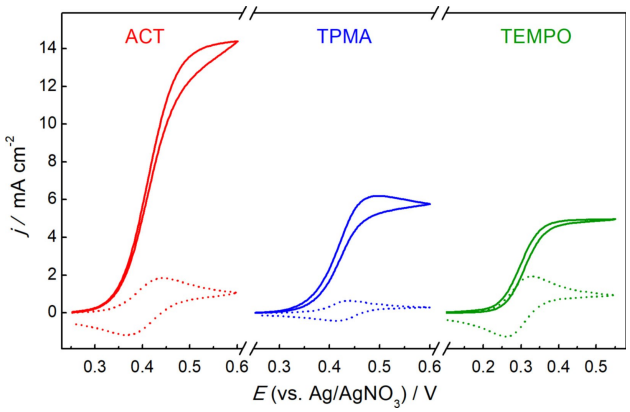

Figure 5. Comparison between background-corrected CVs of ACT (left), TPMA (middle), and TEMPO (right) under non-catalytic and catalytic conditions (c_{TU} = 5 mM, v = 100 mV s^{-1}). Electrolyte: 0.1 M NBu_4ClO_4 in acetonitrile/water (8 : 1). Substrate: 0.1 M 4-methoxybenzyl alcohol (4-MBA). Base: 0.45 M NMI.

For a quantitative treatment of the kinetics of the catalytic process, v was systematically increased to achieve "no substrate consumption – pure kinetic conditions"[29,30] with S-shaped voltammetric profiles (for details see the SI). For homogeneous electrocatalysts, the corresponding plateau current densities (j_{max}) are given by Eq. 2,

$$j_{max} = zFc_{TU}\sqrt{nDk_{cat}c_{sub}} \quad (2)$$

where k_{cat} is the homogeneous rate constant, n the number of catalyst units required per turnover, and c_{sub} the substrate concentration (the other parameters are defined above). A comparison between the catalytic responses of ACT and TPMA is shown in Figure 6A and B. Linear correlations between j_{max} and c_{TU} as well as between j_{max} and $\sqrt{c_{sub}}$ (Figure 6C and D) suggests that *i*) the TPMA-catalyzed process is at least to a large extent a homogeneous one,[31] *ii*) ACT- and TPMA-catalyzed alcohol oxidation is first order both in catalyst and substrate, and *iii*), ACT renders higher j_{max} values over the entire v and c regimes.

The homogeneous rate constants k_{cat} calculated from the j_{max} values (for details see the SI) amount to 397 L mol^{-1} s^{-1} for TPMA and 330 L mol^{-1} s^{-1} for ACT. In comparison, the value for TEMPO (24 L mol^{-1} s^{-1}) turns out to be much lower, confirming that the homogeneous rate of alcohol oxidation is determined by the redox potential of the TEMPO unit rather than by its attachment to the polymer backbone. To generalize the comparison between the polymediator and the low-molecular weight benchmark systems, the catalytic study was extended to 5-(hydroxymethyl)furfural (HMF), glycerol, methanol and prop-

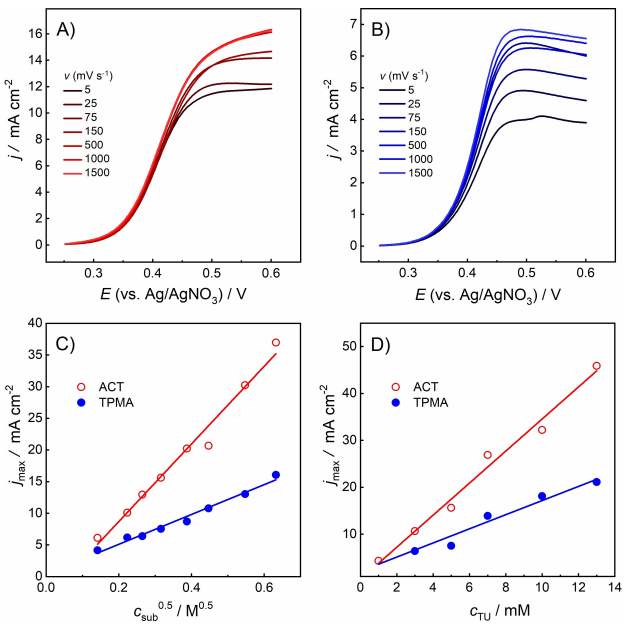

Figure 6. Top: Background-corrected catalytic profiles of 5 mM ACT (A) and 5 mM TPMA (B) in presence of 0.1 M 4-MBA and 0.45 M *N*-methylimidazole (NMI) at varying scan rates. Bottom: Comparison between the achievable j_{max} values of ACT and TPMA at varying substrate concentrations (C) and varying concentrations of TEMPO units (D). Electrolyte: 0.1 M NBu_4ClO_4 in acetonitrile/water (8 : 1).

an-2-ol (see Figure 7 and the SI). In all of these cases, ACT and TPMA exhibit similar rate constants, whereas TEMPO shows comparatively low k_{cat} values (Figure 7B).

Considering the similarity between ACT and TPMA, the impression that the homogeneous kinetics are not strongly affected by the active centers being attached to the polymer backbone thus seems to be strengthened. In other words, the TEMPO units on the polymer appear to be well accessible for the substrate and thus available for catalysis. Furthermore, it is worth mentioning that in the cases of 4-MBA, HMF, methanol and glycerol, despite the much lower diffusion coefficient, the j_{max} values of TPMA are significantly higher than the ones of TEMPO. Thus, in these cases, the higher driving force trumps the curbed mediator transport, leading to more efficient overall kinetics.

2. Conclusions

In the present study, progress was made in understanding the redox behavior and catalytic activity of TEMPO-modified polymethacrylates in view of their application as mediators in electrosynthesis. It was found that the polymer tends to irreversibly adsorb on glassy carbon, thus forming a redox-active layer on the electrode surface. These layers have a pronounced influence on the voltammetric profiles at high scan rates and low mediator concentrations. Electrocatalytic studies at varying concentrations of alcohol substrate and TEMPO units suggest that TPMA-catalyzed alcohol oxidation is a predominantly homogeneous process.

Although TPMA shows significantly slower diffusive behavior compared to TEMPO and ACT, the catalytic current densities achievable with the polymer are intermediate between those of the two low molecular weight mediators for the majority of substrates. Since the homogeneous rate constants of TPMA and ACT resemble each other, being well above the ones of TEMPO for the tested substrates, it can be concluded that the redox potential of the *N*-oxyl unit has a more pronounced effect on the rate of the homogeneous reaction than the active centers being attached to the polymer backbone. This means that curbed mass transfer can be compensated by tuning the redox potential of the catalyst unit, which should be considered as an important design principle for the development of new polymediator generations. Tuning the molecular weight distribution may represent a further possibility for optimization of the overall reaction rate, which is currently under investigation in our laboratory.

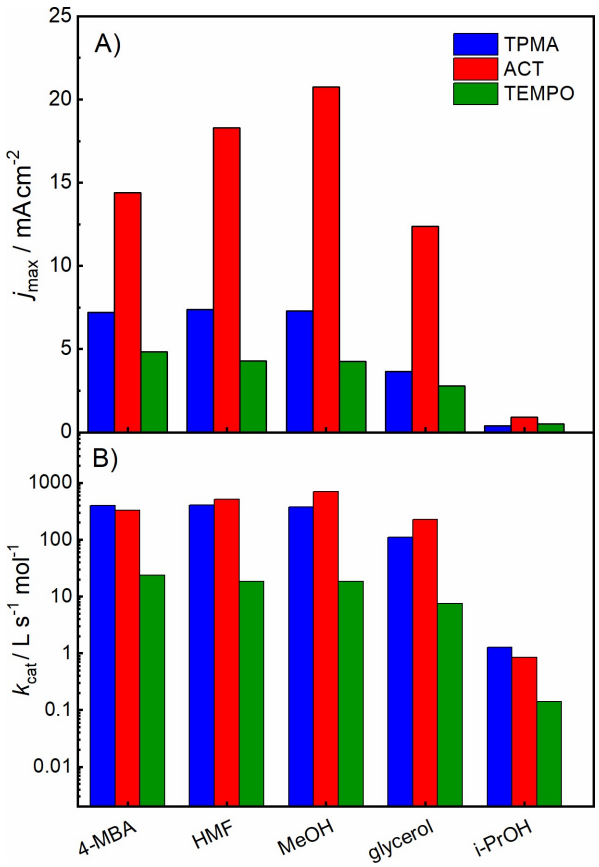

Figure 7. Comparison between the catalytic activities of TPMA, ACT and TEMPO for various substrates. Top: Plateau current densities (j_{max}) achieved under "no substrate consumption – pure kinetic conditions" (c_{TU} = 5 mM, c_{sub} = 0.1 M). Bottom: Rate constants k_{cat} calculated from the j_{max} values.

Acknowledgements

This work has been funded by the German Research Foundation (DFG, project no. FR 3848/2-1). The author is grateful for funding by the DFG Heisenberg Program (FR 3848/4-1). Furthermore, we thank Alina Heckel and Dr. Lutz Nuhn from the Max Planck Institute for Polymer Research (Mainz, Germany) for their helpful support in polymer characterization by size exclusive chromatography. Open Access funding enabled and organized by Projekt DEAL.

Conflict of Interest

The authors declare no conflict of interest.

Keywords: electrosynthesis · electrocatalysis · mediator · TEMPO · polymer

[1] E. Steckhan, *Angew. Chem. Int. Ed. Engl.* **1986**, *25*, 683.
[2] R. Francke, R. D. Little, *Chem. Soc. Rev.* **2014**, *43*, 2492.
[3] a) L. Ackermann, *Acc. Chem. Res.* **2020**, *53*, 84; b) J. C. Siu, N. Fu, S. Lin, *Acc. Chem. Res.* **2020**, *53*, 547; c) C. Ma, P. Fang, T.-S. Mei, *ACS Catal.* **2018**, *8*, 7179; d) J. Strehl, G. Hilt, *Org. Lett.* **2019**, *21*, 5259; e) S. Tang, D. Wang, Y. Liu, L. Zeng, A. Lei, *Nat. Commun.* **2018**, *9*, 798; f) B. R. Walker, S. Manabe, A. T. Brusoe, C. S. Sevov, *J. Am. Chem. Soc.* **2021**, *143*, 6257.
[4] a) P. Qian, Z. Zha, Z. Wang, *ChemElectroChem* **2020**, *7*, 2527–2544; b) Y. N. Ogibin, M. N. Elinson, G. I. Nikishin, *Russ. Chem. Rev.* **2009**, *78*, 89.
[5] a) C.-Y. Cai, X.-M. Shu, H.-C. Xu, *Nat. Commun.* **2019**, *10*, 4953; b) N.-n. Lu, N.-t. Zhang, C.-C. Zeng, L.-M. Hu, S. J. Yoo, R. D. Little, *J. Org. Chem.* **2015**, *80*, 781; c) Y. S. Park, R. D. Little, *J. Org. Chem.* **2008**, *73*, 6807.
[6] a) M. Elsherbini, T. Wirth, *Chem. Eur. J.* **2018**, *24*, 13399; b) R. Francke, *Curr. Opin. Electrochem.* **2019**, *15*, 83; c) R. Francke, *Curr. Opin. Electrochem.* **2021**, *28*, 100719.

[7] a) A. Das, S. S. Stahl, *Angew. Chem. Int. Ed.* **2017**, *56*, 8892; b) M. Rafiee, Z. M. Konz, M. D. Graaf, H. F. Koolman, S. S. Stahl, *ACS Catal.* **2018**, *8*, 6738; c) J. E. Nutting, M. Rafiee, S. S. Stahl, *Chem. Rev.* **2018**, *118*, 4834; d) H.-B. Zhao, P. Xu, J. Song, H.-C. Xu, *Angew. Chem. Int. Ed.* **2018**, *57*, 15153; e) D. P. Hickey, D. A. Schiedler, I. Matanovic, P. V. Doan, P. Atanassov, S. D. Minteer, M. S. Sigman, *J. Am. Chem. Soc.* **2015**, *137*, 16179.
[8] R. Francke, *Chimia* **2020**, *74*, 49.
[9] a) T. Sawamura, S. Kuribayashi, S. Inagi, T. Fuchigami, *Org. Lett.* **2010**, *12*, 644; b) T. Broese, R. Francke, *Org. Lett.* **2016**, *18*, 5896; c) O. Koleda, T. Broese, J. Noetzel, M. Roemelt, E. Suna, R. Francke, *J. Org. Chem.* **2017**, *82*, 11669; d) A. F. Roesel, T. Broese, M. Májek, R. Francke, *ChemElectroChem* **2019**, *6*, 4229.
[10] T. Sawamura, S. Kuribayashi, S. Inagi, T. Fuchigami, *Adv. Synth. Catal.* **2010**, *352*, 2757.
[11] a) H. Tanaka, J. Chou, M. Mine, M. Kuroboshi, *Bull. Chem. Soc. Jpn.* **2004**, *77*, 1745; b) M. Kuroboshi, K. Goto, H. Tanaka, *Synthesis* **2009**, 903.
[12] B. Schille, N. O. Giltzau, R. Francke, *Angew. Chem. Int. Ed.* **2018**, *57*, 422.
[13] J. Wang, Analytical Electrochemistry (3rd Edition), Wiley-VCH, **2006**.
[14] a) For the synthesis of HP-2, a modified procedure from Ref. [14b] was used; b) T. Janoschka, N. Martin, U. Martin, C. Friebe, S. Morgenstern, H. Hiller, M. D. Hager, U. S. Schubert, *Nature* **2015**, *527*, 78.
[15] During conversion of **2** to the TEMPO-modified polymethacrylate, the intermediate precipitates from the aqueous solution prior to complete oxidation. Therefore, the solid is filtered off and dissolved in THF, where the conversion is brought to completion in presence of MCPBA.
[16] T. Janoschka, A. Teichler, A. Krieg, M. D. Hager, U. S. Schubert, *J. Polym. Sci. Part A* **2012**, *50*, 1394.
[17] Direct comparison between the M_w values of HP-2 from Ref. [12] and TPMA is difficult, since different SEC systems and standards were used for SEC measurements.
[18] a) C. P. Jesson, C. M. Pearce, H. Simon, A. Werner, V. J. Cunningham, J. R. Lovett, M. J. Smallridge, N. J. Warren, S. P. Armes, *Macromolecules* **2017**, *50*, 182; b) D. B. Thomas, A. J. Convertine, R. D. Hester, A. B. Lowe, C. L. McCormick, *Macromolecules* **2004**, *37*, 1735.
[19] V. V. Pavlishchuk, A. W. Addison, *Inorg. Chim. Acta* **2000**, *298*, 97.
[20] It should be noted that for the calculation of c_{TU}, the end groups on the polymer chains could not be taken into account, potentially leading to an overestimation of the actual concentration. However, in view of the relatively high molecular weight of TPMA, we assume that this effect is rather small.
[21] R. F. Winter, *Organometallics* **2014**, *33*, 4517.
[22] M. Rafiee, K. C. Miles, S. S. Stahl, *J. Am. Chem. Soc.* **2015**, *137*, 14751.
[23] R. S. Nicholson, I. Shain, *Anal. Chem.* **1964**, *36*, 706.
[24] A slight underestimation of the transferred charge equivalents may result from an overestimation of c_{TU} (see Ref. [20]).
[25] A. J. Bard, L. R. Faulkner, *Electrochemical Methods. Fundamentals and Applications*, Wiley, New York, **2001**.
[26] a) G. Nagarjuna, J. Hui, K. J. Cheng, T. Lichtenstein, M. Shen, J. S. Moore, J. Rodríguez-López, *J. Am. Chem. Soc.* **2014**, *136*, 16309; b) E. C. Montoto, Y. Cao, K. Hernández-Burgos, C. S. Sevov, M. N. Braten, Brett A. Helms, J. S. Moore, J. Rodríguez-López, *Macromolecules* **2018**, *51*, 3539; c) M. Yuan, S. D. Minteer, *Curr. Opin. Electrochem.* **2019**, *14*, 1.
[27] a) B. M. Johnson, R. Francke, R. D. Little, L. A. Berben, *Chem. Sci.* **2017**, *8*, 6493; b) M. A. Pellow, T. D. P. Stack, C. E. D. Chidsey, *Langmuir* **2013**, *29*, 5383; c) M. V. Sheridan, K. Lam, W. E. Geiger, *Angew. Chem. Int. Ed.* **2013**, *52*, 12897.
[28] a) J. B. Flanagan, S. Margel, A. J. Bard, F. C. Anson, *J. Am. Chem. Soc.* **1978**, *100*, 4248; b) B. L. Funt, P. M. Hoang, *J. Electrochem. Soc.* **1984**, *131*, 2295; c) K. H. Hendriks, S. G. Robinson, M. N. Braten, C. S. Sevov, B. A. Helms, M. S. Sigman, S. D. Minteer, M. S. Sanford, *ACS Cent. Sci.* **2018**, *4*, 189.
[29] J.-M. Savéant, *Chem. Rev.* **2008**, *108*, 2348.
[30] J.-M. Savéant, K. B. Su, *J. Electroanal. Chem.* **1984**, *171*, 341.
[31] a) For substrate conversion at active centers attached to the electrode surface, a linear dependency of j_{max} on c_{sub} is expected (see Ref. [25] and Ref. [31b]); b) C. Costentin, J.-M. Savéant, *J. Phys. Chem. C* **2015**, *119*, 12174.

Manuscript received: June 4, 2021
Revised manuscript received: June 23, 2021
Accepted manuscript online: June 25, 2021

Publication II

TEMPO-Modified Polymethacrylates as Mediators in Electrosynthesis: Influence of the Molecular Weight on Redox Properties and Electrocatalytic Activity

Adrian Prudlik (60%), Nayereh Mohebbati (20%), Laura Hildebrandt (5%), Alina Heck (5%), Lutz Nuhn (5%), and Robert Francke (5%).

DOI: 10.1002/chem.202202730

Abstract: Homogeneous catalysts (“mediators”) are frequently employed in organic electrosynthesis to control selectivity. Despite their advantages, they can have a negative influence on the overall energy and mass balance if used only once or recycled inefficiently. Polymediators are soluble redox-active polymers applicable as electrocatalysts, enabling recovery by dialysis or membrane filtration. Using anodic alcohol oxidation as an example, we have demonstrated that TEMPO-modified polymethacrylates (TPMA) can act as efficient and recyclable catalysts. In the present work, the influence of the molecular size on the redox properties and the catalytic activity was carefully elaborated using a series of TPMAs with well-defined molecular weight distributions. Cyclic voltammetry studies show that the polymer chain length has a pronounced impact on the key-properties. Together with preparative-scale electrolysis experiments, an optimum size range was identified for polymediator-guided sustainable reaction control.

My Contribution (20%):

I synthesized all the samples of TPMA with well-defined molecular weight and low molecular weight distribution and carried out their respective materials characterization. A. Prudlik (60%) was in charge of the entire electrochemical analysis and calculations together with L. Hildebrandt (5%) as the assigned bachelor student. A. Heck (5%) and L. Nuhn (5%) carried out the measurements for size exclusion chromatography (SEC) for determination of molecular weights for TPMA samples. R. Francke (5%) supervised the project and revised the manuscript.

Chemistry Europe
European Chemical Societies Publishing

WILEY VCH

Excellence in Chemistry Research

Announcing our new flagship journal

- Gold Open Access
- Publishing charges waived
- Preprints welcome
- Edited by active scientists

Meet the Editors of *ChemistryEurope*

Luisa De Cola
Università degli Studi di Milano Statale, Italy

Ive Hermans
University of Wisconsin-Madison, USA

Ken Tanaka
Tokyo Institute of Technology, Japan

Chemistry–A European Journal
Research Article
doi.org/10.1002/chem.202202730
Chemistry Europe
European Chemical Societies Publishing
www.chemeurj.org

TEMPO-Modified Polymethacrylates as Mediators in Electrosynthesis: Influence of the Molecular Weight on Redox Properties and Electrocatalytic Activity

Adrian Prudlik,[a, b] Nayereh Mohebbati,[a, b] Laura Hildebrandt,[a] Alina Heck,[c, d] Lutz Nuhn,[c, d] and Robert Francke*[a, b]

Abstract: Homogeneous catalysts ("mediators") are frequently employed in organic electrosynthesis to control selectivity. Despite their advantages, they can have a negative influence on the overall energy and mass balance if used only once or recycled inefficiently. Polymediators are soluble redox-active polymers applicable as electrocatalysts, enabling recovery by dialysis or membrane filtration. Using anodic alcohol oxidation as an example, we have demonstrated that TEMPO-modified polymethacrylates (TPMA) can act as efficient and recyclable catalysts. In the present work, the influence of the molecular size on the redox properties and the catalytic activity was carefully elaborated using a series of TPMAs with well-defined molecular weight distributions. Cyclic voltammetry studies show that the polymer chain length has a pronounced impact on the key-properties. Together with preparative-scale electrolysis experiments, an optimum size range was identified for polymediator-guided sustainable reaction control.

Introduction

Indirect electrolysis using redox mediators is a frequently used approach toward controlling selectivity and reducing energy consumption of electro-organic transformations.[1] To address a multitude of synthetic problems, a well-established portfolio of mediators is available including organometallic compounds,[2] metal ions,[3] halides,[4] triarylamines,[5] iodoarenes,[6] and *N*-oxyl radicals.[7] Although the benefits of mediators are undisputed, they may be offset by more difficult separation procedures, increasing waste generation, and additional expenses, which is why concepts to facilitate separation and recycling deserve more attention.[8] The same applies to supporting electrolyte additives, which have to be removed by additional purification steps after completed reaction and, if not recycled, constitute a further source of waste.

The main challenge in recovering mediators from reaction mixtures is the similarity to the product in terms of polarity and molecular size. For example, column chromatography is required for separation of organic mediators such as iodoarenes or 2,2,6,6-tetramethylpiperidinyl-1-oxyl (TEMPO). In this regard, changing the polarity of the mediator by tethering charged groups ("ionic tags") has proven to be a promising approach that enables recovery by extraction while obviating the need for supporting electrolyte additives.[9] Further investigations focused on immobilization of mediators or supporting electrolytes on particles for electrolysis to be carried out in the dispersed phase.[10,11] While this approach allows for recovery by filtration or centrifugation, it is associated with drawbacks such as poor ionic conductivity and difficult electron transfer between electrode and immobilized mediator, respectively. Noteworthy, activation of mediators that are attached to suspended particles requires a homogeneous co-mediator,[10e,f] partially nullifying the benefits achieved by immobilization.

In view of the difficulties caused by the dispersed-phase approach, the installment of mediators on soluble polymer backbones is an interesting alternative, since the resulting polymediators can act as classic homogeneous electrocatalysts that are activated at the electrode surface and react with the substrates in solution. Simultaneously, the increased molecular size allows the use of size exclusion membrane processes for mediator recovery (i.e., dialysis and ultra-/nanofiltration).

Based on the TEMPO-catalyzed anodic alcohol oxidation, we have shown for the first time that indirect electro-organic reactions can efficiently be coupled to dialysis and ultrafiltration

[a] *A. Prudlik, N. Mohebbati, L. Hildebrandt, Prof. Dr. R. Francke*
Leibniz Institute for Catalysis
Albert-Einstein-Str. 29a, 18059 Rostock (Germany)
E-mail: Robert.francke@catalysis.de
[b] *A. Prudlik, N. Mohebbati, Prof. Dr. R. Francke*
Institute of Chemistry
Rostock University
Albert-Einstein-Str. 3a, 18059 Rostock (Germany)
[c] *A. Heck, Prof. Dr. L. Nuhn*
Max Planck Institute for Polymer Research
Ackermannweg 10, 55128 Mainz (Germany)
[d] *A. Heck, Prof. Dr. L. Nuhn*
Chair of Macromolecular Chemistry
Faculty of Chemistry and Pharmacy
Julius-Maximilians-Universität Würzburg
Röntgenring 11, 97070 Würzburg (Germany)

Supporting information for this article is available on the WWW under https://doi.org/10.1002/chem.202202730

when polymediators are employed (Figure 1A–C).[12] Trialkylammonium- and TEMPO-modified polymethacrylates (PTE and TPMA, Figure 1B), which can both be easily prepared on a decagram scale by free radical polymerization, served as polymediators and polyelectrolytes, respectively. The resulting polymer solutions turned out to be sufficiently conductive and exhibited a high electrocatalytic activity toward conversion of various alcohols to the corresponding carbonyl compounds. Recycling tests showed that the polymer solution can be reused multiple times.

In a subsequent electroanalytical study,[13] progress was made in understanding the redox behavior and catalytic activity of TEMPO-modified polymethacrylates using a sample with a number average molecular weight (M_n) of 3.6 kDa and a dispersity ($Đ$) of 1.29 (3.6-TPMA). First, it was found that the polymer adsorbs on the carbon electrode surface, which strongly influences the voltammetric profiles at low mediator concentration and at high scan rates. However, the linear relationship between catalytic current and concentration of TEMPO units suggested that under electrolysis conditions, TPMA-catalyzed alcohol conversion is predominantly a homogeneous process despite polymer adsorption. Second, TPMA shows a significantly slower diffusion rate compared to low molecular *N*-oxyls such as TEMPO and 4-acetoxy-TEMPO (ACT). Third, on average, the achievable catalytic current densities j_{max} are intermediate between those of TEMPO and ACT despite the smaller diffusion coefficient. The homogeneous rate constants k_{cat} of TPMA and ACT that were extracted from j_{max} for five tested substrates are similar to each other and exceed the ones of TEMPO. This suggests *i*) that the redox potential of the mediator unit has a stronger impact on the homogeneous rates than steric effects of the polymer backbone and *ii*), that curbed mass transfer can in part be compensated by tuning the redox potential of the catalyst unit.

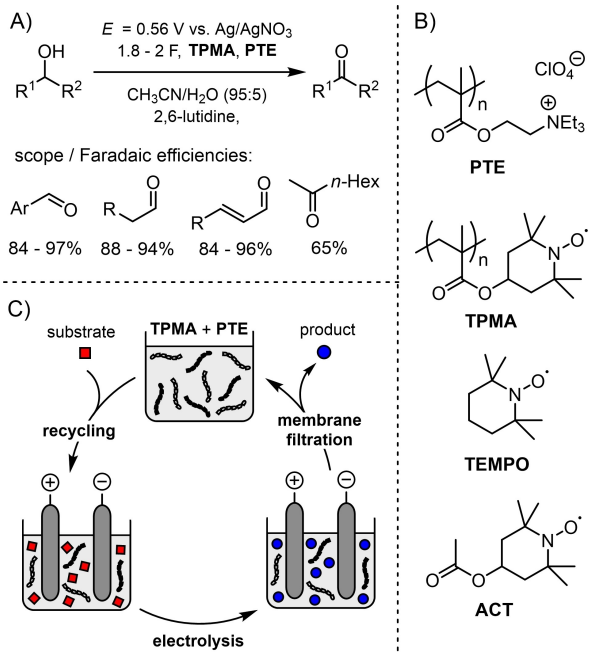

Figure 1. Concept of indirect electrolysis using polymediators and polyelectrolytes.[12,13] A) Preparative-scale anodic oxidation of alcohols using polymediators (TPMA) and polyelectrolytes (PTE).[12] B) Polyelectrolyte and *N*-oxyls under investigation in previous works. C) Schematic illustration of the electrolysis and recycling procedure.

As mentioned above, the results provided by the previous electroanalytical study were obtained from a single TPMA sample with a defined M_n distribution, whereby the relationship between the molecular weight and the electrocatalytic properties thus far remained unknown. Exploring this issue is of great importance, since the molecular weight seems to exert a significant impact on the catalysts diffusion, which is why an impact on the catalytic rate can be expected. Thus, from an electrocatalytic point of view, polymediators with rather small molecular weights appear to be advantageous, whereas larger polymers are desirable with respect to their recovery using size exclusion membranes. In view of these two opposing trends, optimization of the molecular weight appears to be of great importance to find a reasonable compromise between catalytic rates and recyclability. However, no study is yet available on the relationship between the molecular weights of polymediators and their electrocatalytic properties. In general, little is known to date about the influence of molecular size on the behavior of redox-active polymers, even though there is currently a high interest in these materials from further ends, for example in the fields of bioelectrochemistry[14] and electrochemical energy storage.[15] In a seminal work by Bard et al., the influence of the molecular weight on the electrochemical properties of dissolved poly(vinylferrocene) samples was investigated.[16] Later, Rodríguez et al. characterized soluble viologen-modified polystyrenes with varying chain lengths with respect to their redox activity and transport through porous membranes for potential application in redox flow batteries.[17] TPMAs with varying molecular weights have also been systematically characterized, however, thus far exclusively in the solid state as part of composite electrodes with regard to applications in organic radical batteries.[18] Given the limited available knowledge, we have carried out a detailed analysis of the relationship between the key-properties of TPMA-based polymediators and their molecular size, the results of which are presented herein.

Results and Discussion

In our initial feasibility study,[12] TPMA was synthesized via a free radical polymerization of commercially available 2,2,6,6-tetramethylpiperidin-4-yl-methacrylate (**1**), followed by oxidative conversion of the piperidinyl units into *N*-oxyl radicals. The polymerization step involved 2-mercaptoethanol as a modifier, resulting in an M_n value of 1.45 kDa after the oxidation step.[19] In terms of reaction conditions, this approach is very robust, easy to perform, and well scalable. However, it provides only limited control over the length of the polymer chain, which is reflected by a broad molar mass distribution ($Đ = 1.89$). For our subsequent investigation,[13] the dispersity was reduced by RAFT polymerization[20] to exclude possible influences of large molecular weight differences ($M_n = 3.6$ kDa, $Đ = 1.29$). The same

approach has been used in this work to adjust the molecular weights properly (see Scheme 1).

Polymerization of hydrochloride **1·HCl** was achieved using AIBN as a radical starter and dithioester **2** as a chain transfer reagent, followed by oxidation of the resulting intermediate PTM·HCl to yield the desired TPMAs. Since during oxidation with $H_2O_2/NaWO_4$ under alkaline conditions, the intermediate precipitated prior to complete oxidation, the solid was filtered off and dissolved in THF, where the conversion was brought to completion by addition of mCPBA. UV-vis spectroscopic studies confirmed that PTM·HCl initially contains intact thiobenzoylthio end groups, which are cleaved off during reaction to TPMA.[13] End group removal under alkaline and oxidative conditions is also in agreement with literature reports on the stability of thiobenzoylthio moieties.[21] Further details on preparation, purification, and characterization of the polymers are provided in the Supporting Information.

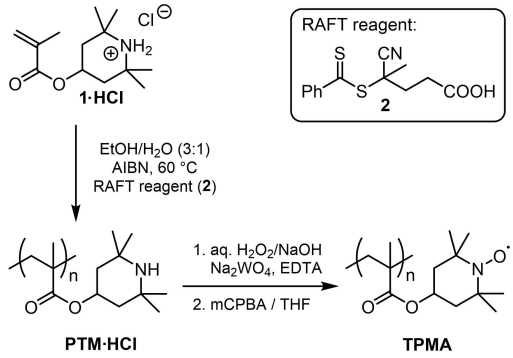

Scheme 1. Preparation of TPMA from monomer **1·HCl**.

Table 1. Results of the two-step polymer syntheses shown in Scheme 1.

Polymer sample	**2** [mol-%]	M_n [kDa]	$Đ$
2.5-TPMA	3.89	2.5	1.16
3.6-TPMA	1.57	3.6	1.30
11.5-TPMA	1.40	11.5	1.38
14.9-TPMA	1.24	14.9	1.45
15.0-TPMA	0.93	15.0	1.32
16.0-TPMA	1.09	16.0	1.44
19.6-TPMA	0.62	19.6	1.31
26.6-TPMA	0.83	26.6	1.25
30.0-TPMA	0.32	30.0	1.30
30.8-TPMA	0.46	30.8	1.29
62.0-TPMA	0.18	62.0	1.26
71.3-TPMA	0.24	71.3	1.26
94.3-TPMA	0.12	94.3	1.34
111.3-TPMA	0.03	111.3	1.99
126.0-TPMA	0.06	126.0	1.68

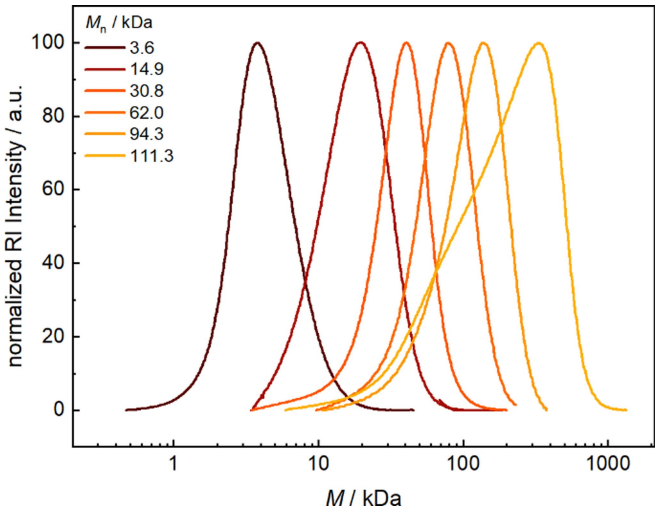

Figure 2. Molecular weight distributions of representative TPMAs (for a complete overview, see the Supporting Information).

The molar mass of the polymers was adjusted by varying the ratio between monomer and chain transfer agent, obtaining a total of 15 samples with M_n values ranging from 2.5 to 126.0 kDa (see Table 1) in isolated yields between 48% and 94% calculated with respect to **1·HCl**. All TPMA samples exhibited a monomodal molecular weight distribution as illustrated by the examples of Figure 2. While the $Đ$ values range from 1.16 to 1.45 for the TPMAs with $M_n < 111.3$ kDa, the two samples with highest M_n provided increased dispersities. The latter is expectable, since low concentrations of RAFT reagents frequently result in a decreased control over radical polymerization.

The electrochemical properties of the TPMA samples were studied by cyclic voltammetry (CV) using a glassy carbon working electrode and a Ag/0.01 M $AgNO_3$ reference electrode ($E_0 = -87$ mV vs. Fc/Fc^+ couple).[22] A 0.1 M solution of NBu_4ClO_4 in a mixture of CH_3CN and water (8:1 vol/vol) served as the electrolyte, in which the polymer content was adjusted to an effective concentration of polymer units (c_{TU}) of 5 mM. To allow a comparison between the TPMAs and low-molecular-weight TEMPO species, 4-acetoxy TEMPO (ACT) and a TEMPO dimer (BTM, see Figure 3A) were subjected to the same analysis. The CVs of ACT, BTM, and four representative polymers (3.6-, 15.0-, 30.8-, and 126.0-TMPA) recorded at 100 mV s^{-1} are shown in Figure 3(B) (key-parameters are summarized in Table 2). Each species exhibits a single reversible redox couple ($R_2N–O^•/R_2N=O^+$), which suggests that there is no significant electronic interaction between the TEMPO units along the polymer backbone.[23] The voltammetric profiles show diffusive character, high chemical reversibility (peak current ratio $j_{p,c}/j_{p,a}$ close to unity, see Table S2), and similar equilibrium redox potentials (E_0, situated in the range between 0.40 V and 0.43 V), suggesting that at 100 mV s^{-1}, the behavior of ACT, BTM, and the PTMAs is essentially the same. That redox-active polymers can exhibit the

Table 2. Parameters extracted from the CVs of the TEMPO species. The shown values are mean values of two measurements.

Species	E_0 vs. $Ag/AgNO_3$[a] [V]	$j_{p,a}$[a] [mA cm^{-2}]	D [cm^2 s^{-1}]
ACT	0.40[b]	1.76[b]	1.53×10^{-5}[b]
BTM	0.41	1.22	7.76×10^{-6}
3.6-TPMA	0.43	0.65	2.36×10^{-6}
15.0-TPMA	0.41	0.45	1.10×10^{-6}
30.8-TPMA	0.42	0.36	7.24×10^{-7}
126.0-TPMA	0.42	0.16	1.37×10^{-7}

[a] Estimated at 100 mV s^{-1}. [b] Values taken from Ref. [13].

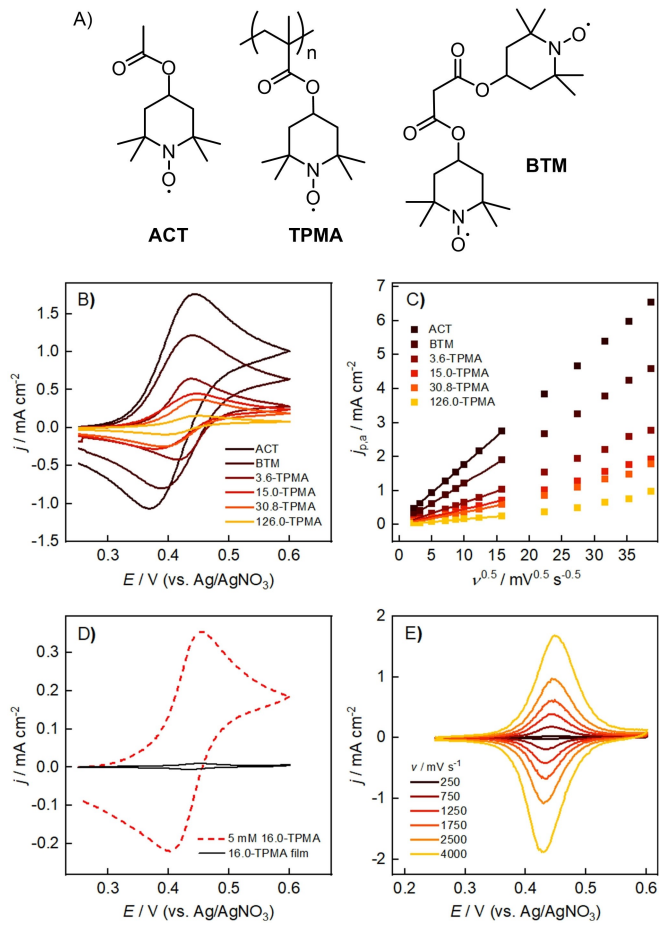

Figure 3. Cyclic voltammetry (CV) of selected *N*-oxyls in a solution of 0.1 M NBu_4ClO_4 in CH_3CN/H_2O (8:1, vol/vol). A) Structures of analyzed species. B) CVs of ACT, BTM, 3.6-, 15.0-, 30.8-, and 126.0-TPMA recorded at 100 mV s^{-1} (c_{TU} = 5 mM). C) Plot of the anodic peak current densities ($j_{p,a}$) vs. $v^{0.5}$. D) CV of 5 mM 16.0-TPMA (red line) recorded at 100 mV s^{-1} and repeated scan after replacing the solution with blank electrolyte (black line). E) CVs of adsorbed 16.0-TPMA recorded at various scan rates.

same form of current-potential responses as molecules with only one corresponding center has already been observed in other studies, for example, in the electrochemical analysis of poly(vinylferrocene).[16]

Large differences are noticeable when comparing the current densities (*j*) of the CVs, which, starting from ACT, decrease with increasing molar weight. This trend suggests that the availability of redox-active units at the electrode surface decreases for the higher-molecular-weight TEMPOs, which may result from curbed mass transfer. This behavior also becomes evident upon varying the scan rate (Figure 3C). Furthermore, with a stepwise increase of *v*, an additional peculiarity is noticeable: While up to 250 mV s^{-1}, ACT, BTM, and the TPMAs show a linear relationship between the anodic peak current density ($j_{p,a}$) and $v^{0.5}$, a deviation from the square root dependency occurs exclusively for the TPMAs above 250 mV s^{-1}. This deviation results from a superposition of adsorptive and diffusive processes, i.e., from charge transfer to both dissolved and adsorbed polymer chains, and has been studied in detail in our previous work.[13] Consequently, the square root dependency of $j_{p,a}$ at low scan rates indicates that at large time scales, the major part of the charge is transferred in diffusive processes. On the other hand, the adsorptive fraction of $j_{p,a}$ that increases linearly with *v*[24] becomes more pronounced at higher scan rates.

To confirm that adsorption of TPMAs on the electrode surface is responsible for the deviation from the square root dependency, additional experiments were performed in which CVs were first recorded in a TPMA solution (c_{TU} = 5 mM), followed by careful rinsing of the electrode with acetonitrile, immersion into a blank electrolyte solution, and repeated cycling. The results are shown exemplarily for 16.0-TPMA: While at 100 mV s^{-1}, voltammetry in the blank electrolyte shows only an extremely weak signal (Figure 3D, black line), well-defined and nearly symmetric features centered around 0.43 V become apparent at high scan rates (Figure 3E). These features exhibit only a small splitting between the oxidative and the reductive peak ($\Delta E_p \sim 15$ mV), which is typical for independent and identical redox-active species attached to the electrode surface.[25] The apparent surface concentration of TEMPO units (Γ_{TU}) calculated from the charge obtained via integration of the anodic peak of the CV recorded at 750 mV s^{-1} corresponds to 1.42×10^{-10} mol cm^{-2}. This value is in the same order of magnitude but well below sterically limited Γ values reported for monolayers of other redox-active molecules (e.g., ferrocene) covalently attached to smooth surfaces.[26] The profiles do not change significantly over ten cycles, indicating high stability of the TPMA layer on the experimental time scale (see Figure S3). The same effect has already been observed in our previous study on 3.6-TPMA.[13] Consequently, polymer adsorption seems to be a general effect that occurs independently from the M_n value of the polymer.

For a quantitative comparison between the transport properties, the diffusion coefficients *D* of the different TEMPO species were calculated from the slope of the j_p vs. $v^{0.5}$ plot using Equation (1),[25]

$$j_p = 0.4463 z F c_{TU} \sqrt{\frac{zFvD}{RT}} \quad (1)$$

where *z* corresponds to the number of transferred electrons per TEMPO unit ($z = 1$), *F* to the Faraday constant, *R* to the ideal gas constant, and *T* to the temperature (the other parameters are defined above). It should be noted that c_{TU} is kept constant (5 mM) and that for the polymer samples, the treatment renders apparent diffusion coefficients that refer to individual TEMPO units rather than to entire polymer chains.[12,13,17] To exclude influences of adsorption, only the *v* range dominated by the diffusive process is evaluated (5–250 mV s^{-1}, see Figure 3C). The resulting *D* values are summarized in Table 2 for the selected examples and in Figure 4 for all studied *N*-oxyl species.

In principle, smaller diffusion coefficients are observed with increasing molecular weight of the polymer, with a rapid initial drop that leads to a 95% decrease in *D* for 19.6-TPMA compared to ACT (Figure 4A). The profile shown is well explained when considering the relationship between *D* and

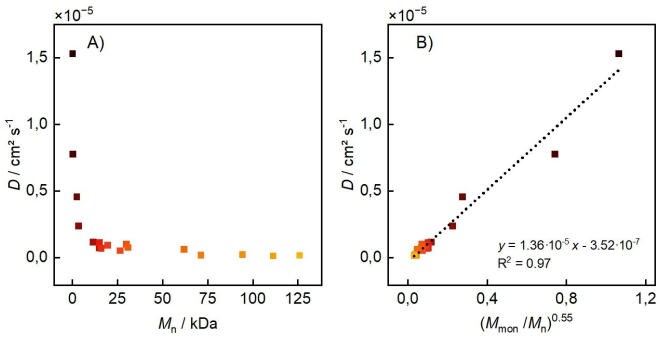

Figure 4. Plot of the diffusion coefficients D derived from Randles-Sevcik analysis vs. A) M_n and B) M_{mon}/M_n. The shown D values are mean values from twofold estimations.

the hydrodynamic radius r of a diffusing species according to the Stokes-Einstein equation ($D \sim r^{-1}$), and substituting r by M_n^a using scaling theory with a being the Flory exponent ($a = 0.5$ for ideal random polymer coils in a theta solvent and $a = 0.6$ for swollen coils in a good solvent).[27] In practice, the following empirical relationship has proven useful,

$$\frac{D}{D_{mon}} = \left(\frac{M_{mon}}{M_n}\right)^{0.55} \quad (2)$$

which relates D to M_n, the (hypothetical) diffusion coefficient, and the molecular weight of the monomer unit (D_{mon} and M_{mon}, respectively).[16–17] In the context of the abovementioned Stokes-Einstein equation and scaling relation, the exponent 0.55 would represent a scenario in which the polymer chain is randomly coiled in a good solvent ($0.5 < a < 0.6$).

As can be seen from the plot in Figure 4(B), D varies linearly with respect to the 0.55 power of the ratio between M_n and M_{mon}. The slope of the linear fit corresponds to D_{mon} and with 1.49×10^{-5} cm^2 s^{-1}, it is well comparable to the diffusion coefficient of the model monomer ACT ($D_{ACT} = 1.72 \times 10^{-5}$ cm^2 s^{-1}). Together with a negligible y-axis intercept (-3.52×10^{-7} cm^2 s^{-1}) and an R^2 value of 0.97, the linear fit is in good agreement with the behavior predicted by Equation (2). Since Equation (2) originally refers to regular diffusion coefficients of polymers, and the D values summarized in Figure 4 are to be considered as apparent diffusion coefficients of individual TEMPO units, some caution must be exercised in interpreting Figure 4(B). However, it seems reasonable to conclude that the observed relationship reflects the impact of the molecular weight on the rate of mass transfer and thereby on the diffusion-limited peak current density. In other words, the relationship between M_n and D follows the behavior predicted by the Stokes–Einstein equation in the sense that diffusion is curbed with increasing molecular size. In view of applications in homogeneous electrocatalysis, the profile shown in Figure 4(A) illustrates that polymers with M_n values smaller than approx. 10 kDa exhibit promising diffusion behavior, whereas diffusion coefficients of larger TPMAs appear rather unfavorable.

The study was continued by analyzing the impact of the molecular weight on the electrocatalytic behavior of the TPMAs. For this purpose, 4-methoxybenzyl alcohol (4-MBA) was used as a test substrate. A comparison between the voltammetric profiles of four representative examples, ACT, BTM, 3.6-, and 26.6-TPMA, recorded at 100 mV s^{-1} in the absence and presence of the alcohol substrate is shown in Figure 5. *N*-Methylimidazole (NMI) was added as a proton scavenger to enable electrocatalytic alcohol oxidation. A control CV recorded without mediator confirmed that direct (uncatalyzed) anodic substrate conversion does not occur in the studied potential range (see Figure S5). In all cases, a typical catalytic response is seen (solid line), where indirect oxidation of the alcohol enhances the anodic current compared to the non-catalytic CV (dashed line), and where the cathodic peak disappears in the reverse scan. Upon comparing the profiles, it becomes clear that *i*) significant catalytic currents can be achieved both with ACT as well as with

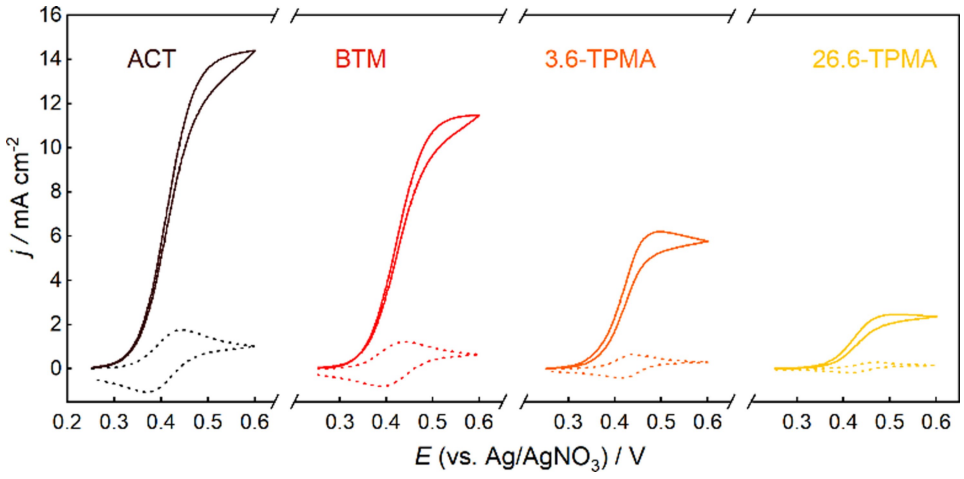

Figure 5. CVs of ACT, BTM, 3.6-TPMA, and 26.6-TPMA, recorded at 100 mV s^{-1}. Conditions: $c_{TU} = 5$ mM, 0.1 M NBu_4ClO_4 in CH_3CN/H_2O (8:1, vol/vol) in the absence (dashed) as well as in the presence of 0.1 M 4-MBA and 0.45 M NMI (solid line).

higher molecular weight TEMPO species and *ii*), that the catalytic peak current densities j_{cat} decrease with increasing molecular size. The latter occurs concomitantly with decreasing $j_{p,a}$ values, whereby the current enhancements do not differ greatly ($j_{cat}/j_{p,a}$ between 8.2 and 9.6). This suggests that the overall reaction rate decreases with increasing M_n due to a curbed diffusion of the mediator.

The catalytic behavior was studied in more detail by variation of the scan rate. In Figure 6(A), the progression of the catalytic response is shown exemplarily for 15.0-TPMA. While initially, an increase in v leads to a strong current enhancement, the profiles remain nearly unchanged at higher scan rates. Together with the canonical S-shape of the curves, this suggests that at high scan rates und sufficiently high electrode potential, only the kinetics of alcohol oxidation determine the current response ('pure kinetic conditions').[28] The same progression of the catalytic profiles is observed for ACT and BTM as well as for the other TPMAs (see the Supporting Information).

Figure 6(B) shows the plots of j_{cat} vs. v for seven representative TEMPO species. Comparison between the plots highlights the relationship between molecular weight and electrocatalytic activity. In all cases studied, j_{cat} reaches a plateau value (j_{max}) at high scan rates. The plot of j_{max} against M_n (Figure 6C) initially shows a sharp drop from 16.3 mA cm^{-2} (ACT) to 6.1 mA cm^{-2} (15.0-TPMA), whereas the decrease is significantly attenuated toward higher M_n values. Interestingly, even polymers with M_n > 60 kDa achieve appreciable j_{max} values despite their extremely low diffusion coefficients. For example, 126.0-TPMA as the largest polymer with a D value of only 1.41×10^{-7} cm^{-2} (as compared to 1.53×10^{-5} cm^{-2} for ACT) still achieves a j_{max} value of 3.2 mA cm^{-2}.

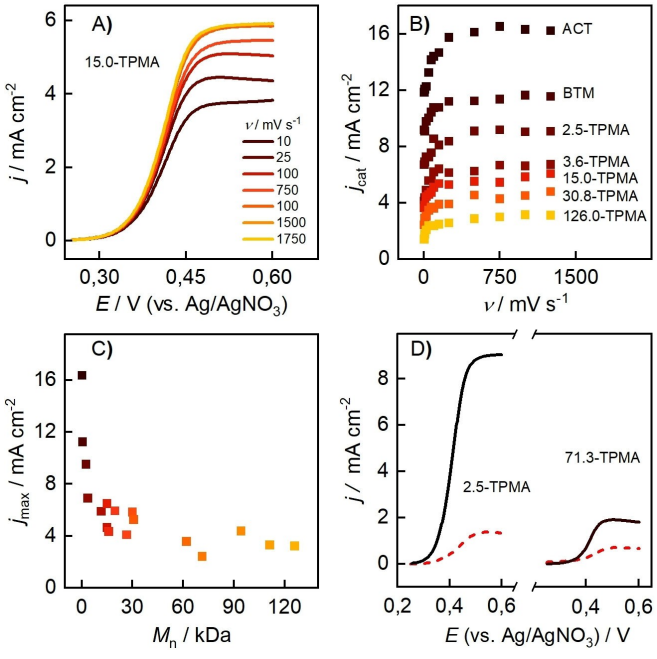

Figure 6. A) LSVs of 15.0-TPMA, recorded at various scan rates. Conditions: c_{TU} = 5 mM, 0.1 M NBu_4ClO_4 in CH_3CN/H_2O (8:1 vol/vol), 0.1 M 4-MBA, and 0.45 M NMI. B) Maximum achievable current densities (j_{cat}) vs. the scan rate for ACT, BTM, and five representative polymers. C) Plot of the plateau current densities achieved under pure kinetic conditions (j_{max}) against M_n (the shown j_{max} values are mean values from two measurements). D) LSVs of 5 mM 2.5-TPMA and 71.3-TPMA recorded at 1 V s^{-1} in presence of 4-MBA and base (black solid line); repeated scan after replacing the solution with TPMA-free, substrate- and base-containing solution (red dashed line).

Assuming pure homogeneous electrocatalysis, j_{max} is given by the following equation,[28a,29]

$$j_{max} = zFc_{TU}\sqrt{nDk_{cat}c_{sub}} \quad (3)$$

with k_{cat} as the homogeneous rate constant, n as the number of catalyst units required per turnover, and c_{sub} as the substrate concentration (the other parameters are defined above). Regarding Equation (3), it appears tempting to determine k_{cat} values for the polymediators. However, in view of the polymer adsorption described above (Figure 3D), caution should be exercised in the kinetic analysis of TPMA-catalyzed reactions. The influence of adsorbed TPMA on the catalytic response is illustrated in Figure 6(D) using the catalytic responses of 2.5-TPMA and 71.3-TPMA recorded at 1 V s^{-1} as examples. In both cases, the measurement was carried out under the same conditions as in Figure 6(A) (black solid lines), followed by removal and rinsing of the electrode, and repeated scan after replacing the electrolyte with a TPMA-free but substrate- and base-containing solution (red dashed lines). A comparison of the profiles recorded before and after change of the solution shows that TPMAs attached to the electrode participate in substrate oxidation, whereby the heterogeneous contribution to j_{cat} is much more pronounced for 71.3-TPMA (35%) than for 2.5-TPMA (15%).

Similar to homogeneous electrocatalysts, adsorbed molecular catalysts exhibit S-shaped profiles under pure kinetic conditions.[28c] An anodic process catalyzed only by adsorbed TEMPO species would lead to plateau currents given by Equation (4),[28b]

$$j_{max} = nF\Gamma_{TU}k_{cat}c_{sub} \quad (4)$$

where Γ_{TU} corresponds to the surface concentration [mol cm^{-2}] of TEMPO units and the other parameters have been defined above. Assuming that no interactions exist between the homogeneously and heterogeneously electrocatalytic processes, the procedure shown on Figure 6(A and D) would in principle allow separation of the contributions of dissolved and adsorbed TPMAs (and thus determination of the homogeneous and heterogeneous k_{cat} values). However, since the catalytic currents of adsorbed TPMAs in TPMA-free solutions are not stable over several cycles, analysis of the individual contributions is not feasible. Still, the j_{max} values summarized in Figure 6(C) are well-suited for characterization of the macroscopic kinetics since they reflect the overall reaction rate as an interplay between catalyst diffusion and microscopic rate.

The previously discussed CV results have proven useful in elucidating the influence of molecule size on redox behavior, transport processes, and electrocatalytic properties. The knowledge gained and intrinsic parameters determined are important for the mechanistic understanding and for the comparison of

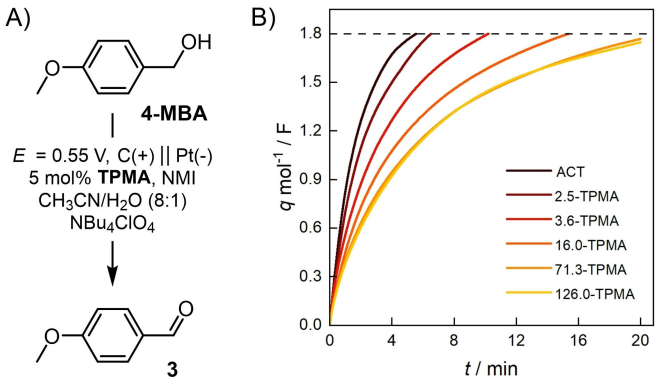

Figure 7. A) TPMA-catalyzed anodic oxidation of 4-MBA to anisaldehyde (**3**) under potentiostatic conditions. B) Corresponding charge-time profiles for ACT and different TPMAs. Electrolyte: 0.1 M Bu_4NClO_4 in CH_3CN/H_2O (8:1, v/v), anode: carbon roving, divided cell, rt. $E = 0.55$ V vs. $Ag/AgNO_3$, 0.075 M 4-MBA (batch size: 0.75 mmol), 0.11 M NMI.

the different *N*-oxyl species. However, it should also be considered that the conditions in preparative-scale applications are significantly more complex than in the CV experiments. Particularly noteworthy are the change of the electrolyte composition during electrolysis as well as forced convection for improved mass transfer. To gain a better insight into the behavior under preparative conditions, controlled potential electrolyses (CPE) were carried out at $E = 0.55$ V with different TPMAs in the presence of 4-MBA (Figure 7A). A divided cell was used in combination with a carbon roving anode[30] and a platinum cathode. An inexpensive size exclusion membrane made of regenerated cellulose served as a separator (for more information see the Supporting Information). The corresponding charge-time profiles are depicted in Figure 7(B). The time periods required to pass 1.8 F per mole of substrate are summarized in Table 3 along with the corresponding Faradaic efficiencies (*FE*).

In all cases, *FE*s between 78% and 95% were achieved. A comparison of the charge-time profiles demonstrates the effect of the molecular weight on the reaction rate. While the electrolysis time differed little between ACT (5.6 h) and 2.5-TPMA (6.6 h), it increased dramatically upon using longer polymer chains. When 71.3- and 126.0-TPMA were employed, electrolysis was stopped after 20 h, achieving a charge transfer of merely 1.77 F and 1.75 F, respectively. Taken together, the CPE experiments show that smaller TPMAs render attractive reaction times and *FE* values. Particularly with 2.5-TPMA, only minimal changes in overall reaction rate can be observed compared to ACT, a very encouraging result in view of future synthetic applications. In contrast, the results obtained with the larger TPMA's are less promising. Especially for 71.3-TPMA and 126.0-TPMA, reactions with $t > 20$ h are inacceptable. The experiments thus highlight the outstanding significance of the M_n distribution for the development of polymediator-guided electrochemical syntheses.

Table 3. Summary of the results of the electrolysis experiments shown in Figure 7.

Species	*q* per mole **4-MBA** [F]	Electrolysis time [h]	*FE* [%][a]
ACT	1.8	5.6	78
2.5-TPMA	1.8	6.6	79
3.6-TPMA	1.8	10.2	93
16.0-TPMA	1.8	15.4	95
71.3-TPMA	1.77	20.0	93
126.0-TPMA	1.75	20.0	80

[a] Faradaic efficiency determined via GC-FID analysis using an internal standard.

Conclusion

In the present study, progress has been made in understanding electrocatalysis involving TEMPO-modified polymethacrylates (TPMA) as mediators. It was shown how the molecular weight affects the key properties of the polymers, revealing that this aspect plays an important role in the development of poly-mediated processes. At this point, it is worth summarizing the most important findings:

1. Cyclic voltammetry is shown to be a simple and effective method for studying the key-properties of polymediators. At low to medium scan rates, the non-catalytic voltammetric profiles of the studied TPMAs are very similar to 4-acetoxy-TEMPO (ACT) in terms of equilibrium potential, chemical reversibility, and diffusive character, indicating a non-interacting electron exchange between electrode and TEMPO units attached to the polymer chain. Major differences between the TPMAs are observed for the achievable redox currents, which is explained by a decrease of the diffusion rate with increasing molecular size, following the behavior predicted by the Stokes–Einstein equation. In other words, short-chain TPMAs can be more rapidly charged than the larger polymers.
2. To quantify the effect of number-average molecular weight (M_n) on the diffusion rate, diffusion coefficients (*D*) conveniently estimated via CV turned out useful. For the TPMA series, the relationship between *D* and M_n is in good agreement with an empirical equation reported in the literature representing random coil polymers in good solvents.[16,27]
3. The affinity of the polymer to the electrode surface should be taken into account when studying reactions involving polymediators. In the present case, all TPMAs tend to adsorb on the electrode surface regardless of molecular weight. Polymer adsorption affects the non-catalytic voltammetric response, especially at low TPMA concentrations and high scan rates. Both dissolved and adsorbed TPMAs participate in the catalytic process, whereby the relative heterogeneous contribution is small for short-chain TPMAs and increases with increasing M_n.
4. The catalytic currents diminish with increasing molecular weight, which can be assigned to the decreasing diffusion coefficients. The maximum achievable catalytic current under pure kinetic conditions (j_{max}) is a parameter that can be conveniently determined for all *N*-oxyl species and reflects the interplay between catalyst diffusion, homoge-

neous rate, and catalysis by adsorbed TEMPO units. It can therefore serve as a useful measure for comparing the activity of the polymediators. Compared to ACT, the long-chain TPMAs provide only about one-fifth of the j_{max} value. In contrast, good results are achieved with shorter chains (2.5 and 3.6 kDa).

5. The trends observed in the CV studies translate well to controlled potential electrolysis. While all polymers provide good to very good Faradaic efficiencies, the electrolysis time prolongs with increasing molecular weight. Promising results were obtained with short-chain polymers (2.5 and 3.6 kDa), whereas the large TPMAs tend to give low currents and long reaction times.

Together with our previous mechanistic work on the subject,[13] it is now possible to assemble a coherent picture. From the insights gained, important criteria and design principles can be derived for future developments.

The current work clearly shows that short-chain polymediators are needed to achieve useful reaction rates, with consequences for coupling between electrolysis and membrane filtration (the latter serving to separate and recycle the polymers). Preliminary recycling studies on short-chain TPMAs using dialysis with commercially available porous size-exclusion membranes (regenerated cellulose, molecular weight cut-off: 1 kDa) already yielded promising results.[12] However, in pressure-driven ultrafiltration using the same membrane material, short-chain TPMAs were not sufficiently retained to enable multiple reuse with stable electrolysis performance. Thus, nanofiltration with dense membranes seems more suitable for quantitative recovery. However, more studies on polymer recovery and recycling are needed before applying the concept under industrially relevant conditions. For the latter, a continuous process in which an electrochemical flow reactor is coupled with a cross-flow membrane filtration cell appears particularly promising. Efforts to advance polymediator-guided electrosynthesis are ongoing in our laboratory.

Experimental Section

General remarks: All chemicals were purchased from Alfa Aesar, Sigma Aldrich or TCI and used as received. The supporting electrolyte (tetrabutylammonium perchlorate) was purchased from Sigma Aldrich in electrochemical grade. Acetonitrile was purchased in HPLC grade from Acros Organics and used as received. Synthesis and spectroscopic characterization of the TEMPO catalysts is described in the Supporting Information.

Size exclusion chromatography (SEC): The polymer samples were dissolved in 1,1,1,3,3,3-hexaflouropropan-2-ol (HFIP) (Fluorochem, Hadfield, UK) containing 3 gL^{-1} of potassium trifluoroacetate. The SEC instrument was equipped with a PU2080+ pump, an auto sampler AS1555 and an RI-detector RI2080+ from JASCO. Columns packed with modified silica were obtained from PSS (Mainz, Germany): PFG columns, particle size 7 μm, porosity 100 Å and 1000 Å. The column was kept in an oven at constant temperature of 40 °C. Calibration was carried out with poly(methyl methacrylate) (PMMA) standards, purchased from PSS (Mainz, Germany). The samples were prepared at 1–2 mg mL^{-1} and filtered through PVDF syringe filters (pore size 0.2 μm) prior to analysis.

Cyclic voltammetry (CV): The experiments were carried out in a custom-made three-electrode cell using a PGSTAT 302N (Metrohm Autolab) or a PGSTAT 128N (Metrohm Autolab). A glassy carbon disk (diameter: 1.6 mm) served as the working electrode and a platinum wire as the counter electrode. The glassy carbon disk was polished using polishing alumina suspension (0.05 μm) prior to each experiment. As reference, a $Ag/AgNO_3$ electrode (silver wire in 0.1 M NBu_4ClO_4/CH_3CN solution; $c(AgNO_3) = 0.01$ M; $E_0 = -87$ mV vs. ferrocene/ferrocenium couple)[22] was used, and this compartment was separated from the rest of the cell with a Vycor frit. NBu_4ClO_4 (0.1 M, electrochemical grade) was employed as supporting electrolyte in an acetonitrile-water mixture (8:1, vol./vol.). The electrolyte was purged with Ar for at least 5 min prior to recording. In order to account for the *iR* drop at high catalytic currents, positive feedback *iR* compensation was used. The resistance *R* was determined by electrochemical impedance spectroscopy prior to each experiment. Background corrections were made by subtracting the blank voltammograms from the CVs of the analytes.

Controlled potential electrolysis (CPE): The electrolyses were carried out in an H-type divided cell using a Vionic Potentiostat (Metrohm). A size exclusion membrane (regenerated cellulose, MW cut-off: 1 kDa, Merck) was used as a separator, a carbon roving wrapped around a PTFE sheet as a working electrode, and a Pt sheet as a counter electrode. A solution of 0.1 M NBu_4ClO_4 in CH_3CN/H_2O (8:1) served as the electrolyte, whereby 75 mM 4-methoxybenzyl alcohol, 110 mM 1-methylimidazol, and 5 mol-% TPMA (with respect to starting material and TEMPO units) were added to the anolyte. The anolyte and catholyte solutions (10 mL each) were prepared separately and filled simultaneously into the corresponding half-cells with syringes. During electrolysis, the working electrode potential was maintained at 0.55 V vs. Ag/0.01 M $AgNO_3$ using the same reference electrode as described for the cyclic voltammetry experiments. The yields were determined with a calibrated GC-FID (Trace 1310, Thermo Fisher) equipped with a HP-5 column (Agilent) using an internal standard (1,3,5-trimethoxy benzene).

Acknowledgements

This work has been funded by the German Research Foundation (DFG, project no. FR 3848/2-1). The author is grateful for funding by the DFG Heisenberg Program (FR 3848/4-1). Open Access funding enabled and organized by Projekt DEAL.

Conflict of Interest

The authors declare no conflict of interest.

Data Availability Statement

The data that support the findings of this study are available in the supplementary material of this article.

Keywords: electrosynthesis · electrocatalysis · mediators · redox-active polymers · TEMPO

[1] a) R. Francke, R. D. Little, *Chem. Soc. Rev.* **2014**, *43*, 2492–2521; b) L. F. T. Novaes, J. Liu, Y. Shen, L. Lu, J. M. Meinhardt, S. Lin, *Chem. Soc. Rev.* **2021**, *50*, 7941–8002.
[2] a) N. Kaeffer, W. Leitner, *JACS Au* **2022**, *2*, 1266–1289; b) L. Ackermann, *Acc. Chem. Res.* **2020**, *53*, 84–104; c) C. Ma, P. Fang, T.-S. Mei, *ACS Catal.* **2018**, *8*, 7179–7189; d) A. Jutand, *Chem. Rev.* **2008**, *108*, 2300–2347.
[3] a) J. Strehl, G. Hilt, *Org. Lett.* **2019**, *21*, 5259–5263; b) J. C. Siu, N. Fu, S. Lin, *Acc. Chem. Res.* **2020**, *53*, 547–560.
[4] a) P. Qian, Z. Zha, Z. Wang, *ChemElectroChem* **2020**, *7*, 2527–2544; b) N. Dagar, P. P. Sen, S. R. Roy, *ChemSusChem* **2021**, *14*, 1229–1257; c) F. Lian, K. Xu, C. Zeng, *Chem. Rec.* **2021**, *21*, 2290–2305.
[5] a) C. Y. Cai, X. M. Shu, H. C. Xu, *Nat. Commun.* **2019**, *10*, 4953; b) Y. S. Park, R. D. Little, *J. Org. Chem.* **2008**, *73*, 6807–6815; c) N. N. Lu, N. T. Zhang, C. C. Zeng, L. M. Hu, S. J. Yoo, R. D. Little, *J. Org. Chem.* **2015**, *80*, 781–789.
[6] a) R. Francke, *Curr. Opin. Electrochem.* **2019**, *15*, 83–88; b) R. Francke, *Curr. Opin. Electrochem.* **2021**, *28*; c) M. Elsherbini, T. Wirth, *Chem. Eur. J.* **2018**, *24*, 13399–13407.
[7] a) J. E. Nutting, M. Rafiee, S. S. Stahl, *Chem. Rev.* **2018**, *118*, 4834–4885; b) M. Rafiee, Z. M. Konz, M. D. Graaf, H. F. Koolman, S. S. Stahl, *ACS Catal.* **2018**, *8*, 6738–6744; c) H. B. Zhao, P. Xu, J. Song, H. C. Xu, *Angew. Chem. Int. Ed.* **2018**, *57*, 15153–15156; *Angew. Chem.* **2018**, *130*, 15373–15376; d) J. C. Siu, J. B. Parry, S. Lin, *J. Am. Chem. Soc.* **2019**, *141*, 2825–2831.
[8] a) Y. Yuan, A. Lei, *Nat. Commun.* **2020**, *11*, 802; b) R. Francke, *Chimia* **2020**, *74*, 49–56; c) J. Yoshida, K. Kataoka, R. Horcajada, A. Nagaki, *Chem. Rev.* **2008**, *108*, 2265–2299; d) R. Francke, *Curr. Opin. Electrochem.* **2022**, *36*, 101111.
[9] a) T. Broese, R. Francke, *Org. Lett.* **2016**, *18*, 5896–5899; b) O. Koleda, T. Broese, J. Noetzel, M. Roemelt, E. Suna, R. Francke, *J. Org. Chem.* **2017**, *82*, 11669–11681; c) A. F. Roesel, T. Broese, M. Májek, R. Francke, *ChemElectroChem* **2019**, *6*, 4229–4237.
[10] a) T. Tajima, T. Fuchigami, *J. Am. Chem. Soc.* **2005**, *127*, 2848–2849; b) T. Tajima, T. Fuchigami, *Angew. Chem. Int. Ed.* **2005**, *44*, 4760–4763; *Angew. Chem.* **2005**, *117*, 4838–4841; c) T. Tajima, H. Kurihara, T. Fuchigami, *J. Am. Chem. Soc.* **2007**, *129*, 6680–6681; d) S. J. Yoo, L. J. Li, C. C. Zeng, R. D. Little, *Angew. Chem. Int. Ed.* **2015**, *54*, 3744–3747; *Angew. Chem.* **2015**, *127*, 3815–3818; e) T. Sawamura, S. Kuribayashi, S. Inagi, T. Fuchigami, *Adv. Synth. Catal.* **2010**, *352*, 2757–2760; f) M. Kuroboshi, K. Goto, H. Tanaka, *Synthesis* **2009**, 903–908.
[11] Another option is the immobilization of molecular catalysts on electrode surfaces for heterogeneously electrocatalyzed transformations as exercised in refs. [11a–d]. a) D. P. Hickey, R. D. Milton, D. Chen, M. S. Sigman, S. D. Minteer, *ACS Catal.* **2015**, *5*, 5519–5524; b) F. C. Macazo, D. P. Hickey, S. Abdellaoui, M. S. Sigman, S. D. Minteer, *Chem. Commun.* **2017**, *53*, 10310–10313; c) A. Das, S. S. Stahl, *Angew. Chem. Int. Ed.* **2017**, *56*, 8892–8897; *Angew. Chem.* **2017**, *129*, 9018–9023.
[12] B. Schille, N. O. Giltzau, R. Francke, *Angew. Chem. Int. Ed.* **2018**, *57*, 422–426; *Angew. Chem.* **2018**, *130*, 429–433.
[13] N. Mohebbati, A. Prudlik, A. Scherkus, A. Gudkova, R. Francke, *ChemElectroChem* **2021**, *8*, 3837–3843.
[14] Applications of redox-active polymers in bioelectrochemistry have been recently reviewed: a) M. Kaneko, K. Ishihara, S. Nakanishi, *Small* **2020**, *16*, 2001849; b) M. Yuan, S. D. Minteer, *Curr. Opin. Electrochem.* **2019**, *15*, 1–6. For selected applications in bioelectrocatalysis, see: c) M. Kanekoa, M. Ishikawa, J. Song, S. Kato, K. Hashimoto, S. Nakanishi, *Electrochem. Commun.* **2017**, *75*, 17–20; d) K. Hasan, M. Grattieri, T. Wang, R. D. Milton, S. D. Minteer, *ACS Energy Lett.* **2017**, *2*, 1947–1951; e) Y. S. Lee, M. Yuan, R. Cai, K. Lim, S. D. Minteer, *ACS Catal.* **2020**, *10*, 6854–6861; f) G. Pankratova, D. Pankratov, R. D. Milton, S. D. Minteer, L. Gorton, *Adv. Energy Mater.* **2019**, *9*, 1900215. For selected applications in biosensors, see: g) S. M. Oja, B. Feldman, M. W. Eshoo, *Anal. Chem.* **2018**, *90*, 1536–1541; h) A. Ruff, P. Pinyou, M. Nolten, F. Conzuelo, W. Schuhmann, *ChemElectroChem* **2017**, *4*, 890–897.
[15] Applications of redox-active polymers in energy storage have been recently reviewed: a) K.-A. Hansen, J. P. Blinco, *Polym. Chem.* **2018**, *9*, 1479–1516; b) A. A. Vereshchagin, A. Y. Kalnin, A. I. Volkov, D. A. Lukyanov, O. V. Levin, *Energies* **2022**, *15*; c) J. Kim, J. H. Kim, K. Ariga, *Joule* **2017**, *1*, 739–768. For an outstanding example of TEMPO-modified polymers in redox flow batteries, see: d) T. Janoschka, N. Martin, U. Martin, C. Friebe, S. Morgenstern, H. Hiller, M. D. Hager, U. S. Schubert, *Nature* **2015**, *527*, 78–81.
[16] J. B. Flanagan, S. Margel, A. J. Bard, F. C. Anson, *J. Am. Chem. Soc.* **1978**, *100*, 4248–4253.
[17] G. Nagarjuna, J. Hui, K. J. Cheng, T. Lichtenstein, M. Shen, J. S. Moore, J. Rodríguez-López, *J. Am. Chem. Soc.* **2014**, *136*, 16309–16316.
[18] K. Zhang, Y. Hu, L. Wang, J. Fan, M. J. Monteiro, Z. Jia, *Polym. Chem.* **2017**, *8*, 1815–1823.
[19] Direct comparison between the M_n values of the TPMA samples used in this study and the one from Ref. [12] is not possible, since different SEC systems and standards were used for molecular weight analysis.
[20] T. Janoschka, A. Teichler, A. Krieg, M. D. Hager, U. S. Schubert, *J. Polym. Sci. Part A* **2012**, *50*, 1394–1407.
[21] a) D. B. Thomas, A. J. Convertine, R. D. Hester, A. B. Lowe, C. L. McCormick, *Macromolecules* **2004**, *37*, 1735–1741; b) C. P. Jesson, C. M. Pearce, H. Simon, A. Werner, V. J. Cunningham, J. R. Lovett, M. J. Smallridge, N. J. Warren, S. P. Armes, *Macromolecules* **2017**, *50*, 182–191.
[22] V. V. Pavlishchuk, A. W. Addison, *Inorg. Chim. Acta* **2000**, *298*, 97–102.
[23] R. F. Winter, *Organometallics* **2014**, *33*, 4517–4536.
[24] J. Wang, in *Analytical Electrochemistry*, Wiley-VCH, **2006**.
[25] A. J. F. Bard, in *Electrochemical Methods. Fundamentals and Applications*, Wiley, **2001**.
[26] a) B. M. Johnson, R. Francke, R. D. Little, L. A. Berben, *Chem. Sci.* **2017**, *8*, 6493–6498; b) M. A. Pellow, T. D. P. Stack, C. E. D. Chidsey, *Langmuir* **2013**, *29*, 5383–5387; c) M. V. Sheridan, K. Lam, W. E. Geiger, *Angew. Chem. Int. Ed.* **2013**, *52*, 12897–12900; *Angew. Chem.* **2013**, *125*, 13135–13138.
[27] a) M. D. Lechner, K. Gehrke, E. Nordmeier, *Makromolekulare Chemie*, Springer, **2020**; b) S. F. Sun, *Physical Chemistry of Macromolecules*, John Wiley & Sons, **2004**.
[28] a) J.-M. Savéant, *Chem. Rev.* **2008**, *108*, 2348–2378; b) C. Costentin, J.-M. Saveant, *J. Phys. Chem. C* **2015**, *119*, 12174–12182; c) C. Costentin, J.-M. Savéant, *Phys. Chem. Chem. Phys.* **2015**, *17*, 19350–19359.
[29] a) Preconditions for validity of Equation (3) are, among others, rate limitation by a single chemical step. In the present catalytic cycle (see Ref. [29b]), the reaction between the alcohol and the anodically formed oxoammonium species is generally assumed to be the rate-limiting step, while comproportionation between $TEMPO^+$ and TEMPOH is fast and thermodynamically favorable (see Refs. [29c] and [29d]). Consequently, Equation (3) has been used before for kinetic analysis of anodic alcohol oxidations mediated by TEMPO derivatives (see Refs. [29e] and [29f]); b) M. F. Semmelhack, C. R. Schmid, D. A. Cortés, *Tetrahedron Lett.* **1986**, *27*, 1119–1122; c) S. Kishioka, T. Ohsaka, K. Tokuda, *Chem. Lett.* **1998**, *27*, 343–344; d) A. Israeli, M. Patt, M. Oron, A. Samuni, R. Kohen, S. Goldstein, *Free Radical Biol. Med.* **2005**, *38*, 317–324; e) M. Rafiee, K. C. Miles, S. S. Stahl, *J. Am. Chem. Soc.* **2015**, *137*, 14751–14757; f) M. Rafiee, B. Karimi, S. Alizadeh, *ChemElectroChem* **2014**, *1*, 455–462.
[30] During optimization of the electrolysis conditions in our previous work, carbon roving was identified as the material with the best performance in view of product yield and long-term stability toward passivation.

Manuscript received: August 31, 2022
Accepted manuscript online: November 25, 2022
Version of record online: ■■, ■■■

RESEARCH ARTICLE

The polymeric electrosynthesis mediators: Polymediators are soluble redox-active polymers applicable as catalysts in electrosynthesis. Their difference in size relative to typical product molecules enables recovery by dialysis or membrane filtration. Using anodic alcohol oxidation as an example, the relationship between the molecular weight of TEMPO-modified polymethacrylates and their catalytic properties was elaborated using cyclic voltammetry and preparative-scale electrolysis.

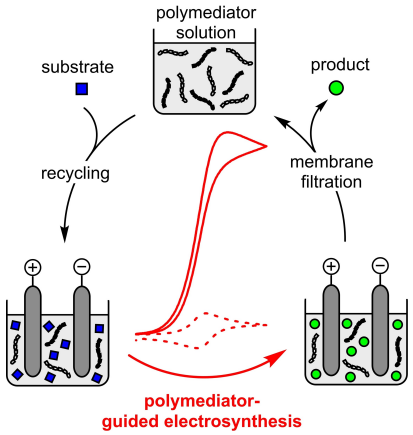

*A. Prudlik, N. Mohebbati, L. Hildebrandt, A. Heck, Prof. Dr. L. Nuhn, Prof. Dr. R. Francke**

1 – 10

TEMPO-Modified Polymethacrylates as Mediators in Electrosynthesis: Influence of the Molecular Weight on Redox Properties and Electrocatalytic Activity

Publication III

Electrochemical Generation of Hypervalent Bromine(III) Compounds

Igors Sokolovs (60%), Nayereh Mohebbati (20%), Robert Francke (10%), and Edgars Suna (10%)

DOI: 10.1002/anie.202104677.

Abstract: In sharp contrast to hypervalent iodine(III) compounds, the isoelectronic bromine(III) counterparts have been little studied to date. This knowledge gap is mainly attributed to the difficult-to-control reactivity of l3-bromanes as well as to their challenging preparation from the highly toxic and corrosive BrF3 precursor. In this context, we present a straightforward and scalable approach to chelation-stabilized l3-bromanes by anodic oxidation of parent aryl bromides possessing two coordinating hexafluoro-2-hydroxypropanyl substituents. A series of para-substituted l3-bromanes with remarkably high redox potentials spanning a range from 1.86 V to 2.60 V vs. Ag/AgNO3 was synthesized by the electrochemical method. We demonstrate that the intrinsic reactivity of the bench-stable bromine(III) species can be unlocked by addition of a Lewis or a Brønsted acid. The synthetic utility of the l3-bromane activation is exemplified by oxidative C-C, C-N, and C-O bond forming reactions.

My Contribution (20%):

I carried out all the electroanalytical measurements. I. Sokolovs (60%) was responsible for synthetic studies and application screening. R. Francke (10%) and E. Suna (10%) had the initial idea of the topic, supervised the project, and wrote the manuscript.

Zitierweise: *Angew. Chem. Int. Ed.* **2021**, *60*, 15832–15837
Internationale Ausgabe: doi.org/10.1002/anie.202104677
Deutsche Ausgabe: doi.org/10.1002/ange.202104677

Electrochemistry

Electrochemical Generation of Hypervalent Bromine(III) Compounds

Igors Sokolovs, Nayereh Mohebbati, Robert Francke, and Edgars Suna**

Abstract: *In sharp contrast to hypervalent iodine(III) compounds, the isoelectronic bromine(III) counterparts have been little studied to date. This knowledge gap is mainly attributed to the difficult-to-control reactivity of λ^3-bromanes as well as to their challenging preparation from the highly toxic and corrosive BrF_3 precursor. In this context, we present a straightforward and scalable approach to chelation-stabilized λ^3-bromanes by anodic oxidation of parent aryl bromides possessing two coordinating hexafluoro-2-hydroxypropanyl substituents. A series of para-substituted λ^3-bromanes with remarkably high redox potentials spanning a range from 1.86 V to 2.60 V vs. $Ag/AgNO_3$ was synthesized by the electrochemical method. We demonstrate that the intrinsic reactivity of the bench-stable bromine(III) species can be unlocked by addition of a Lewis or a Brønsted acid. The synthetic utility of the λ^3-bromane activation is exemplified by oxidative C–C, C–N, and C–O bond forming reactions.*

The chemistry of hypervalent halogen species has experienced tremendous development in the last decades, and hypervalent iodine(III) compounds have become mainstream reagents in contemporary organic synthesis.[1] Recent selected applications of hypervalent iodine(III) compounds involve oxidative heterocycle formation,[2] atom transfer reactions[3] such as alkynylation[4] and trifluoromethylation,[5] oxidative rearrangements,[6] and C–H functionalization.[7] Additionally, electrochemically generated iodine(III) derivatives have been frequently utilized as ex-cell mediators (electro-generated reagents) in organic electrosynthesis.[8] The corresponding isoelectronic hypervalent bromine(III) species feature superior reactivity to that of iodine(III) counterparts owing to the higher oxidizing ability, stronger electrophilicity and better nucleofugality of the bromanyl unit.[9] Not surprisingly, the unique properties of bromine(III) reagents have allowed for the development of unprecedented synthetic transformations such as Hofmann rearrangement of sulfonamides to the corresponding *N*-arylsulfamoyl fluorides,[10] unusual Bayer–Villiger-type oxidation of open-chain aliphatic aldehydes,[9a] oxidative coupling of alkynes and primary alcohols to form conjugated enones[11] as well as transition metal-free regioselective C-H amination of non-activated alkanes.[12] Although these notable accomplishments highlight the remarkable synthetic potential of bromine(III) species,[13a] the hypervalent bromine chemistry appears to be significantly less developed as compared to that of iodine(III) compounds. This striking bias apparently is to be attributed to the relatively poor stability and the high oxidizing power of bromine(III) reagents,[13b] properties that have created a common perception of difficult-to-control reactivity and poor functional group compatibility. Furthermore, there is an apparent lack of convenient methods for the synthesis of bromine(III) species.

The synthesis of Br^{III} reagents is typically accomplished by a ligand exchange reaction between bromine trifluoride (BrF_3) and nucleophilic arene derivatives such as arylsilanes and arylstannanes.[13] For example, BrF_3 reacts with phenyl trifluorosilane to form a relatively unstable phenyl-λ^3-bromane **1**[14] that is suitable both as reagent and as entry point for the synthesis of other derivatives via ligand exchange (Figure 1, top).[15,16]

[*] Dr. I. Sokolovs, Prof. Dr. E. Suna
Latvian Institute of Organic Synthesis
Aizkraukles 21, 1006 Riga (Latvia)
E-mail: edgars@osi.lv
N. Mohebbati, Dr. R. Francke
Leibniz Institute for Catalysis
Albert-Einstein-Str. 29a, 18059 Rostock (Germany)
E-mail: robert.francke@catalysis.de
Dr. I. Sokolovs, N. Mohebbati, Dr. R. Francke
Institute of Chemistry, Rostock University
Albert-Einstein-Str. 3a, 18059 Rostock (Germany)
Prof. Dr. E. Suna
Faculty of Chemistry, University of Latvia
Jelgavas 1, 1004 Riga (Latvia)
Supporting information and the ORCID identification number(s) for the author(s) of this article can be found under: https://doi.org/10.1002/anie.202104677.

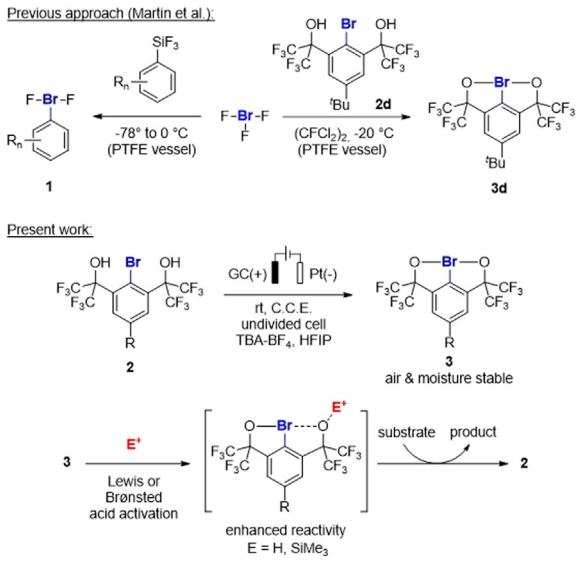

Figure 1. New approach to aryl-λ^3-bromanes.

Bromine trifluoride has been also used by Martin et al. for the preparation of chelation-stabilized aryl-λ^3-bromane **3d**.[17] However, an important limitation of these approaches is the use of BrF_3, a highly toxic and extremely reactive liquid that requires dedicated equipment (such as PTFE vessels etc.) and specific experimental techniques for its safe handling. Notably, high oxidation potentials of aryl bromides (e.g. 2.0 V vs. Ag/0.01 M $AgNO_3$ for PhBr in CH_3CN)[18] and poor stability of the resulting bromine(III) species complicates the direct two-electron oxidation by chemical oxidants, a method that is routinely employed for the synthesis of hypervalent iodine(III) counterparts from iodoarenes.[19] Clearly, the development of a convenient synthetic approach to λ^3-bromanes would open the door for the rapid development of hypervalent Br^{III} chemistry. Herein we report a straightforward and high yielding synthesis of Martin's hypervalent bromine(III) species **3** by anodic oxidation of the parent aryl bromide **2** (Figure 1, bottom). The extremely high reactivity of arylbromonium species[13a] is tamed by the two coordinating *ortho* substituents, allowing **3** to be stored as a bench-stable reagent for extended periods of time. However, the reactivity of the electrochemically generated Br^{III} species can be unlocked by a Lewis acid (such as TMSOTf and $BF_3{\cdot}OEt_2$) or a Brønsted acid (TfOH) additive as described below.

Recently we reported on electrosynthesis of hypervalent iodine(III) species by anodic oxidation of aryl iodides in an undivided cell using HFIP as solvent.[20] We hypothesized that the electrochemical oxidation would be suitable also for the synthesis of aryl-λ^3-bromanes provided that they are compatible with anodic oxidation conditions. Hence, the air- and moisture-stable[17b] aryl-λ^3-bromane **3a** was chosen as the target substrate to verify the feasibility of its electrochemical synthesis. The published conditions for anodic oxidation of iodoarenes into λ^3-iodanes were used as the starting point for the preparation of λ^3-bromane **3a** (Table 1).

Table 1: Optimization of the electrochemical synthesis of **3a**.

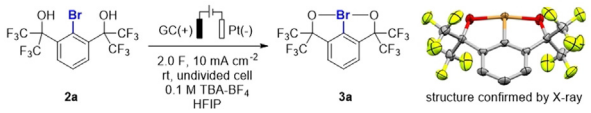

2a **3a**

Entry	Deviations from standard conditions	**2a** [%][a]	**3a** [%][a]	Mass balance [%][a]
1	none	43	55	98
2	TFE	40	52	92
3	CH_3CN	93	6	99
4	BDD(+)	54	46	100
5	RVC(+)	60	40	100
6	0.1 TBA-ClO_4	50	44	94
7	0.1 TBA-PF_6	44	55	99
8	$j = 5$ mA cm^{-2}	51	47	98
9	$j = 15$ mA cm^{-2}	38	56	94
10	$j = 20$ mA cm^{-2}	37	60	97
11	q/mol = 3.0 F	30	67	97
12	q/mol = 4.0 F	17	75 (63)[b]	92
13	q/mol = 5.0 F	18	71	89

[a] Yields and mass balances determined by ^{1}H NMR spectroscopy of the post-electrolysis solution using 1,2,3,4-tetrafluorobenzene as the internal standard (0.3 mmol scale). [b] Isolated yield.

Gratifyingly, electrochemical oxidation using glassy carbon (GC) as the working electrode and platinum foil as the counter electrode in a TBA-BF_4/HFIP electrolyte at 10 mA cm^{-2} afforded the desired **3a** in 55% yield (entry 1) after passing 2 F per mole of starting material. The molecular structure of **3a** was confirmed by single crystal X-ray analysis (Table 1, graphics). Although the use of 2,2,2-trifluoroethanol (TFE) as a solvent gave similar results (entry 2), we refrained from using it in further experiments because of its high toxicity. In contrast, acetonitrile turned out to be unsuitable due to anodic degradation (Supporting Information, p. S47), resulting in poor conversion to **3a** (entry 3). The replacement of working electrode material to BDD or RVC (entry 4 and 5) gave no increase in product yield. TBA-PF_6 can be used as an alternative to TBA-BF_4 (entry 7 vs. 1), whereas TBA-ClO_4 turned out to be inferior in terms of yield (entry 6). Lower current density (5 mA cm^{-2}) resulted in two-fold increase of the reaction time and slightly reduced product yield (entry 8 vs. entry 1). Higher current densities (15 and 20 mA cm^{-2}, entries 9 and 10, respectively) led to increased conversion at the expense of selectivity. Thus, a current density of 10 mA cm^{-2} was used in further optimization experiments. The increase of passed charge equivalents from 2.0 F up to 3.0 F resulted in the increase of λ^3-bromane **3a** yield from 55% to 67% (entry 11 vs. 1). Higher yields of **3a** and improved conversion was observed after passing 4.0 F. Nevertheless, further increase of the passed charge amount did not result in significant improvements, and a concomitant formation of degradation products was observed (entry 13 vs. 12).

With the optimized conditions in hand (entry 12), the scalability of the developed electrochemical synthesis of λ^3-bromane **3a** was examined. We were pleased to find that the galvanostatic electrolysis in an undivided electrochemical cell could be readily performed on a 10 mmol scale to afford 3.50 g of **3a** in a single-batch (72% yield). Notably, λ^3-bromane **3a** was isolated from the electrolysis mixture as >95% pure (^{1}H-NMR assay) pale-yellow solid by simple filtration through a short silica plug followed by extractive workup (see Figure 2, bottom right).

After elaboration of the electrochemical protocol for synthesis of λ^3-bromane **3a**, we intended to vary the substitution in *para* position to create a reagent platform with tunable reactivity and electrochemical properties. To establish access to compounds **3a–f**, the synthetic routes depicted in Figure 4 were developed. Introduction of 2-hydroxy-1,1,1,3,3,3-hexafluoropropanyl group in positions 2 and 5 of an aryl bromide was readily accomplished in two steps from 2-bromoisophthalic acids **5a–f**. The first step involved elaboration of acids **5a–f** into the corresponding acid chlorides, followed by the reaction with 2,2,2-trifluoroethanol to afford *bis*-trifluoroethyl esters **6a–f**. Subsequent treatment of esters **6a,d,e** with $TMSCF_3$ (7 equiv) in the presence of catalytic TBAF (10 mol%)[21] afforded the desired alcohols **2a,d,e** in 57–72% yields. The synthesis of **2b,c,f** required the addition of excess (4 equiv) of TBAF[22] and $TMSCF_3$ (6 equiv)[23] to furnish products in 62–69% yields. The nitration of **2a** afforded bromide **2f**. The starting 2-bromoisophthalic acids **5a–e** were obtained by the oxidation of the

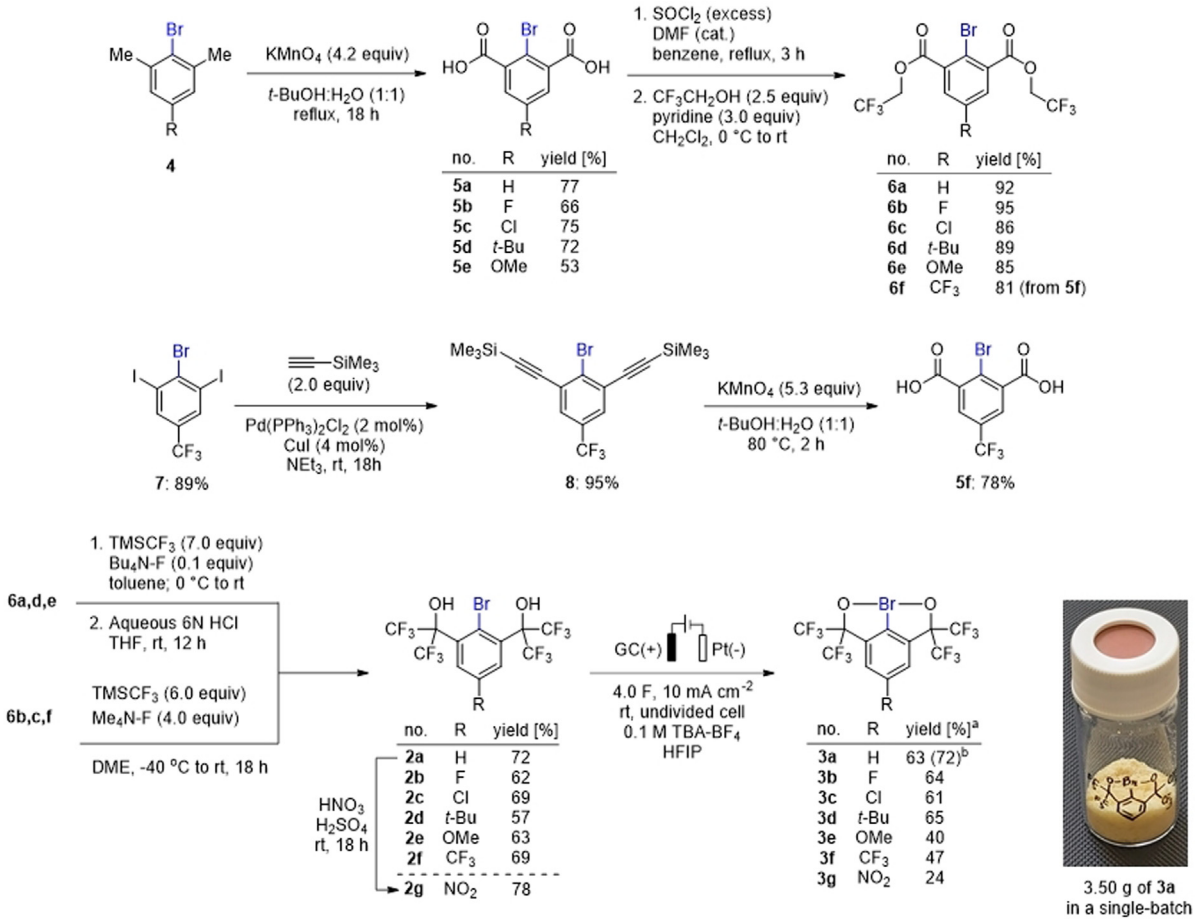

Figure 2. Synthesis of bromides **2a–g**. [a] Average yield of two runs on 0.3 mmol scale. [b] Yield on 10.0 mmol scale.

corresponding commercially available 2-bromo-*m*-xylenes **4a–e** with $KMnO_4$.[24] Acid **5f** was synthesized by chemoselective cross-coupling of the two iodo-moieties in **7** (prepared by iodination of 4-bromobenzotrifluoride)[25] with ethynyltrimethylsilane under Sonogashira cross-coupling conditions,[26] followed by oxidative cleavage of the acetylene subunit in **8** with $KMnO_4$ (Figure 2). Finally, application of the optimized electrolysis conditions (Table 1, entry 12) to the oxidation of **2b–g** rendered λ^3-bromanes **3b–g** in 24–66% yields. It should also be noted that attempts toward oxidation of **5a** and bromoarene related to **2a** carrying one chelating moiety remained unsuccessful (for details see the Supporting Information, p. S21).

For characterization of the electrochemical properties of the bromoarene/λ^3-bromane redox couples, all synthesized bromides **2a–g** were studied by cyclic voltammetry, using a 0.1 M NBu_4BF_4/HFIP electrolyte, a glassy carbon working electrode and a Ag/0.01 M $AgNO_3$ reference ($E_0 = -87$ mV vs. Fc/Fc^+ couple;[27] for more details, see p. S43). In the range between 0 and 2.7 V, each of the bromoarenes exhibits a single irreversible feature associated with the oxidation of Br^I to Br^{III}. The corresponding half-peak potentials ($E_{P/2}$) are situated in the range between 1.86 V (**2e**, R = OMe) and 2.60 V (**2g**, R = NO_2; see table in Figure 3). It follows that i) the anodically generated bromanes can be considered as strong oxidants due to the high $E_{P/2}$ values and ii) that with the compounds synthesized thus far, the potential of **2** is flexibly tunable within a range of 0.66 V. A Hammett treatment (Figure 3, bottom right) using σ_P^+ substituent coefficients[28] shows that $E_{P/2}$ is dependent on the electron donating or withdrawing ability of the substituent R and follows a linear trend according to Equation (1),

$$E_{P/2}(2) = 2.25\,\text{V} + 0.47\,\text{V}\,\sigma_P^+ \quad (1)$$

wherein the slope provides a measure of the influence of the substituents upon the observed potential, while the intercept refers to the $E_{P/2}$ of the unsubstituted compound of the series.[29]

The stabilization of the characteristic pseudo-trigonal bipyramidal geometry of λ^3-bromanes **3** by 2-benzobromaoxole rings (for X-ray structure of **3a**, see Table 1 graphics)[30] endows Martin's bromine(III) species with remarkable stability. Given the high oxidizing power and strong electrophilicity of λ^3-bromanes,[13a] the observed stability is striking. Not only it allowed for the electrosynthesis, isolation and purification of λ^3-bromanes **3a–g**, but also made possible their convenient handling and storage for extended periods of time. In the meantime, the synthetic application of λ^3-bromanes **3a–g** would require activation to unlock their intrinsic

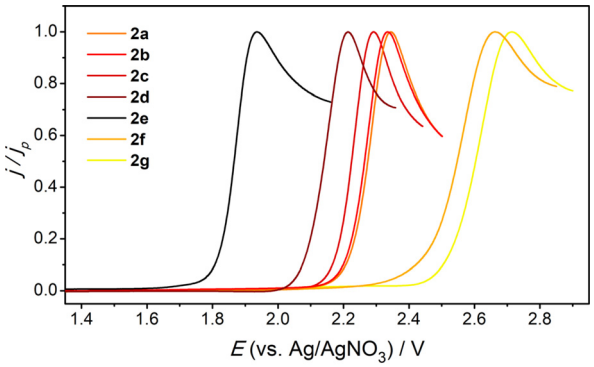

compound	$E_{P/2}$ [V]	σ_p^+
2a (R = H)	2.27	0
2b (R = F)	2.26	-0.07
2c (R = Cl)	2.22	0.11
2d (R = *t*Bu)	2.13	-0.26
2e (R = OMe)	1.86	-0.78
2f (R = CF_3)	2.54	0.61
2g (R = NO_2)	2.60	0.79

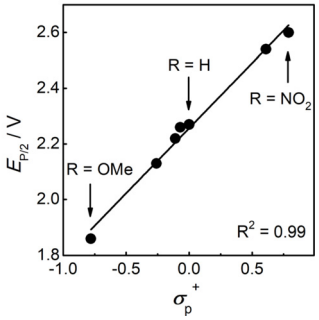

Figure 3. Top: Background and *iR* drop corrected linear sweep voltammograms (LSV) of aryl bromides **2a–g** ($c = 5$ mM) recorded at 10 mV s^{-1}. Bottom: Plot of the half-peak potentials $E_{P/2}$ (extracted from the LSVs) vs. the σ_p^+ substituent constants.

reactivity. To this end, oxidative biaryl coupling[31] was chosen as a model reaction to develop the in situ bromane activation (Figure 4). As anticipated, the non-activated **3a** did not effect the homocoupling of benzodioxole **9a** in DCM at room temperature after 18 h. We envisioned that the reactivity of λ^3-bromane **3a** could be enhanced by weakening the stabilizing effect of the two chelating *ortho*-substituents using a suitable Lewis acid.[32] Indeed, a nearly quantitative formation of biaryl **10a** (98% yield) was observed after 3 h at −30 °C (Figure 4) when **3a** was used together with TMSOTf[33] (1:2 ratio, respectively). Alternatively, $BF_3{\cdot}OEt_2$ could be employed for the activation of bromane **2a** in HFIP as the solvent (35% yield of **10a**). Finally, TfOH as additive (1.05 equiv) also effected the **3a**-mediated biaryl formation in DCM (93% yield of **10a**). Hence, both Lewis and Brønsted acids are suitable for the enhancement of λ^3-bromane reactivity possibly by increase of cationic character of **3a** upon interactions with the Lewis basic oxygen atom.[32,34] Noteworthy, CV studies showed that an in-cell mediated biaryl coupling is not possible, since the substrates are easier to oxidize than the bromoarenes (for details see the Supporting Information, p. S46).

The scope of substrates for the λ^3-bromane-mediated biaryl formation was briefly explored using TMSOTf as the activator (Figure 4 A). The reaction features remarkable functional group compatibility. Not only halides are tolerated (biaryls **10a–d**) but also allylic and propargylic subunits as

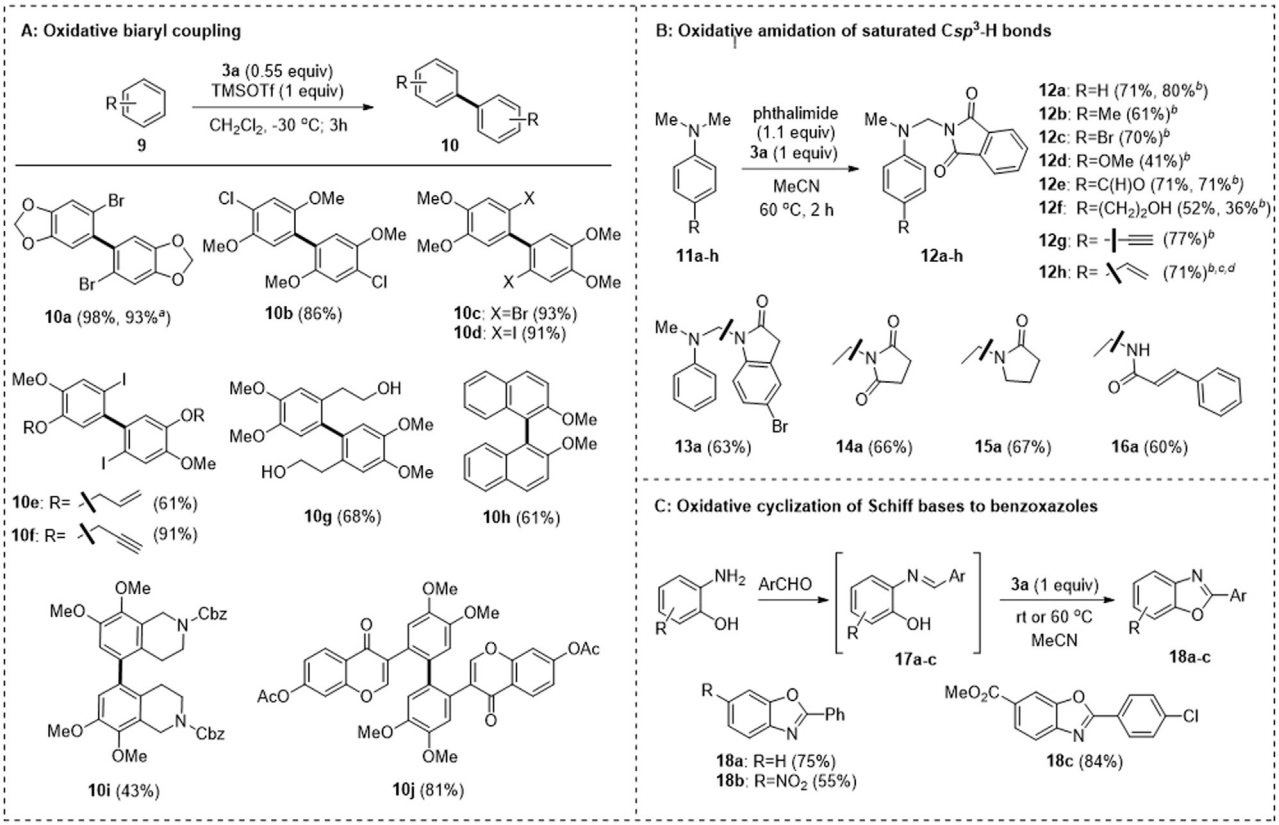

[a] Activation with 1.05 equiv. TfOH; [b] with K-phthalimide (1.1 equiv); [c] ^{1}H-NMR yields (mesitylene as an internal standard); [d] 51% isolated yield.

Figure 4. Synthetic applications of electrogenerated bromane reagent **3a**.

well as primary alcohols (**10e**,**f**,**g**, respectively) are compatible with the **3a**-mediated biaryl formation. Biaryls **10h** and **10i** as well as bi-isoflavone derivative **10j** can be also obtained using TMS-OTf activation of λ^3-bromane **3a** (Figure 4A).

We were pleased to find that λ^3-bromane **3a** also effected the oxidative amidation of *N*,*N*-dimethylanilines **11a–h** with imides (phthalimide and succinimide) as well as with various amides such as pyrrolidin-2-one, oxindole and cinnamamide (Figure 4B).[35] Relatively electron-rich anilines **11a,b,d** are suitable as substrates. Notably, the oxidative amination with λ^3-bromane **3a** is compatible with the presence of vinylic, propargylic and primary alcohol moieties in anilines (**11f–h**) as well as with bromine and aldehyde substituents (**11c**,**e**). Finally, λ^3-bromane **3a** was also found to be suitable for the oxidative cyclization of Schiff bases **17a–c** to benzoxazoles (**18a–c**; Figure 4C). Further studies to expand the application scope of λ^3-bromane **3a** are ongoing in our laboratories.

In summary, an efficient, reliable, and inexpensive approach to Martin's hypervalent bromine (III) species is reported. The key step of the synthesis is anodic oxidation of the parent aryl bromides in an undivided cell using a glassy carbon as the working electrode, platinum as the counter electrode, TBA-BF_4 as the supporting electrolyte and HFIP as the solvent. The use of an undivided cell under constant current conditions allowed for easy scale-up of the electrolysis as demonstrated by the preparation of the bench-stable λ^3-bromane in multi-gram quantities. A series of aryl bromides with oxidation half-peak potentials spanning the range from 1.86 V to 2.60 V were converted into the corresponding λ^3-bromanes. Cyclic voltammetry studies showed good correlation between the half-peak potentials and Hammett substituent coefficients for aryl bromides. The aryl bromides could be readily obtained from 2-bromoisophthalic acids in three steps. The reactivity of Martin's λ^3-bromane is sufficient for oxidative amidation and benzoxazole formation and could be further enhanced by Lewis or Brønsted acid additives as demonstrated by the successful application of the reagent in the biaryl coupling. The developed electrochemical approach to λ^3-bromanes offers considerable advantages as compared to the existing methods that rely on highly toxic, hazardous, and difficult-to-handle BrF_3 as the key reagent. Therefore, we believe that our approach may open the door to the development of unprecedented synthetic transformations that would benefit from the unique properties of hypervalent bromine(III) species.

Acknowledgements

This work was funded by ERDF (Post-Doc Latvia) project No. 1.1.1.2/VIAA/2/18/377 for I. Sokolovs and the German Research Foundation (DFG, Grant No. FR 3848/1-2). R.F. is grateful for financial support by the DFG (Heisenberg Program, Grant No. FR 3848/4-1). We thank Dr. Alexander Villinger (Institute of Chemistry, Rostock University) for X-ray structural analysis. Open access funding enabled and organized by Projekt DEAL.

Conflict of interest

The authors declare no conflict of interest.

Keywords: anodic oxidation · cyclic voltammetry · electrochemistry · hypervalent bromine · oxidative coupling

[1] a) V. V. Zhdankin, *Hypervalent Iodine Chemistry: Preparation, Structure and Synthetic Applications of Polyvalent Iodine Compounds*, Wiley, Chichester, **2013**; b) *Hypervalent Iodine Chemistry; Topics in Current Chemistry, Vol. 373* (Ed.: T. Wirth), Springer International Publishing, Cham, **2016**; c) A. Yoshimura, V. V. Zhdankin, *Chem. Rev.* **2016**, *116*, 3328–3435.

[2] "Oxidative Heterocycle Formation Using Hypervalent Iodine(III) Reagents": S. Murarka, A. P. Antonchick, in *Hypervalent Iodine Chemistry*; *Topics in Current Chemistry, Vol. 373* (Ed.: T. Wirth), Springer International Publishing, Cham, **2015**, pp. 75–104.

[3] Y. Li, D. P. Hari, M. V. Vita, J. Waser, *Angew. Chem. Int. Ed.* **2016**, *55*, 4436–4454; *Angew. Chem.* **2016**, *128*, 4512–4531.

[4] "Alkynylation with Hypervalent Iodine Reagents": J. Waser, in *Hypervalent Iodine Chemistry; Topics in Current Chemistry, Vol. 373* (Ed.: T. Wirth), Springer International Publishing, Cham, **2015**, pp. 187–222.

[5] J. Charpentier, N. Früh, A. Togni, *Chem. Rev.* **2015**, *115*, 650–682.

[6] F. Singh, T. Wirth, *Synthesis* **2013**, *45*, 2499–2511.

[7] a) Pioneering work in C–H arylation: O. Daugulis, V. G. Zaitsev, *Angew. Chem. Int. Ed.* **2005**, *44*, 4046–4048; *Angew. Chem.* **2005**, *117*, 4114–4116; b) For a seminal contribution of C–H oxidation, see: A. R. Dick, K. L. Hull, M. S. Sanford, *J. Am. Chem. Soc.* **2004**, *126*, 2300–2301; c) L. Massignan, X. Tan, T. H. Meyer, R. Kuniyil, A. M. Messinis, L. Ackermann, *Angew. Chem. Int. Ed.* **2020**, *59*, 3184–3189; *Angew. Chem.* **2020**, *132*, 3210–3215; d) Y. Kita, K. Morimoto, M. Ito, C. Ogawa, A. Goto, T. Dohi, *J. Am. Chem. Soc.* **2009**, *131*, 1668–1669; e) A. P. Antonchick, R. Samanta, K. Kulikov, J. Lategahn, *Angew. Chem. Int. Ed.* **2011**, *50*, 8605–8608; *Angew. Chem.* **2011**, *123*, 8764–8767.

[8] a) M. Elsherbini, T. Wirth, *Chem. Eur. J.* **2018**, *24*, 13399–13407; b) R. Francke, *Curr. Opin. Electrochem.* **2019**, *15*, 83–88; c) M. Elsherbini, B. Winterson, H. Alharbi, A. A. Folgueiras-Amador, C. Génot, T. Wirth, *Angew. Chem. Int. Ed.* **2019**, *58*, 9811–9815; *Angew. Chem.* **2019**, *131*, 9916–9920; d) S. Doobary, A. T. Sedikides, H. P. Caldora, D. L. Poole, A. J. J. Lennox, *Angew. Chem. Int. Ed.* **2020**, *59*, 1155–1160; *Angew. Chem.* **2020**, *132*, 1171–1176; e) J. D. Herszman, M. Berger, S. R. Waldvogel, *Org. Lett.* **2019**, *21*, 7893–7896; f) A. Maity, B. L. Frey, N. D. Hoskinson, D. C. Powers, *J. Am. Chem. Soc.* **2020**, *142*, 4990–4995; g) R. Möckel, E. Babaoglu, G. Hilt, *Chem. Eur. J.* **2018**, *24*, 15781–15785; h) R. Francke, *Curr. Opin. Electrochem.* **2021**, *28*, 100719; i) Y. N. Ogibin, M. N. Elinson, G. I. Nikishin, *Russ. Chem. Rev.* **2009**, *78*, 89.

[9] a) M. Ochiai, A. Yoshimura, K. Miyamoto, S. Hayashi, W. Nakanishi, *J. Am. Chem. Soc.* **2010**, *132*, 9236–9239; b) M. Ochiai, N. Tada, T. Okada, A. Sota, K. Miyamoto, *J. Am. Chem. Soc.* **2008**, *130*, 2118–2119.

[10] M. Ochiai, T. Okada, N. Tada, A. Yoshimura, K. Miyamoto, M. Shiro, *J. Am. Chem. Soc.* **2009**, *131*, 8392–8393.

[11] M. Ochiai, A. Yoshimura, T. Mori, Y. Nishi, M. Hirobe, *J. Am. Chem. Soc.* **2008**, *130*, 3742–3743.

[12] M. Ochiai, K. Miyamoto, T. Kaneaki, S. Hayashi, W. Nakanishi, *Science* **2011**, *332*, 448–451.

[13] a) U. Farooq, A.-H. A. Shah, T. Wirth, *Angew. Chem. Int. Ed.* **2009**, *48*, 1018–1020; *Angew. Chem.* **2009**, *121*, 1036–1038; b) K. Miyamoto, *Chemistry of Hypervalent Bromine* in *PATAI'S*

Chemistry of Functional Groups (Ed.: Z. Rappoport), Wiley, Chichester, **2018**; pp. 1 – 25.
[14] H. J. Frohn, M. Giesen, *J. Fluorine Chem.* **1998**, *89*, 59 – 63.
[15] M. M. Hoque, K. Miyamoto, N. Tada, M. Shiro, M. Ochiai, *Org. Lett.* **2011**, *13*, 5428 – 5431.
[16] M. Ochiai, Y. Nishi, S. Goto, M. Shiro, H. J. Frohn, *J. Am. Chem. Soc.* **2003**, *125*, 15304 – 15305.
[17] a) T. T. Nguyen, J. C. Martin, *J. Am. Chem. Soc.* **1980**, *102*, 7382 – 7383; b) T. T. Nguyen, S. R. Wilson, J. C. Martin, *J. Am. Chem. Soc.* **1986**, *108*, 3803 – 3811.
[18] N. L. Weinberg, H. R. Weinberg, *Chem. Rev.* **1968**, *68*, 449 – 523.
[19] E. A. Merritt, B. Olofsson, *Eur. J. Org. Chem.* **2011**, 3690 – 3694.
[20] a) T. Broese, R. Francke, *Org. Lett.* **2016**, *18*, 5896 – 5899; b) O. Koleda, T. Broese, J. Noetzel, M. Roemelt, E. Suna, R. Francke, *J. Org. Chem.* **2017**, *82*, 11669 – 11681; c) A. F. Roesel, T. Broese, M. Májek, R. Francke, *ChemElectroChem* **2019**, *6*, 4229 – 4237.
[21] H. Lenormand, V. Corcé, G. Sorin, C. Chhun, L.-M. Chamoreau, L. Krim, E.-L. Zins, J.-P. Goddard, L. Fensterbank, *J. Org. Chem.* **2015**, *80*, 3280 – 3288.
[22] A. A. Kolomeitsev, F. U. Seifert, G.-V. Röschenthaler, *J. Fluorine Chem.* **1995**, *71*, 47 – 49.
[23] Y. Imada, T. Kukita, H. Nakano, Y. Yamamoto, *Bull. Chem. Soc. Jpn.* **2016**, *89*, 546 – 548.
[24] Y. Motoyama, M. Okano, H. Narusawa, N. Makihara, K. Aoki, H. Nishiyama, *Organometallics* **2001**, *20*, 1580 – 1591.
[25] L. Kraszkiewicz, M. Sosnowski, L. Skulski, *Synthesis* **2006**, 1195 – 1199.
[26] Z. U. Levi, T. D. Tilley, *J. Am. Chem. Soc.* **2009**, *131*, 2796 – 2797.
[27] V. V. Pavlishchuk, A. W. Addison, *Inorg. Chim. Acta* **2000**, *298*, 97 – 102.
[28] C. Hansch, A. Leo, R. W. Taft, *Chem. Rev.* **1991**, *91*, 165 – 195.
[29] R. Francke, R. D. Little, *J. Am. Chem. Soc.* **2014**, *136*, 427 – 435.
[30] Deposition number 2053433 contains the supplementary crystallographic data for λ^3-bromane **3a**. These data are provided free of charge by the joint Cambridge Crystallographic Data Centre and Fachinformationszentrum Karlsruhe Access Structures service.
[31] T. Dohi, M. Ito, N. Yamaoka, K. Morimoto, H. Fujioka, Y. Kita, *Tetrahedron* **2009**, *65*, 10797 – 10815.
[32] S. Izquierdo, S. Essafi, I. del Rosal, P. Vidossich, R. Pleixats, A. Vallribera, G. Ujaque, A. Lledós, A. Shafir, *J. Am. Chem. Soc.* **2016**, *138*, 12747 – 12750.
[33] V. V. Zhdankin, A. Y. Koposov, L. Su, V. V. Boyarskikh, B. C. Netzel, V. G. Young, *Org. Lett.* **2003**, *5*, 1583 – 1586.
[34] J. N. Brantley, A. V. Samant, F. D. Toste, *ACS Cent. Sci.* **2016**, *2*, 341 – 350.
[35] a) K. Kiyokawa, T. Kosaka, T. Kojima, S. Minakata, *Angew. Chem. Int. Ed.* **2015**, *54*, 13719 – 13723; *Angew. Chem.* **2015**, *127*, 13923 – 13927; b) V. V. Zhdankin, M. McSherry, B. Mismash, J. T. Bolz, J. K. Woodward, R. M. Arbit, S. Erickson, *Tetrahedron Lett.* **1997**, *38*, 21 – 24.

Manuscript received: April 5, 2021
Accepted manuscript online: April 24, 2021
Version of record online: June 9, 2021

Publication IV

Electrochemistry and Reactivity of Chelation-stabilized Hypervalent Bromine(III) Compounds

N. Mohebbati (40%), I. Sokolovs (15%), P. Woite (10%), M. Lokov (5%), E. Parman (5%), M. Ugandi (5%), I. Leito (5%), M. Roemelt (5%), E. Suna (5%), and R. Francke (5%).

DOI: 10.1002/chem.202200974

Abstract: Hypervalent bromine(III) reagents possess a higher electrophilicity and a stronger oxidizing power compared to their iodine(III) counterparts. Despite the superior reactivity, bromine(III) reagents have a reputation of hard-to-control and difficult-to-synthesize compounds. This is partly due to their low stability, and partly because their synthesis typically relies on the use of the toxic and highly reactive BrF_3 as a precursor. Recently, we proposed chelation-stabilized hypervalent bromine(III) compounds as a possible solution to both problems. First, they can be conveniently prepared by electro-oxidation of the corresponding bromoarenes. Second, the chelation endows bromine(III) species with increased stability while retaining sufficient reactivity, comparable to that of iodine(III) counterparts. Finally, their intrinsic reactivity can be unlocked in the presence of acids. Herein, an in-depth mechanistic study of both the electrochemical generation and the reactivity of the bromine(III) compounds is disclosed, with implications for known applications and future developments in the field.

My Contribution (40%):

I carried out all the electrochemical measurements, including mechanistic studies of bromine(IIII) generation. I. Sokolovs (15%) performed the studies on activation of λ^3-bromanes and their application as reagents. P. Woite (10%) carried out the quantum chemical calculations for investigation of the mechanism of λ^3-bromanes formation together with M. Ugandi (5%) under supervision of M. Roemelt (5%). Acid titration experiments with λ^3-bromanes were performed by E. Parman (5%) together with M. Lokov (5%),supervised by I. Leito (5%). E. Suna (5%) and R. Francke (5%) had the idea of the project and supervised the progress, as well as writing the manuscript.

Chemistry Europe Amplifying Great Science

Chemistry Europe
European Chemical Societies Publishing

Stop by our **booth #3**

EuChemS Chemistry Congress
28 August to 1 September
2022 · LISBON.PT

Chemistry Europe Symposium

Monday, August 29, 9:15 – 12:30
Room #9

- We will celebrate the 10th anniversaries of *ChemistryOpen* and *ChemPlusChem*
- Mark the launch of *Chemistry-Methods* and *Analysis & Sensing*
- And introduce the redesign of *ChemistryViews* on a new platform

Join us for five fascinating talks by top scientists

Célia Fonseca-Guerra
Vrije Universiteit Amsterdam

Francesco Ricci
Rome Tor Vergata

Javier García Martínez
Universidad de Alicante
Current President of IUPAC

Anat Milo
Ben Gurion University

Ramón Martínez Mánez
Universitat Politècnica de Valènzia

We look forward to seeing you in Lisbon

chemistry-europe.org

Chemistry–A European Journal | Research Article
doi.org/10.1002/chem.202200974
Chemistry Europe
European Chemical Societies Publishing
www.chemeurj.org

Electrochemistry and Reactivity of Chelation-stabilized Hypervalent Bromine(III) Compounds

Nayereh Mohebbati,[a, b] Igors Sokolovs,[c] Philipp Woite,[d] Märt Lõkov,[e] Elisabeth Parman,[e] Mihkel Ugandi,[d] Ivo Leito,*[e] Michael Roemelt,*[d] Edgars Suna,*[c, f] and Robert Francke*[a, b]

Abstract: Hypervalent bromine(III) reagents possess a higher electrophilicity and a stronger oxidizing power compared to their iodine(III) counterparts. Despite the superior reactivity, bromine(III) reagents have a reputation of hard-to-control and difficult-to-synthesize compounds. This is partly due to their low stability, and partly because their synthesis typically relies on the use of the toxic and highly reactive BrF_3 as a precursor. Recently, we proposed chelation-stabilized hypervalent bromine(III) compounds as a possible solution to both problems. First, they can be conveniently prepared by electro-oxidation of the corresponding bromoarenes. Second, the chelation endows bromine(III) species with increased stability while retaining sufficient reactivity, comparable to that of iodine(III) counterparts. Finally, their intrinsic reactivity can be unlocked in the presence of acids. Herein, an in-depth mechanistic study of both the electrochemical generation and the reactivity of the bromine(III) compounds is disclosed, with implications for known applications and future developments in the field.

Introduction

The chemistry of hypervalent halogen species has experienced tremendous progress in recent decades, with hypervalent iodine(III) compounds playing an increasingly important role in modern organic synthesis.[1] The related isoelectronic hypervalent bromine(III) reagents exhibit stronger electrophilicity, better nucleofugality of the bromanyl unit, and more driving force for oxidations,[2–4] as evidenced by a series of unprecedented synthetic transformations involving oxidative coupling of alkynes and primary alcohols to conjugated enones,[5] Hofmann rearrangement of sulfonamides to the corresponding *N*-arylsulfamoyl fluorides,[6] regioselective C–H functionalization of non-activated alkanes,[7,8a] and a rare Bayer-Villiger-type oxidation of open-chain aliphatic aldehydes.[9] Recently, the application of diaryl-λ^3-bromanes in catalysis[10] and in cycloaddition reactions[11] was also reported. Although these notable achievements underscore the remarkable synthetic potential of this reagent class, hypervalent bromine(III) chemistry appears to be underdeveloped in comparison to that of the iodine(III) counterparts. This notable disparity has been ascribed to two unfavorable factors. First, bromine(III) reagents exhibit poor stability and high oxidizing power, which has led to the general perception of difficult-to-control reactivity and poor compatibility with functional groups.[2,3] Second, conventional routes to λ^3-bromane reagents rely eventually on the use of BrF_3, a highly toxic and extremely reactive liquid that demands for specific equipment and experimental techniques for its safe handling.[8]

Recently, a chelation-stabilized λ^3-bromane reagent[12] (Martin's bromane **2**, Scheme 1) was proposed as a possible solution to both the stability and the accessibility issue. Inspired by the successful *in situ* generation of reactive hypervalent iodine species via anodic oxidation of iodoarene precursors,[13,14] we presented a convenient electrochemical approach toward synthesis of **2**.[15] The method is based on the anodic oxidation of parent aryl bromides **1** containing two coordinating hexafluoro-2-hydroxy-propanyl substituents under galvanostatic conditions in an undivided cell (Eq. (1) in Scheme 1). The protocol was used to prepare a series of *para*-substituted derivatives of

[a] *N. Mohebbati, Prof. Dr. R. Francke*
Leibniz Institute for Catalysis
Albert-Einstein-Str. 29a, 18059 Rostock (Germany)
E-mail: robert.francke@catalysis.de
[b] *N. Mohebbati, Prof. Dr. R. Francke*
Institute of Chemistry
Rostock University
Albert-Einstein-Str. 3a, 18059 Rostock (Germany)
[c] *Dr. I. Sokolovs, Prof. Dr. E. Suna*
Latvian Institute of Organic Synthesis
Aizkraukles 21, 1006 Riga (Latvia)
E-mail: edgars@osi.lv
[d] *P. Woite, M. Ugandi, Prof. Dr. M. Roemelt*
Department of Chemistry
Humboldt-University of Berlin
Brook-Taylor-Str. 2, 12489 Berlin (Germany)
E-mail: michael.roemelt@hu-berlin.de
[e] *Dr. M. Lõkov, E. Parman, Prof. Dr. I. Leito*
Institute of Chemistry
University of Tartu
Ravila 14a, 50411 Tartu (Estonia)
E-mail: ivo.leito@ut.ee
[f] *Prof. Dr. E. Suna*
Faculty of Chemistry
University of Latvia
Jelgavas 1, 1004 Riga (Latvia)

Supporting information for this article is available on the WWW under https://doi.org/10.1002/chem.202200974

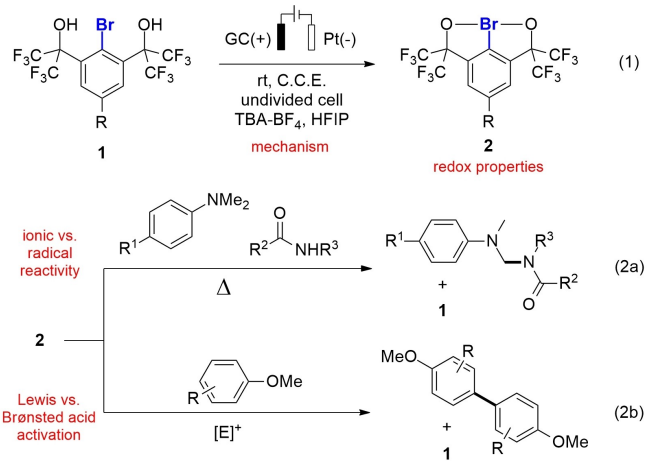

Scheme 1. Electrochemical generation of aryl-λ^3-bromanes **2** (Eq. (1)) and applications as reagent (Eq. (2)).

Martin's bromane **2** that revealed remarkably high redox potentials covering a range from 1.86 V to 2.60 V versus Ag/$AgNO_3$. The compounds are benchtop-stable and have proven useful as reagents in various transformations. Thus, λ^3-bromane **2a** (R=H) was shown to be sufficiently reactive to effect clean oxidative amidation of aniline derivatives (Eq. (2a) in Scheme 1). Furthermore, the intrinsic reactivity of hypervalent bromine(III) species can be unlocked by addition of Brønsted or Lewis acids, for example to achieve dehydrogenative homocoupling of substituted anisoles (Eq. (2b) in Scheme 1). Herein, mechanistic insights into both the electrochemical generation and the reactivity of chelation-stabilized bromine(III) compounds are disclosed.

Results and Discussion

Anodic bromane generation

To better understand the mechanism of bromane formation, we intended to combine detailed electroanalytical studies with quantum chemical modeling. In our previous work,[15] we have already obtained some information about bromoarene oxidation by performing preliminary electroanalytical experiments. Thus, voltammetric analysis of **1** at 10 mV s^{-1} between 0 and 2.7 V versus Ag/0.01 M $AgNO_3$ (E_{ref} = −87 mV vs. Fc/Fc^+ couple)[16] using an electrolyte consisting of 0.1 M NBu_4BF_4 in HFIP showed that each of the bromoarenes exhibits a single irreversible anodic feature. The corresponding half-peak potentials ($E_{P/2}$) are situated between 1.86 V (**1e**, R=OMe) and 2.60 V (**1g**, R=NO_2), which means that the potential of **1** is flexibly tunable within a range of 0.74 V (see Table 1). A linear relationship between $E_{p/2}$ and σ_P^+ substituent coefficients showed that the oxidizability is dependent on the electron donating or withdrawing ability of the substituent R and that the redox potential of the **1**/**2** couple thus exhibits a somewhat predictable behavior.

Table 1. Summary of the half-peak potentials ($E_{P/2}$, determined at v = 10 mV s^{-1}) and slopes of the j_p vs. $v^{0.5}$ plots for the anodic oxidation of **1** in HFIP.

compound	R	$E_{P/2}$ [V]	slope j_p vs. $v^{0.5}$ [mA $s^{0.5}$ $mV^{-0.5}$ cm^{-2}]
1a	H	2.27	0.156
1b	F	2.26	0.161
1c	Cl	2.22	0.194
1d	*t*Bu	2.13	0.168
1e	OMe	1.86	0.088
1f	CF_3	2.54	0.150
1g	NO_2	2.60	0.140

For the present study, one of the aims was to learn more about the mechanism of the formation of **2**. For this purpose, the scan rate v was increased stepwise from 10 mV s^{-1} to 1 V s^{-1}. The observed voltammetric responses of **1a** are characteristic for the bromoarene series with the signal shape indicating that one or more chemical steps are coupled to the electron transfer ("chemical irreversibility", see representative CVs in Figure 1A).[17] Bromoarenes **1b–d**, **1f** and **1g** exhibit analogous behavior (see the Supporting Information), whereas the voltammetry of **1e** (R=OMe) is rather exceptional (Figure 1B). Initially, **1e** displays irreversible behavior at low scan rates (dashed curve), followed by a gradual change to almost full reversibility with increasing v (dotted and solid lines, for $j_{p,ox}/j_{p,red}$ ratios see Table S2 in the Supporting Information),

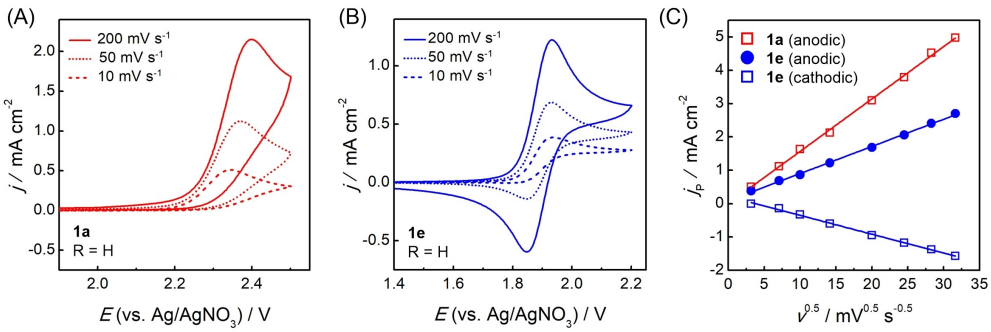

Figure 1. A and B: Background and *iR* drop-corrected CVs of 5 mM **1a** and 5 mM **1e** at different scan rates (solvent: HFIP, working electrode: glassy carbon, supporting electrolyte: 0.1 M Bu_4NBF_4). C: Plot of the peak current densities (j_P) vs. $v^{0.5}$.

indicating that the intermediate formed upon electron transfer is stable on the voltammetry time scale.

Another striking difference between **1e** and the other bromoarenes is that the anodic peak current density j_p of the 4-OMe-substituted compound is significantly smaller. Both j_P and the slope of the linear fit of j_p versus $v^{0.5}$ are approximately half as high as the average values for the other compounds (see Figure 1C and Table 1). One-electron oxidation of **1e** and two-electron oxidation of the other bromoarenes, provide a reasonable rationale for this difference. In fact, it is well-established that a j_p value (and a j_p vs. $v^{0.5}$ slope, respectively) twice as high as for a comparable one-electron transfer is characteristic of a two-electron process in which *i*), the second oxidation is energetically more favorable than the first one and *ii*), in which a fast chemical reaction is interposed between the two electrochemical steps.[18]

A mechanism consistent with the observations described above is shown in Figure 2. Accordingly, bromanes **2** are generally formed via two electrochemical oxidation steps in an ECEC pathway, which includes initial electron abstraction, deprotonation, further oxidation, and a second deprotonation (leading to $\mathbf{1}^{\bullet+}$, $\mathbf{1}^{\bullet}$, $\mathbf{2}^{+}$, and **2**, respectively). Competitive homogeneous disproportionation of $\mathbf{1}^{\bullet}$ (or between $\mathbf{1}^{\bullet+}$ and $\mathbf{1}^{\bullet}$) within the diffusion layer would also be in agreement with the diagnostic criteria (ECE_{disp} pathway).[17] However, when the deprotonation step $\mathbf{1}^{\bullet+}\rightarrow\mathbf{1}^{\bullet}$ is slow due to a stabilization of $\mathbf{1}^{\bullet+}$,

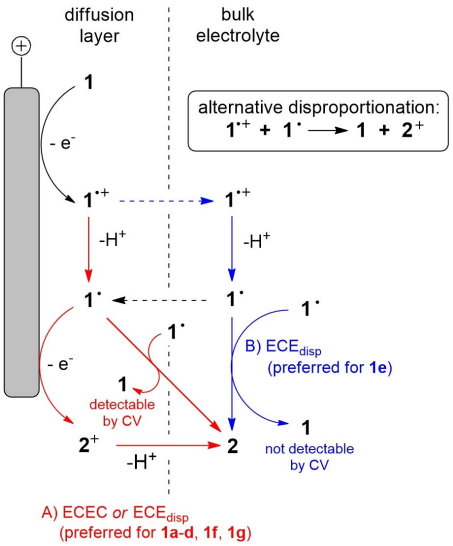

Figure 2. Proposed mechanism for anodic bromane formation.

the radical cation has sufficient time to diffuse into the bulk solution, where $\mathbf{1}^{\bullet}$ is slowly formed (Figure 2, pathway highlighted in blue). Subsequent disproportionation again leads to the formation of **2** and **1** ($\mathbf{2}^{+}$ and **1**, respectively). Such a delayed disproportionation would explain the distinct behavior of **1e**, as it is in agreement both with the one electron peak in the CV and the observed formation of **2e** in the preparative-scale electrolysis. Here, the electron-donating ability of the 4-methoxy substituent seems to be responsible for the enhancement of the lifetime of $\mathbf{1e}^{\bullet+}$.

Further probing into the mechanism of bromane formation was carried out with a series of quantum chemical calculations using a state-of-the-art combination of density functional theory and coupled cluster methods (see computational details in the Supporting Information). The obtained results presented in Table 2 confirm the feasibility of the reaction sequence $\mathbf{1}\rightarrow\mathbf{1}^{\bullet+}\rightarrow\mathbf{1}^{\bullet}\rightarrow\mathbf{2}^{+}\rightarrow\mathbf{2}$ in terms of reaction free energies for all investigated derivatives. For all proton transfer reactions, cathodically generated HFIP anions have been assumed as proton acceptors, as has been established previously.[14] The investigated deprotonations occur spontaneously without any barrier *in silico*. Similarly, the outer sphere electron transfer is expected to be associated with reaction barriers that are readily overcome under the given reaction conditions, since the redox-active sites are well accessible in all cases.

A closer look at the individual reaction steps yields interesting insight into certain aspects of the observed reactivity and provides further support for the proposed reaction mechanism (Table 2). For example, in good agreement with the experimental observations, the calculated ionization energy of $\mathbf{1}^{\bullet}$ is lower than that of **1**, rendering the second electron transfer more favorable than the first one. In contrast, the ionization free energy of $\mathbf{1}^{\bullet+}$ is predicted to be significantly higher. On the basis of these results, the possibility for formation of **2** via an EEC mechanism appears unlikely.

It is furthermore interesting to consider the calculated free energy of the disproportionation reactions $\mathbf{1}^{\bullet+}+\mathbf{1}^{\bullet}\rightarrow\mathbf{2}+\mathbf{2}^{+}$ as well as $2\ \mathbf{1}^{\bullet}\rightarrow\mathbf{1}+\mathbf{2}$, which are favorable for all investigated derivatives with predicted free energies of approx. $-30\ kcal\,mol^{-1}$. Only for $\mathbf{1e}^{\bullet+}+\mathbf{1e}^{\bullet}\rightarrow\mathbf{2e}+\mathbf{2e}^{+}$ the reaction free energy is significantly less negative ($-14.5\ kcal\,mol^{-1}$). This finding can be attributed to the relative stability of $\mathbf{1e}^{\bullet+}$ that originates from the electron-donating character of the 4-methoxy group. The spin density plots shown in Figure 3 reflect this assessment. Moreover, our calculations indicate that $\mathbf{1e}^{+\bullet}$ is less prone to deprotonation than all other $\mathbf{1}^{+\bullet}$ derivatives ($-34.0\ kcal\,mol^{-1}$ vs. approx. $-50\ kcal\,mol^{-1}$) and thereby cor-

Table 2. Calculated [DFT + DLPNO-CCSD(T)] reaction free energies (in kcal mol^{-1}) for all elementary steps of the electrochemical conversion of **1** to **2**.

Derivative	$1\rightarrow1^{\bullet+}$	$1^{\bullet+}\rightarrow1^{\bullet}$	$1^{\bullet+}\rightarrow1^{2+}$	$1^{\bullet}\rightarrow2^{+}$	$2^{+}\rightarrow2$	$1\rightarrow2$	$2\ 1^{\bullet}\rightarrow1+2$	$1^{\bullet+}+1^{\bullet}\rightarrow2+2^{+}$
a	169.9	−49.2	180.3	139.2	−49.5	210.5	−31.1	−30.7
b	170.8	−49.8	181.4	141.4	−50.1	212.4	−29.6	−29.4
c	170.4	−49.4	180.8	141.8	−51.3	211.5	−30.5	−28.6
d	169.0	−48.0	178.9	139.7	−49.1	211.6	−30.3	−29.3
e	154.5	−34.0	169.6	140.0	−50.0	210.5	−30.5	−14.5
f	170.9	−50.5	180.5	143.0	−52.7	210.7	−30.1	−28.0
g	171.5	−51.3	182.2	143.5	−52.3	211.4	−29.1	−28.1

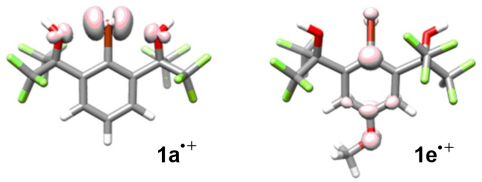

Figure 3. Comparison between the spin density distributions of **1a**$^{\bullet+}$ and **1e**$^{\bullet+}$.

roborate the proposed mechanism for the formation of **2e**. Considering the significant driving force for both disproportionation reactions, we assume that the predominant reaction type will most likely be determined by the availability of the involved species (**1e**$^{\bullet+}$ vs. **1e**$^{\bullet}$) rather than by thermodynamic factors.

Another experimental observation supports the proposed ECE_{disp} mechanism for **1e**→**2e**. During preparative-scale electrolysis of **1**, the electrolyte solution usually remains colorless or, sometimes, becomes slightly yellowish. Only the oxidation of **1e** leads to a deep red coloration of the electrolyte solution, which disappears shortly after switching off the current. This prompted us to perform a spectroelectrochemical (SEC) analysis of the oxidation of **1e** (see Figure 4). After applying a potential of 2.0 V, two bands arise simultaneously at 336 nm and 534 nm (Figure 4, bottom) in addition to the band of **1e** at 288 nm. An apparent increase of the latter can be assigned to formation of **2e**, which absorbs at similar wavelengths (284 nm, see pure component spectrum in Figure 4, top). The new features are in good agreement with the bands predicted by quantum chemical calculations (321 nm and 487 nm). Noteworthy, no bands in the respective energy regimes are predicted for **1e**$^{\bullet}$ and **2e**$^{+}$ (see Table S8 in the Supporting Information). After switching off the potential, the bands at 336 nm and 534 nm rapidly disappear, while the signal for **2e** continues to increase, which is further evidence for the proposed disproportionation mechanism.

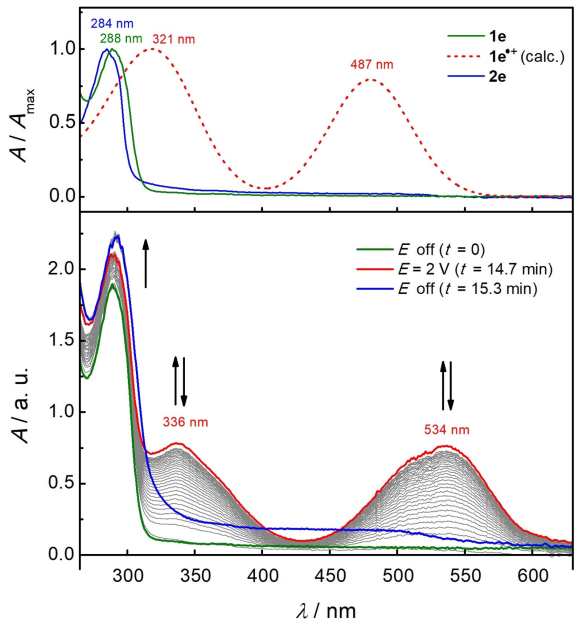

Figure 4. Top: Absorption spectra of pure **1e** (green line) and **2e** (blue line) recorded in HFIP along with the predicted spectrum of **1e**$^{\bullet+}$ (dotted red line). Bottom: Spectroelectrochemical analysis of the anodic oxidation of **1e** at $E = 2.0$ V vs. $Ag/AgNO_3$ (anode: Pt grid).

Cathodic reduction of bromanes

As described in the previous section, the CVs of the bromoarenes recorded in HFIP show that with the exception of **1e**, the compounds are irreversibly oxidized, meaning that there is no associated reduction peak in the reverse scan. Thus, the anodically generated bromanes appear to be surprisingly robust toward reduction at the cathode. Knowledge of the cathodic behavior is still desirable, as it allows conclusions to be drawn about the properties of **2** as a chemical oxidant (see below). In this regard, an electroanalytical study demands for employing solvents that were used in the synthetic applications, that is, acetonitrile for C–H amidations and dichloromethane for arene-arene homocouplings (Eq. (2a) and (2b) in Scheme 1).[15] CV studies of the cathodic reduction were thus carried out in each of these solvents using a glassy carbon working electrode and NBu_4BF_4 as the supporting electrolyte, whereby both the shape of the profiles and the half-peak potentials are quite similar.

In the range between 0.1 and −0.9 V, each of the bromanes exhibits a single irreversible feature, indicating that electron transfer is followed by a rapid chemical step. The forward scans are shown in Figure 5 exemplarily for acetonitrile (for full CVs, see the Supporting Information). The corresponding $E_{P/2}$ values are situated in the range between −0.35 V (**2g**, R=NO_2) and −0.53 V (**2e**, R=OMe; see table in Figure 5). It follows that *i*) electrochemical reduction of **2** is relatively difficult, *ii*) with 0.18 V, the range of reduction potentials covered by series **2** is relatively narrow compared to the range of oxidation potentials of **1** (0.74 V). A good match was found between the experimental half-peak potentials and $E_{P/2}$ values predicted on the basis of a two-parameter correlation with σ_F and σ_R substituent constants (Figure 5, bottom right; for details see Tables S5 and S6 in the Supporting Information), the latter two explicitly accounting for inductive (σ_F) and resonance effects (σ_R).[19] Accordingly, there is a correlation between $E_{P/2}$ and electron-donating/withdrawing ability of R, indicating the inclusion of the aromatic ring in the reduction process (albeit, apparently, to a much lesser extent than for the oxidation of **1**).

Surprisingly, further analysis of the reduction peaks shows that the process, both in CH_3CN and CH_2Cl_2, is associated with merely a single electron exchange (see the Supporting Information). To better understand the underlying mechanism, **2a** was subjected to controlled potential electrolysis (CPE, Scheme 2). In acetonitrile, bromoarene **1a** could be isolated in 74% yield after passing 1.0 F at −0.78 V versus Ag/0.01 M $AgNO_3$ (11% recovered **2a**). This result is in agreement with the one electron peak observed in the CV experiments, and can be explained by initial formation of radical anion **2a**$^{\bullet-}$, followed by

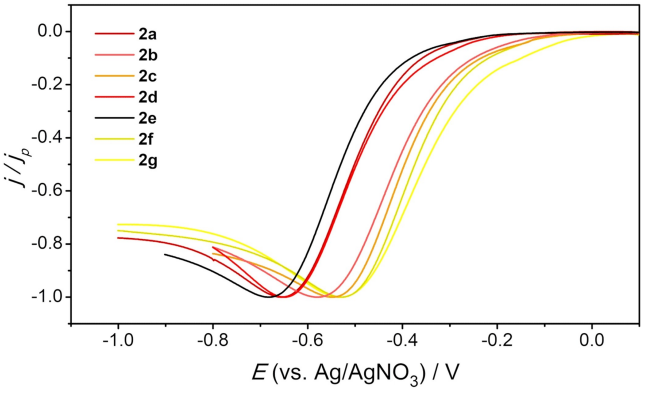

compound (group R)	$E_{P/2}$ (obs.) [V]	$E_{P/2}$ (pred.) [V]
2a (H)	-0.50	-0.50
2b (F)	-0.41	-0.42
2c (Cl)	-0.39	-0.43
2d (*t*-Bu)	-0.50	-0.50
2e (OMe)	-0.53	-0.50
2f (CF_3)	-0.37	-0.38
2g (NO_2)	-0.35	-0.33

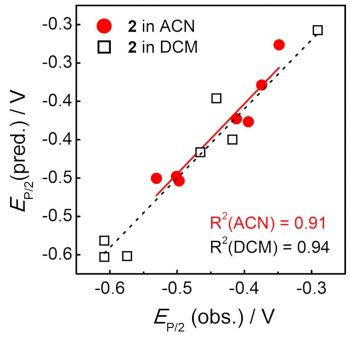

Figure 5. Top: Background and *iR* drop corrected linear sweep voltammograms (LSV) of bromanes **2a-g** (c = 5 mM) recorded at 10 mV s^{-1} in CH_3CN. Bottom left: Half-peak potentials $E_{P/2}$(obs.) measured in CH_3CN and the values predicted using σ_R and σ_F substituent constants ($E_{P/2}$(pred.), for details see the Supporting Information). Bottom right: Correlation between $E_{P/2}$(obs.) and $E_{P/2}$(pred.) for **2** in CH_2Cl_2 and CH_3CN.

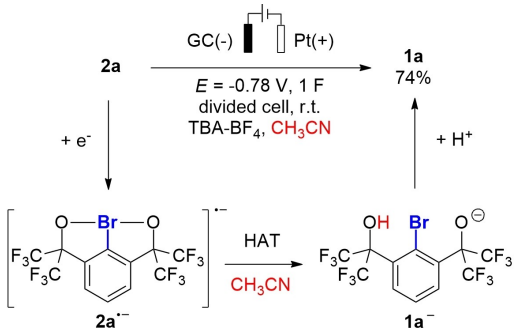

Scheme 2. Results of preparative-scale cathodic reduction of **2a** in CH_3CN.

hydrogen atom transfer (HAT) from a solvent molecule leading to **1a**$^-$.[20] The latter is protonated either by anodically generated acids (the anodic half-cell reaction is electrolyte degradation)[21] or during workup.

Ionic versus radical reactivity

The results of the cathodic scans and CPE suggest that although formation of **2a**$^{\bullet-}$ is in principle feasible, the one electron reduction is unfavorable and proceeds at negative potentials. For applications in synthetic organic chemistry, λ^3-bromane **2a** can thus be considered a poor single electron oxidant. This important finding prompted us to study mechanisms of the recently published reactions involving **2a**, such as oxidative amination of *N*,*N*-dimethylanilines **3** (Eq. (1), Scheme 3).[15] The oxidative amination apparently proceeds through the addition of phthalimide **5** to iminium ion **4a** that is formed *in situ* from parent aniline **3a** and hypervalent bromine(III) reagent **2a**. A calculated free energy of −19.3 kcal mol^{-1} confirms the thermodynamical feasibility of iminium **4a** formation induced by **2a**. However, a literature survey returns controversial mechanisms for iminium **4a** formation from aniline **3a** and hypervalent iodine(III) species, related to **2a**. Thus, a single electron transfer (SET) from aniline **3a** to hydroxybenziodoxole[22] or PIDA[23] was proposed to generate transient radical cation **3a**$^{\bullet+}$ *en route* to the iminium ion **4a** (Eq. (2), Scheme 3). An alternative mechanistic scenario towards iminium ion **4a** involves β-deprotonation of transient aniline-containing iodine(III) species **TS-2** (Eq. (3), Scheme 3).[24] Given the apparent inconsistency in the mechanism of the iodine(III)-mediated oxidative amination reaction, we decided to examine in more detail the reaction of aniline **3a** with λ^3-bromane **2a**.

The comparison of the measured oxidation potential for aniline **3a** ($E_{P/2}$ = 0.40 V) with the reduction potential of λ^3-bromane **2a** ($E_{P/2}$ = −0.50 V) in MeCN shows a large potential gap of 0.9 V, suggesting that SET oxidation of aniline **3a** by **2a** is thermodynamically unfavorable. This assessment is supported by calculations showing that the formation of **2a**$^{\bullet-}$ and **3a**$^{\bullet+}$ is endergonic (ΔG = 20.1 kcal mol^{-1}). Of note, electrochemically generated radical cation **3a**$^{\bullet+}$ was found to be highly unstable and short-lived in MeCN with a half-life on the order of microseconds.[25] Furthermore, radical cation **3a**$^{\bullet+}$ was reported to undergo rapid dimerization to *N*,*N*,*N*,*N*-tetramethylbenzidene (TMB; see Scheme 2, Eq. (2)) with an extremely high rate constant ($k = 2.5 \times 10^8$ M^{-1} s^{-1}).[26] The lack of evidence for the formation of TMB upon mixing the equimolar amounts of **2a** and **3a** in MeCN (in absence of **5**) renders highly unlikely the involvement of radical cation **3a**$^{\bullet+}$ in the oxidative amination.[27]

Additional experimental evidence against the intermediacy of radical cation **3a**$^{\bullet+}$ in the oxidative amination was obtained by a control experiment using aniline **3b** as the radical clock probe.[28] Assuming that SET between **3b** and λ^3-bromane **2a** is feasible, the generated radical cation **3b**$^{\bullet+}$ should feature aryl radical character (shown are only two resonance forms for **3b**$^{\bullet+}$; see Eq. (4), Scheme 3). The *O*-allyl-substituted aryl radicals such as **3b**$^{\bullet+}$ are well-known to undergo the radical 5-*exo* cyclization to **7**$^{\bullet+}$ with an extremely high rate constant (k = 6.3×10^9 s^{-1} at 30 °C).[29] Subsequent deprotonation and hydrogen atom transfer from MeCN would furnish 2,3-dihydrobenzofurane **8**. Notably, the formation of **8** was not observed in the crude reaction mixture of the oxidative amination. Instead, the desired oxidative amination product **6b** was isolated in 63% yield (Eq. (1), Scheme 3). Finally, important evidence against the intermediacy of radical cation **3a**$^{\bullet+}$ was obtained by EPR studies. Specifically, the formation of radicals could not be observed upon mixing λ^3-bromane **2a** (0.1 M solution in MeCN)

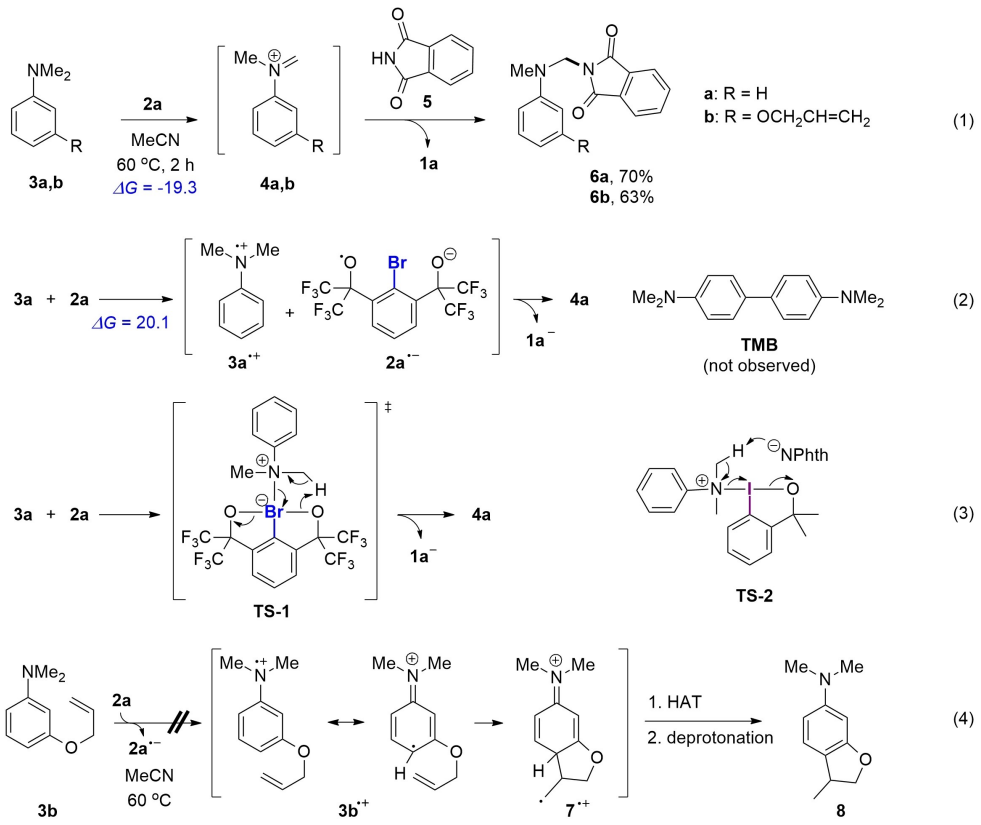

Scheme 3. Mechanistic studies of oxidative aminations induced by **2a** (calculated free energies in kcal mol^{-1}).

with aniline **3a** (0.1 M solution in MeCN) at room temperature. In striking contrast, the formation of a persistent radical intermediate from **2a** and **3a** was clearly observed when HFIP was used as the solvent at room temperature (for details see Figure S5 in the Supporting Information). Furthermore, the oxidative amination experiment in HFIP using aniline **3b** as the radical clock probe (Eq. (4), Scheme 3) returned a highly complex mixture of unidentified products. This result implies a change of the reaction mechanism upon replacing MeCN by HFIP as the solvent. Consequently, the combined mechanistic evidence suggests the SET oxidation of anilines to radical cations **3**$^{\bullet+}$ by λ^3-bromane **2a** is unlikely under the published oxidative amination conditions in MeCN as the solvent.[15] The formation of iminium ion **4a** in MeCN apparently follows an ionic pathway, involving intramolecular β-deprotonation within a transient [12-Br-4] complex **TS-1** between aniline **3a** and Lewis acidic λ^3-bromane **2a** (Eq. (3), Scheme 3). In agreement with the abundant experimental evidence, quantum chemical calculations suggest that an ionic pathway to **6a** via **4a** is thermodynamically well feasible as illustrated by Figure S8 in the Supporting Information.

Acidic bromane activation

In contrast to the efficiency of λ^3-bromane **2a** in the oxidative amination of anilines, the activation of bromine(III) reagent **2a** by the addition of Lewis or Brønsted acids was found to be necessary to accomplish the homocoupling of arenes such as **9** to biaryl **10** in CH_2Cl_2 (Eq. (1), Scheme 4).[15] Importantly, the closely related hypervalent iodine(III)-mediated oxidative biaryl coupling was shown to proceed through SET oxidation of electron-rich arenes to the corresponding cation radicals **11**$^{\bullet+}$ (Eq. (2), Scheme 4),[30] and Lewis acid additives such as $BF_3{\cdot}OEt_2$ were required to enhance the SET oxidizing ability of $PhI(OCOCF_3)_2$.[31,32] Assuming a similar mechanism for iodine(III) and bromine(III)-mediated biaryl coupling, the requirement for a Lewis acid additive to enhance the SET oxidizing ability of λ^3-bromane **2a** becomes evident given its more negative reduction potential ($E_{P/2} = -0.57$ V) compared to $PhI(OCOCF_3)_2$ ($E_{P/2} = -0.20$ V, see the Supporting Information).

TMS-OTf was chosen as Lewis acid additive for the bromine(III)-mediated biaryl coupling.[33] A nearly quantitative formation of biaryl **10** (98% yield) was observed after 3 h at −30 °C (Eq. (1), Scheme 4), when **2a** was used together with 1 equiv. TMS-OTf.[34] It should be noted that the formation of **10** was not observed with added TMS-OTf in the absence of **2a**. Importantly, TfOH as the additive (1.05 equiv) also resulted in the **2a**-mediated formation of biaryl in DCM as the solvent (93% yield of **10**). This observation led us to hypothesize that partial hydrolysis of TMSOTf by traces of water under the biaryl coupling conditions may take place to form TfOH, which is the actual activator of **2a**.[35] To verify this hypothesis, the TMSOTf-mediated biaryl coupling was performed under standard

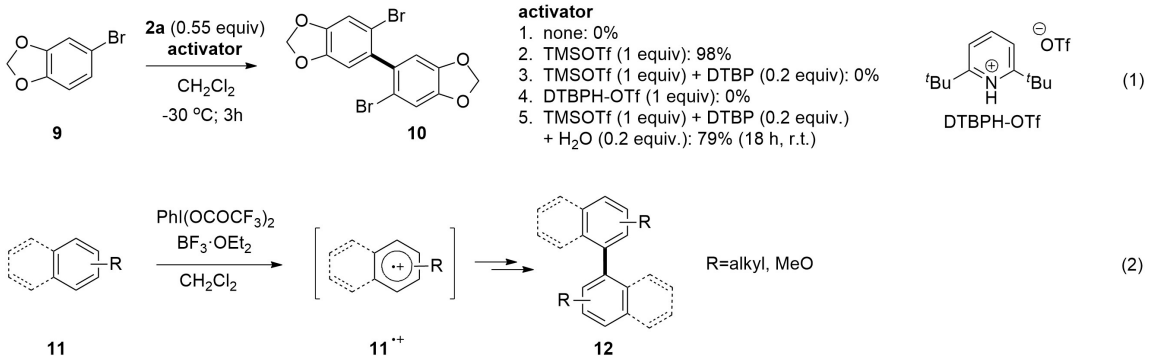

Scheme 4. Activation of **2a** for oxidative biaryl homo-coupling.

reaction conditions in the presence of sub-stoichiometric amounts of DTBP (0.2 equiv) as a proton scavenger (Eq. (1), Scheme 4). The formation of **10** was not observed with the added DTBP. Furthermore, the biaryl coupling also did not proceed in the presence of 2,6-di-*tert*-butylpyridinium triflate (1.0 equiv; prepared *in situ* from equimolar amounts of TfOH and DTBP), a relatively weak Brønsted acid that is generated upon proton quench by DTBP. However, biaryl **10** was slowly formed in 79% yield using TMSOTf (1 equiv) with added DTBP (0.2 equiv) and water (0.2 equiv) at room temperature. Possibly, a small excess of TfOH (trace amounts of the acid present in TMSOTf combined with TfOH that was formed upon hydrolysis of TMSOTf) with respect to DTBP was sufficient to catalyze the formation of biaryl **10**. Taken together, these experiments provide evidence favoring the activation of the biaryl coupling by TfOH that is generated *in situ* from TMS-OTf.

Additional support for the acid-base interactions between λ^3-bromane **2a** and Brønsted acid was obtained by NMR experiments. Thus, a downfield displacement of ^{1}H NMR signals ($\delta = 0.03$ and 0.04 ppm) and ^{19}F NMR signal ($\delta = 0.19$ ppm) for λ^3-bromane **2a** was observed upon addition of two equivalents of TfOH (see table, Figure 6B). In sharp contrast, the addition of TMSOTf (2 equiv) or $BF_3{\cdot}OEt_2$ (2 equiv) did not lead to noticeable changes in the NMR spectra of **2a**. Apparently, TMS-OTf is not a sufficiently strong Lewis acid to form a stable complex with the moderately Lewis basic oxygen atom of the bromaoxole subunit in **2a**. Overall, the experiments above provide evidence that the activation of λ^3-bromane **2a** requires protonation by a strong Brønsted acid such as TfOH (Figure 6A).

Quantum chemical calculations were performed to provide additional insights into the protonation of λ^3-bromane **2a** with TfOH. According to our results on the local coupled cluster level of theory, the protonation of **2a** to **2a–TfOH** is associated with a free reaction energy of $\triangle G = 5.8$ kcal mol^{-1} and virtually no reaction barrier (see Figure 6A; the optimized geometry of the adduct is shown in Figure 6C). This implies that only a small fraction of **2a** is protonated by added stoichiometric TfOH which agrees well with the relatively small displacements in chemical shifts observed in ^{19}F and ^{1}H NMR spectra for the 1:2 mixture of **2a**:**TfOH** (Figure 6B). In contrast, the computed ^{19}F and ^{1}H chemical shift values for **2a–TfOH** show more pronounced displacements; the calculated average displace-

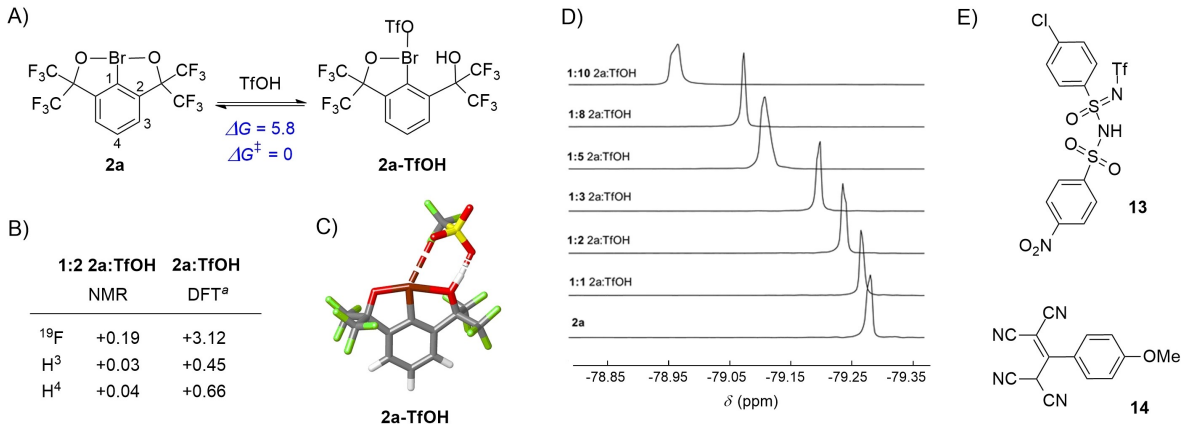

Figure 6. A) Adduct formation between TfOH and **2a** with calculated Gibbs free energy in kcal mol^{-1}. B) Comparison between the observed shifts of ^{1}H and ^{19}F signals for **2a** upon the addition of TfOH (2.0 equiv) in CD_2Cl_2 (trifluorotoluene as the internal standard) and the computed shifts. The positive signs refer to downfield displacements. [a] Averaged chemical shifts. C) Computed optimized geometry of **2a**-**TfOH**. D) Displacement of ^{19}F chemical shifts for **2a** in the presence of various amounts of TfOH. E) Reference compounds for titration experiments.

ment value for chemical shifts of the two protons at position 3 amounts to $\delta = 0.45$ ppm when going from **2a** to **2a-TfOH**, while that for a proton at position 4 amounts to 0.66 ppm. Furthermore, an average shift of $\delta = 3.12$ ppm is predicted for the ^{19}F signals. When compared with the observed displacements of the ^{1}H and ^{19}F NMR shifts for a 1:2 mixture of **2a**:**TfOH**, the computed values have the correct sign and roughly the correct relative size. Therefore, taking into account the small fraction of formed **2a-TfOH** under these conditions and considering the progression of the signal position for higher acid concentrations shown in Figure 6D, the computed NMR shifts agree well with our experimental observations and thus support the proposed mechanistic picture of equilibrium protonation of **2a** by the added TfOH. These findings, together with the absence of any displacement of the NMR shifts for a 1:2 mixture of **2a**:**TMSOTf**, provide further evidence for the indirect role of **TMSOTf** in terms of activating **2**.

The observed equilibrium protonation of λ^3-bromane **2a** called for additional experiments to estimate the approximate acidity of the solution needed for protonating **2a**, in terms of the unified pH ($pH_{abs}^{H_2O}$) scale.[36] The term "$pH_{abs}^{H_2O}$" stands for unified pH (pH_{abs}) "aligned" with the aqueous pH scale, that is, the $pH_{abs}^{H_2O}$ values in any solvent are directly comparable with the conventional aqueous pH values. In other words, in a solution with a given $pH_{abs}^{H_2O}$, made in any solvent, the chemical potential of the solvated proton is equal to the chemical potential of solvated proton in water at the same value of conventional pH.[37]

The acidity necessary for protonation of **2a** is expressed as "buffer point $pH_{abs}^{H_2O}$ ", that is, $pH_{abs}^{H_2O}$, at which approximately half of **2a** is free and half has TfOH added (**2a-TfOH**, Figure 6A). Experiments for determination of the buffer point were carried out in 1,2-dichloroethane, where a self-consistent acidity scale has been previously established and linked to the unified pH ($pH_{abs}^{H_2O}$) scale.[38] The experiments consisted in titration of a mixture of **2a** and a reference compound, for which the pK_a and buffer point $pH_{abs}^{H_2O}$ estimates are available in 1,2-dichloroethane.[38] Different reference compounds were tried. The titration experiments gave a clearly interpretable outcome only with **13** (monitored by ^{19}F NMR) and **14** (monitored by UV-Vis spectrometry; see Figure 6E and the Supporting Information). The obtained buffer points are as follows: the buffer point $pH_{abs}^{H_2O}$ from titration of **13** was −6.8 and from titration of **14** was −8.5. Thus, the average value of the buffer point $pH_{abs}^{H_2O}$, together with an uncertainty estimate would be (-7.7 ± 1.2). This value has high uncertainty but allows qualitative interpretation: it means that by its acidity, in terms of the chemical potential of the solvated proton, such solution corresponds approximately to a hypothetical aqueous solution with pH −7.7. The uncertainty estimate embraces the full range of variability that we have seen in our experiments. Additional explanations, descriptions of experiments, and the obtained NMR and UV-Vis spectra are presented in the Supporting Information.

Conclusion

A combination of experimental and quantum chemical methods provided important insight into electrochemical properties and reactivity of chelation-stabilized λ^3-bromanes. Cyclic voltammetry studies in HFIP show that the anodic oxidation of parent bromoarenes that are equipped with coordinating hexafluoro-2-hydroxy-propanyl units in positions 2 and 6 proceeds via parallel ECEC and ECE_{disp} sequences, whereby the initially formed cation radical intermediate could be detected in the case of the *para*-methoxy-substituted bromoarene by UV-Vis spectroelectrochemistry. In contrast, cathodic conversion of the chelation-stabilized λ^3-bromanes to parent bromoarenes in acetonitrile occurs via single electron reduction, followed by hydrogen atom abstraction from the solvent and protonation. The corresponding half-peak potentials indicate that Martin's-type λ^3-bromanes are rather poor single electron oxidants. This important finding was corroborated by mechanistic studies of bromine(III)-mediated oxidative amidation of *N*,*N*-dimethylanilines in MeCN that provided compelling evidence against the involvement of a SET mechanism. The oxidative amidation in MeCN apparently proceeds through an ionic mechanism, involving an inner-sphere redox process within a transient [12-Br-4] complex. On the other hand, chelation-stabilized λ^3-bromanes possess comparable SET oxidizing ability to that of hypervalent iodine(III) reagents such as PIFA. The latter requires activation by Lewis acid to effect SET oxidation in, for example, oxidative biaryl coupling, whereas the activation by a strong Brønsted acid such as TfOH turned out to be the most efficient for Martin's-type λ^3-bromanes. The observed displacements of chemical shifts in ^{1}H and ^{19}F NMR spectra for λ^3-bromane suggests its equilibrium protonation by the added TfOH with a buffer point $pH_{abs}^{H_2O}$ determined to be -7.7 ± 1.2 by titration experiments in 1,2-dichloroethane. The protonation presumably leads to the cleavage of benzabromooxole ring and the formation of more reactive bromonium(III) triflate that features enhanced $[Ar{-}Br]^+$ cationic character as reflected by a LUMO energy reduction of 1.01 eV and a slight increase of the Mulliken charge population by 0.07 units and, hence, increased Lewis acidity and oxidizing ability.[32] Overall, we believe that the detailed mechanistic understanding of electrochemical properties and reactivity of the chelation-stabilized λ^3-bromanes will help to widen the use of hypervalent bromine(III) species in contemporary organic synthesis and accelerate the development of unprecedented synthetic transformations. Our ongoing work on the electrochemical synthesis of various bromine(III) species and their application in organic synthesis will be reported in due course.

Acknowledgements

This work was funded by the German Research Foundation (DFG, Grant No. FR 3848/1-2 and RO 5688/1-1), ERDF (Post-Doc Latvia) project No. 1.1.1.2/VIAA/2/18/377, by the EMPIR program (project 17FUN09 "UnipHied", www.uniphied.eu) co-financed by the Participating States and from the European Union's Horizon

2020 research and innovation program and by the Estonian Research Council grant (PRG690). R.F. is grateful for financial support by the DFG (Heisenberg Program, Grant No. FR 3848/4-1). The authors thank Dr. Larisa Baumane (Latvian Institute of Organic Synthesis) for EPR experiments. Open Access funding enabled and organized by Projekt DEAL.

Conflict of Interest

The authors declare no conflict of interest.

Data Availability Statement

The data that support the findings of this study are available in the supplementary material of this article.

Keywords: hypervalent halogen · bromane · oxidative coupling · cyclic voltammetry · unified pH

[1] a) T. Wirth (Ed.) *Top. Curr. Chem., Vol. 373*, Springer, **2016**; b) I. Marek (Ed.) *Patai's Chemistry of Functional Groups*, John Wiley & Sons, Hoboken, **2018**; c) A. Yoshimura, V. V. Zhdankin, *Chem. Rev.* **2016**, *116*, 3328; d) R. Francke, *Curr. Opin. Electrochem.* **2021**, *28*, 100719; e) M. Elsherbini, T. Wirth, *Chem. Eur. J.* **2018**, *24*, 13399; f) R. Francke, *Curr. Opin. Electrochem.* **2019**, *15*, 83.
[2] U. Farooq, A.-U.-H. A. Shah, T. Wirth, *Angew. Chem. Int. Ed.* **2009**, *48*, 1018.
[3] K. Miyamoto in *Patai's Chemistry of Functional Groups* (Ed.: I. Marek), John Wiley & Sons, Hoboken, **2018**, DOI: 10.1002/9780470682531.pat0956.
[4] B. Winterson, T. Patra, T. Wirth, *Synthesis* **2022**, *54*, 1261.
[5] M. Ochiai, A. Yoshimura, T. Mori, Y. Nishi, M. Hirobe, *J. Am. Chem. Soc.* **2008**, *130*, 3742.
[6] M. Ochiai, T. Okada, N. Tada, A. Yoshimura, K. Miyamoto, M. Shiro, *J. Am. Chem. Soc.* **2009**, *131*, 8392.
[7] M. Ochiai, K. Miyamoto, T. Kaneaki, S. Hayashi, W. Nakanishi, *Science* **2011**, *332*, 448.
[8] a) K. Miyamoto, M. Saito, S. Tsuji, T. Takagi, M. Shiro, M. Uchiyama, M. Ochiai, *J. Am. Chem. Soc.* **2021**, *143*, 9327; b) Md. M. Hoque, K. Miyamoto, N. Tada, M. Shiro, M. Ochiai, *Org. Lett.* **2011**, *13*, 5428; c) M. Ochiai, T. Kaneaki, N. Tada, K. Miyamoto, H. Chuman, M. Shiro, S. Hayashi, W. Nakanishi, *J. Am. Chem. Soc.* **2007**, *129*, 12938; d) M. Ochiai, Y. Nishi, S. Goto, M. Shiro, H. Frohn, *J. Am. Chem. Soc.* **2003**, *125*, 15304; e) H. J. Frohn, M. Giesen, *J. Fluorine Chem.* **1998**, *89*, 59.
[9] M. Ochiai, A. Yoshimura, K. Miyamoto, S. Hayashi, W. Nakanishi, *J. Am. Chem. Soc.* **2010**, *132*, 9236.
[10] Y. Yoshida, S. Ishikawa, T. Mino, M. Sakamoto, *Chem. Commun.* **2021**, *57*, 2519.
[11] M. Lanzi, R. A. Ali Abdine, M. de Abreu, J. Wencel-Delord, *Org. Lett.* **2021**, *23*, 9047.
[12] a) T. T. Nguyen, J. C. Martin, *J. Am. Chem. Soc.* **1980**, *102*, 7382; b) T. T. Nguyen, S. R. Wilson, J. C. Martin, *J. Am. Chem. Soc.* **1986**, *108*, 3803.
[13] a) T. Broese, R. Francke, *Org. Lett.* **2016**, *18*, 5896; b) W.-C. Gao, Z.-Y. Xiong, S. Pirhaghani, T. Wirth, *Synthesis* **2019**, *51*, 276; c) A. F. Roesel, T. Broese, M. Májek, R. Francke, *ChemElectroChem* **2019**, *6*, 4229–4237; d) M. Elsherbini, B. Winterson, H. Alharbi, A. A. Folgueiras-Amador, C. Génot, T. Wirth, *Angew. Chem. Int. Ed.* **2019**, *58*, 9811; e) A. Maity, B. L. Frey, N. D. Hoskinson, D. C. Powers, *J. Am. Chem. Soc.* **2020**, *142*, 11, 4990; f) J. D. Herszman, M. Berger, S. R. Waldvogel, *Org. Lett.* **2019**, *21*, 7893; g) S. Doobary, A. T. Sedikides, H. P. Caldora, D. L. Poole, A. J. J. Lennox, *Angew. Chem. Int. Ed.* **2020**, *59*, 1155; h) B. Devadas, J. Svoboda, M. Krupička, T. Bystron, *Electrochim. Acta* **2020**, *342*, 136080.
[14] O. Koleda, T. Broese, J. Noetzel, M. Roemelt, E. Suna, R. Francke, *J. Org. Chem.* **2017**, *82*, 11669.
[15] I. Sokolovs, N. Mohebbati, R. Francke, E. Suna, *Angew. Chem. Int. Ed.* **2021**, *60*, 15832.
[16] V. V. Pavlishchuk, A. W. Addison, *Inorg. Chim. Acta* **2000**, *298*, 97.
[17] J. Heinze, *Angew. Chem. Int. Ed. Engl.* **1984**, *23*, 831.
[18] R. F. Nelson, *J. Electroanal. Chem.* **1968**, *18*, 329.
[19] C. Hansch, A. Leo, R. W. Taft, *Chem. Rev.* **1991**, *91*, 165.
[20] F. M'Halla, J. Pinson, J. M. Saveant, *J. Am. Chem. Soc.* **1980**, *102*, 4120.
[21] E. Oberem, A. F. Roesel, A. Rosas-Hernández, T. Kull, S. Fischer, A. Spannenberg, H. Junge, M. Beller, R. Ludwig, M. Roemelt, R. Francke, *Organometallics* **2019**, *38*, 1236.
[22] D. Zhu, Y. Yao, R. Zhao, Y. Liu, L. Shi, *Chem. Eur. J.* **2018**, *24*, 4805.
[23] N. Döben, H. Yan, M. Kischkewitz, J. Mao, A. Studer, *Org. Lett.* **2018**, *20*, 7933.
[24] K. Kiyokawa, T. Kosaka, T. Kojima, S. Minakata, *Angew. Chem. Int. Ed.* **2015**, *54*, 13719.
[25] T. A. Brown, H. Chen, R. N. Zare, *Angew. Chem. Int. Ed.* **2015**, *54*, 11183.
[26] F. Cao, J. Kim, A. J. Bard, *J. Am. Chem. Soc.* **2014**, *136*, 18163.
[27] The major product identified in the reaction mixture was *N*-methylaniline that was presumably formed from iminium ion **4a** upon aqueous workup.
[28] D. Griller, K. U. Ingold, *Acc. Chem. Res.* **1980**, *13*, 317.
[29] L. J. Johnston, J. Lusztyk, D. D. M. Wayner, A. N. Abeywickreyma, A. L. J. Beckwith, J. C. Scaiano, K. U. Ingold, *J. Am. Chem. Soc.* **1985**, *107*, 4594.
[30] Y. Kita, K. Morimoto, M. Ito, C. Ogawa, A. Goto, T. Dohi, *J. Am. Chem. Soc.* **2009**, *131*, 1668.
[31] T. Dohi, M. Ito, N. Yamaoka, K. Morimoto, H. Fujioka, Y. Kita, *Tetrahedron* **2009**, *65*, 10797.
[32] S. Izquierdo, S. Essafi, I. Del Rosal, P. Vidossich, R. Pleixats, A. Vallribera, G. Ujaque, A. Lledós, A. Shafir, *J. Am. Chem. Soc.* **2016**, *138*, 12747.
[33] V. V. Zhdankin, A. Y. Koposov, L. Su, V. V. Boyarskikh, B. C. Netzel, V. G. Young, *Org. Lett.* **2003**, *5*, 1583.
[34] Alternatively, $BF_3{\cdot}OEt_2$ could be used for the activation of bromane **2a** in HFIP as the solvent (35% yield of **10**).
[35] Y.-B. Kang, L. H. Gade, *J. Am. Chem. Soc.* **2011**, *133*, 3658.
[36] a) D. Himmel, S. K. Goll, I. Leito, I. Krossing, *Angew. Chem. Int. Ed.* **2010**, *49*, 6885; b) A. Suu, L. Jalukse, J. Liigand, A. Kruve, D. Himmel, I. Krossing, M. Rosés, I. Leito, *Anal. Chem.* **2015**, *87*, 2623.
[37] V. Radtke, D. Stoica, I. Leito, F. Camões, I. Krossing, B. Anes, M. Roziková, L. Deleebeeck, S. Veltzé, T. Näykki et al., *Pure Appl. Chem.* **2021**, *93*, 1049.
[38] E. Paenurk, K. Kaupmees, D. Himmel, A. Kütt, I. Kaljurand, I. A. Koppel, I. Krossing, I. Leito, *Chem. Sci.* **2017**, *8*, 6964.

Manuscript received: March 29, 2022
Accepted manuscript online: May 5, 2022
Version of record online: June 10, 2022

Part VII. Appendix

References

[1] E. J. Horn, B. R. Rosen, P. S. Baran, *ACS Central Science* **2016**, *2*, 302-308.

[2] M. Faraday, *Annalen der Physik* **1834**, *109*, 481-520.

[3] H. Kolbe, *Justus Liebigs Annalen der Chemie* **1849**, *69*, 257-294.

[4] a) J. E. B. Randles, *Transactions of the Faraday Society* **1948**, *44*, 322-327; b) A. Hickling, *Transactions of the Faraday Society* **1942**, *38*, 27-33; c) J. J. Lingane, C. G. Swain, M. Fields, *Journal of the American Chemical Society* **1943**, *65*, 1348-1353; d) J. E. B. Randles, *Transactions of the Faraday Society* **1948**, *44*, 327-338; e) O. Hammerich, H. Lund, *Organic Electrochemistry, Fourth Edition*, Taylor & Francis, **2000**.

[5] J. H. Simons, *Journal of The Electrochemical Society* **1949**, *95*, 47.

[6] P. Sartori, N. Ignat'ev, *Journal of Fluorine Chemistry* **1998**, *87*, 157-162.

[7] a) G. G. Botte, *Interface magazine* **2014**, *23*, 49-55; b) D. S. P. Cardoso, B. Šljukić, D. M. F. Santos, C. A. C. Sequeira, *Organic Process Research & Development* **2017**, *21*, 1213-1226.

[8] A. Wiebe, T. Gieshoff, S. Möhle, E. Rodrigo, M. Zirbes, S. R. Waldvogel, *Angewandte Chemie International Edition* **2018**, *57*, 5594-5619.

[9] B. A. Frontana-Uribe, R. D. Little, J. G. Ibanez, A. Palma, R. Vasquez-Medrano, *Green Chemistry* **2010**, *12*, 2099-2119.

[10] a) M. A. Matthews, *Pure and Applied Chemistry* **2001**, *73*, 1305-1308; b) R. Francke, *Current Opinion in Electrochemistry* **2022**, *36*, 101111.

[11] S. R. Waldvogel, B. Janza, *Angewandte Chemie International Edition* **2014**, *53*, 7122-7123.

[12] Y. Yuan, A. Lei, *Nature Communications* **2020**, *11*, 802.

[13] a) P. Anastas, N. Eghbali, *Chemical Society Reviews* **2010**, *39*, 301-312; b)R. A. Sheldon, *ACS Sustainable Chemistry & Engineering* **2018**, *6*, 32-48.

[14] R. A. Sheldon, I. W. Arends, G. J. Ten Brink, A. Dijksman, *Acc Chem Res* **2002**, *35*, 774-781.

[15] G. Tojo, M. I. Fernandez, *Oxidation of Alcohols to Aldehydes and Ketones: A Guide to Current Common Practice*, Springer US, **2006**.

[16] a) R. R. Fernandes, J. Lasri, M. F. C. Guedes da Silva, J. A. L. da Silva, J. J. R. Fraústo da Silva, A. J. L. Pombeiro, *Journal of Molecular Catalysis A:*

Chemical **2011**, *351*, 100-111; b) S. Gowrisankar, H. Neumann, D. Gördes, K. Thurow, H. Jiao, M. Beller, *Chemistry – A European Journal* **2013**, *19*, 15979-15984.

[17] M. N. Kopylovich, A. P. C. Ribeiro, E. C. B. A. Alegria, N. M. R. Martins, L. M. D. R. S. Martins, A. J. L. Pombeiro, in *Advances in Organometallic Chemistry, Vol. 63* (Ed.: P. J. Pérez), Academic Press, **2015**, pp. 91-174.

[18] D. Pollok, S. R. Waldvogel, *Chemical Science* **2020**, *11*, 12386-12400.

[19] R. Cernansky, *Nature* **2015**, *519*, 379-380.

[20] J.-i. Yoshida, K. Kataoka, R. Horcajada, A. Nagaki, *Chemical Reviews* **2008**, *108*, 2265-2299.

[21] R. Francke, R. D. Little, *Chemical Society Reviews* **2014**, *43*, 2492-2521.

[22] a) E. Steckhan, T. Arns, W. R. Heineman, G. Hilt, D. Hoormann, J. Jörissen, L. Kröner, B. Lewall, H. Pütter, *Chemosphere* **2001**, *43*, 63-73; b) S. Cembellín, B. Batanero, *The Chemical Record* **2021**, *21*, 2453-2471; c) R. Francke, *Current Opinion in Electrochemistry* **2021**, *28*, 100719.

[23] C. A. Paddon, M. Atobe, T. Fuchigami, P. He, P. Watts, S. J. Haswell, G. J. Pritchard, S. D. Bull, F. Marken, *Journal of Applied Electrochemistry* **2006**, *36*, 617-634.

[24] A. J. Bard, L. R. Faulkner, H. S. White, *Electrochemical Methods: Fundamentals and Applications*, Wiley, **2022**.

[25] O. Hammerich, B. Speiser, *Organic Electrochemistry: Revised and Expanded*, CRC Press, **2015**.

[26] a) C. Zhu, N. W. J. Ang, T. H. Meyer, Y. Qiu, L. Ackermann, *ACS Cent Sci* **2021**, *7*, 415-431; b) R. Francke, T. Broese, A. F. Roesel, in *PATAI'S Chemistry of Functional Groups* **2018**, pp. 1-22.

[27] Y. Yuan, A. Lei, *Nat Commun* **2020**, *11*, 802.

[28] T. Fuchigami, M. Atobe, S. Inagi, *Fundamentals and Applications of Organic Electrochemistry: Synthesis, Materials, Devices*, Wiley, **2014**.

[29] E. S. Rountree, B. D. McCarthy, T. T. Eisenhart, J. L. Dempsey, *Inorganic Chemistry* **2014**, *53*, 9983-10002.

[30] H. A. Beejapur, Q. Zhang, K. Hu, L. Zhu, J. Wang, Z. Ye, *ACS Catalysis* **2019**, *9*, 2777-2830.

[31] a) R. Gracia, D. Mecerreyes, *Polymer Chemistry* **2013**, *4*, 2206-2214; b) T. Janoschka, M. D. Hager, U. S. Schubert, *Advanced Materials* **2012**, *24*, 6397-

6409; c) S. Muench, A. Wild, C. Friebe, B. Häupler, T. Janoschka, U. S. Schubert, *Chemical Reviews* **2016**, *116*, 9438-9484.

[32] a) L. Tebben, A. Studer, *Angewandte Chemie International Edition* **2011**, *50*, 5034-5068; b) T. Vogler, A. Studer, *ChemInform* **2008**, *39*; c) R. A. Sheldon, *Catalysis Today* **2015**, *247*, 4-13.

[33] a) B. P. Soule, F. Hyodo, K. Matsumoto, N. L. Simone, J. A. Cook, M. C. Krishna, J. B. Mitchell, *Free Radic Biol Med* **2007**, *42*, 1632-1650; b) E. J. Rivera, R. Sethi, F. Qu, R. Krishnamurthy, R. Muthupillai, M. Alford, M. A. Swanson, S. S. Eaton, G. R. Eaton, L. J. Wilson, *Advanced Functional Materials* **2012**, *22*, 3691-3698; c) R. Weishaupt, G. Siqueira, M. Schubert, P. Tingaut, K. Maniura-Weber, T. Zimmermann, L. Thöny-Meyer, G. Faccio, J. Ihssen, *Biomacromolecules* **2015**, *16*, 3640-3650; d) T. Yoshitomi, Y. Nagasaki, *Nanomedicine (Lond)* **2011**, *6*, 509-518.

[34] a) A. C. Greene, R. B. Grubbs, *Macromolecules* **2010**, *43*, 10320-10325; b) D. Yang, C. Feng, J. Hu, *Polymer Chemistry* **2013**, *4*, 2384-2394.

[35] a) K. Herr, M. Fleckenstein, M. Brodrecht, M. V. Höfler, H. Heise, F. Aussenac, T. Gutmann, M. Reggelin, G. Buntkowsky, *Scientific Reports* **2021**, *11*, 13714; b) F. Torricella, A. Pierro, E. Mileo, V. Belle, A. Bonucci, *Biochim Biophys Acta Proteins Proteom* **2021**, *1869*, 140653.

[36] R. Ciriminna, M. Pagliaro, *Organic Process Research & Development* **2010**, *14*, 245-251.

[37] P. Lucio Anelli, C. Biffi, F. Montanari, S. Quici, *The Journal of Organic Chemistry* **1987**, *52*, 2559-2562.

[38] a) M. F. Semmelhack, C. R. Schmid, *Journal of the American Chemical Society* **1983**, *105*, 6732-6734; b) R. Kempt, A. Kuc, T. Heine, *Angewandte Chemie International Edition* **2020**, *59*, 9242-9254; c) N. Prakash, R. Rajeev, A. John, A. Vijayan, L. George, A. Varghese, *ChemistrySelect* **2021**, *6*, 7691-7710.

[39] a) Y. Kashiwagi, J. Anzai, *Chem Pharm Bull (Tokyo)* **2001**, *49*, 324-326; b) Y. Fang, X.-Y. Yu, X. W. Lou, *Matter* **2019**, *1*, 90-114; c) A. A. Vereshchagin, A. Y. Kalnin, A. I. Volkov, D. A. Lukyanov, O. V. Levin, *Energies* **2022**, *15*, 2699.

[40] X.-Y. Qian, S.-Q. Li, J. Song, H.-C. Xu, *ACS Catalysis* **2017**, *7*, 2730-2734.

[41] P. Parpot, K. Servat, A. P. Bettencourt, H. Huser, K. B. Kokoh, *Cellulose* **2010**, *17*, 815-824.

[42] T. Isogai, T. Saito, A. Isogai, *Biomacromolecules* **2010**, *11*, 1593-1599.

[43] T. Sawamura, S. Kuribayashi, S. Inagi, T. Fuchigami, *Advanced Synthesis & Catalysis* **2010**, *352*, 2757-2760.

[44] a) M. Kuroboshi, K. Goto, H. Tanaka, *Synfacts* **2009**, *2009*, 0694-0694; b) K. Mitsudo, T. Kaide, E. Nakamoto, K. Yoshida, H. Tanaka, *Journal of the American Chemical Society* **2007**, *129*, 2246-2247.

[45] a) T. Janoschka, N. Martin, U. Martin, C. Friebe, S. Morgenstern, H. Hiller, M. D. Hager, U. S. Schubert, *Nature* **2015**, *527*, 78-81; b) B. Schille, N. O. Giltzau, R. Francke, *Angewandte Chemie International Edition* **2018**, *57*, 422-426.

[46] E. Steckhan, *Angewandte Chemie International Edition in English* **1986**, *25*, 683-701.

[47] a) R. Francke, *Current Opinion in Electrochemistry* **2019**, *15*, 83-88; b) N. Mohebbati, A. Prudlik, A. Scherkus, A. Gudkova, R. Francke, *ChemElectroChem* **2021**, *8*, 3837-3843.

[48] a) B. Winterson, T. Patra, T. Wirth, *Synthesis* **2021**, *54*, 1261-1271; bV. V. Zhdankin, *Hypervalent Iodine Chemistry: Preparation, Structure, and Synthetic Applications of Polyvalent Iodine Compounds*, Wiley, **2013**.

[49] a) B. Olofsson, I. Marek, Z. Rappoport, *The Chemistry of Hypervalent Halogen Compounds, 2 Volume Set*, Wiley, **2019**; b) K. Miyamoto, M. Uchiyama, *Chemistry Letters* **2021**, *50*, 832-838; c) A. A. Sikalov, *Theoretical Chemistry Accounts* **2019**, *139*, 8; d) T. Wirth, *Hypervalent Iodine Chemistry*, Springer International Publishing, **2016**.

[50] T. Wirth, Y. Kita, T. Wirth, *Hypervalent iodine chemistry, Vol. 373*, Springer, **2016**.

[51] M. Lanzi, Q. Dherbassy, J. Wencel-Delord, *Angewandte Chemie International Edition* **2021**, *60*, 14852-14857.

[52] O. Koleda, T. Broese, J. Noetzel, M. Roemelt, E. Suna, R. Francke, *The Journal of Organic Chemistry* **2017**, *82*, 11669-11681.

[53] C. Hartmann, V. Meyer, *Berichte der deutschen chemischen Gesellschaft* **1894**, *27*, 426-432.

[54] a) M. Ochiai, N. Tada, T. Okada, A. Sota, K. Miyamoto, *Journal of the American Chemical Society* **2008**, *130*, 2118-2119; b) M. Ochiai, A.

Yoshimura, K. Miyamoto, S. Hayashi, W. Nakanishi, *Journal of the American Chemical Society* **2010**, *132*, 9236-9239.

[55] a) M. R. Leach, *Foundations of Chemistry* **2013**, *15*, 13-29; b) D. R. Lide, *CRC handbook of chemistry and physics, Vol. 85*, CRC press, **2004**; c) K. Miyamoto, M. Saito, S. Tsuji, T. Takagi, M. Shiro, M. Uchiyama, M. Ochiai, *Journal of the American Chemical Society* **2021**, *143*, 9327-9331.

[56] R. B. Sandin, A. S. Hay, *Journal of the American Chemical Society* **1952**, *74*, 274-275.

[57] a) A. N. Nesmeyanov, L. G. Makarova, T. P. Tolstaya, *Tetrahedron* **1957**, *1*, 145-157; b) G. A. Olah, T. Sakakibara, G. Asensio, *The Journal of Organic Chemistry* **1978**, *43*, 463-468.

[58] H. J. Frohn, M. Giesen, *Journal of Fluorine Chemistry* **1984**, *24*, 9-15.

[59] T. T. Nguyen, J. C. Martin, *Journal of the American Chemical Society* **1980**, *102*, 7382-7383.

[60] I. Sokolovs, N. Mohebbati, R. Francke, E. Suna, *Angewandte Chemie International Edition* **2021**, *60*, 15832-15837.

[61] A. Prudlik, N. Mohebbati, L. Hildebrandt, A. Heck, L. Nuhn, R. Francke, *Chemistry – A European Journal*, *n/a*, e202202730.

[62] M. Rafiee, K. C. Miles, S. S. Stahl, *Journal of the American Chemical Society* **2015**, *137*, 14751-14757.

[63] J. Wang, J. Schultze, *Angewandte Chemie-English Edition* **1996**, *35*, 1998-1998.

[64] a) J.-M. Savéant, *Chemical Reviews* **2008**, *108*, 2348-2378; b) J. M. Savéant, K. B. Su, *Journal of Electroanalytical Chemistry and Interfacial Electrochemistry* **1984**, *171*, 341-349.

[65] Y. Li, D. P. Hari, M. V. Vita, J. Waser, *Angewandte Chemie International Edition* **2016**, *55*, 4436-4454.

[66] a) K. Miyamoto, *PATAI'S Chemistry of Functional Groups* **2009**, 1-25; b) U. Farooq, A.-u.-H. A. Shah, T. Wirth, *Angewandte Chemie International Edition* **2009**, *48*, 1018-1020.

[67] N. Mohebbati, I. Sokolovs, P. Woite, M. Lõkov, E. Parman, M. Ugandi, I. Leito, M. Roemelt, E. Suna, R. Francke, *Chemistry – A European Journal* **2022**, *28*, e202200974.

[68] C. J. Li, *From C-H to C-C Bonds: Cross-Dehydrogenative-Coupling*, Royal Society of Chemistry, **2014**.

[69] T. Dohi, M. Ito, N. Yamaoka, K. Morimoto, H. Fujioka, Y. Kita, *Tetrahedron* **2009**, *65*, 10797-10815.

[70] R. F. Nelson, *Journal of Electroanalytical Chemistry and Interfacial Electrochemistry* **1968**, *18*, 329-332.

[71] J. Heinze, *Angewandte Chemie International Edition in English* **1984**, *23*, 831-847.

[72] C. Hansch, A. Leo, R. W. Taft, *Chemical Reviews* **1991**, *91*, 165-195.

[73] F. M'Halla, J. Pinson, J. M. Saveant, *Journal of Electroanalytical Chemistry and Interfacial Electrochemistry* **1978**, *89*, 347-361.

[74] a) S. Seiffert, C. Kummerlöwe, N. Vennemann, *Lechner, Gehrke, Nordmeier - Makromolekulare Chemie: Ein Lehrbuch für Chemiker, Physiker, Materialwissenschaftler und Verfahrenstechniker*, Springer Berlin Heidelberg, **2020**; b) S. F. Sun, *Physical Chemistry of Macromolecules: Basic Principles and Issues*, Wiley, **2004**.

Curriculum Vitae

Personal Details

Address	Albrechtstraße 27, 65185 Wiesbaden
Email	Nayereh.Mohebbati@outlook.de
Telephone	+49(176)695-03785
Date and place of birth	29.04.1993, Tehran-Iran

Work Experience

10/2022 - Present	**Sustainability Manager**, SE Tylose GmbH & Co. KG • Responsibility as a central contact for sustainability topics • Interface between internal decision-makers and external consultants • Identification, application and realization of fundings in the field of sustainability • Monitoring of the current legislation and application landscape in Germany and EU.
11/2018 - 04/2022	**Research Assistant**, Universität Rostock • Organization and implementation of interdisciplinary projects • Teaching assistant for practical courses in the department of technical chemistry • Supervision and guidance of students • Management of chemicals and safe storage in the department of electrochemistry in LIKAT.
10/2017 - 11/2018	**Assistant Student**, Leibniz Institute for Catalyse e. V., Prof. Dr. Udo Kragl • Synthesis of silicone based polymers
07/2014 - 09/2014	**Internship**, Iran Behnoush Company, Teheran • Quality control

Education

11/2018 - present	**PhD candidate**, Universität Rostock, Prof. Dr. Robert Francke • Focus topics: Electrochemistry, Polymer Chemistry, Technical Chemistry (DFG Funding) • Preparation and investigation of electrochemical properties of redox-active polymers • Mechanistic studies on electrochemical reagents

10/2016 - 11/2018	**Master**, Universität Rostock, Degree: Master of Science in Chemistry • Master thesis topic: „Propoxylation of Polyorganosiloxanes to Produce Brush Copolymers", Technical Chemistry, Dr. Esteban Mejia
09/2012 - 06/2015	**Bachelor**, Alzahra University, Teheran • Degree: Bachelor of Science in Chemistry
10/2012 - 06/2013	**Training**, Private college of Goftogoo,Teheran • Degree: English teaching training
09/2009 - 06/2011	**High school,** Ridgemont high school, Ottawa, Ontario, Canada • Degree: High school diploma
09/2007 - 06/2009	**High school,** Moalem Gymnasium, Teheran, Iran

Language and work related skills

Languages

- Persian: Native speaker
- German: Fluent (Goethe Institut C1 Zertifikat)
- English: Fluent (IELTS 7.5 score)

IT skills

- Office Programs: Word, Excel, PowerPoint, Outlook
- Other specialized programs: Xcalibur, ClarityChrom (Knauer), Origin, EndNote, Citavi, ChemBioDraw, TopSpin, MestReNova, NOVA

Analytical skills

- NMR, Elemental analysis, cyclic voltametry, galvanic processes, EPR, HPLC, GC, MS, GC-MS, HPLC-MS und GPC.

Further trainings

- Qualification course „Project and Time Management for Scientists "
- Qualification course „Zeit- & Selbstmanagement"
- Qualification course „Projektmanagement für Akademiker*innen"
- Qualification course „Führungskompetenzen für Akademiker*innen"
- Qualification course „Grundlagen der Betriebswirtschaft in Finanzen und Controlling für Wissenschafler*innen"

- DECHEMA training course „Elektrochemie für Naturwissenschaftler, Ingenieure und Techniker“

Memberships

- DECHEMA
- GDCh

Personal Competence

- - Volunteer work at German Red Cross (support of refugees)

References

Prof. Dr. Robert Francke
Tel. : +49 381 1281 306
Email: robert.francke@catalysis.de

Dr. Esteban Mejia
Tel.: +49 381 1281 362
Email: esteban.mejia@catalysis.de

Prof. Dr. Udo Kragl
Tel.: +49 381 4896 450
Email: udo.kragl@uni-rostock.de

Patente, Publications and Front Cover and Awards

Patents

(1) A. Guthacker, T. Hemery, J. Klein, A. Dietrich, E. Mejia, **N. Mohebbati**
Henkel AG and Co KGaA
Preparation of Polysiloxane Polyalkyleneglycol Brush Copolymers WO2020114770A1, 06.12.**2018**.

Publications

(4) A. Prudlik, N. Mohebbati, L. Hildebrandt, A. Heck, L. Nuhn, R. Francke (2022).
TEMPO-Modified Polymethacrylates as Mediators in Electrosynthesis: Influence of the Molecular Weight on Redox Properties and Electrocatalytic Activity.
Chem. Eur. J. **2023**, e202202730.
DOI: 10.1002/chem.202202730

(3) **N. Mohebbati**, I. Sokolovs, P. Woite, M. Lokov, E. Parman, M. Ugandi, I. Leito, M. Roemelt, E. Suna, R. Francke(2022).
Electrochemistry and Reactivity of Chelation-stabilized Hypervalent Bromine(III) Compounds.
Chem. Eur. J.. **2022**
DOI: 10.1002/chem.202200974

(2) **N. Mohebbati,** A. Prudlik, A. Scherkus, A. Gudkova, R. Francke
TEMPO-Modified Polymethacrylates as Mediators in Electrosynthesis – Redox Behavior and Electrocatalytic Activity towards Alcohol Substrates.
ChemElectroChem **2021**, *8*, 3837.
DOI: 10.1002/celc.202100768.

(1) I. Skolovs, **N. Mohebbati**, R. Francke, E. Suna
Electrochemical Generation of Hypervalent Bromine(III) compounds.
Angew. Chem. Int. Ed. **2021**, *60*, 15832.
DOI: 10.1002/anie.202104677

Front Cover

Front Cover: TEMPO-Modified Polymethacrylates as Mediators in Electrosynthesis – Redox Behavior and Electrocatalytic Activity toward Alcohol Substrates (ChemElectroChem 20/2021).

Award

DAAD Prize of the German Academic Exchange Service (DAAD) 2021 for outstanding academic achievements and high social or intercultural commitment of international students at the University of Rostock. (03.12.2021)

Conference Participation, Talks and Posters

Conferences

(4) Virtual LIKAT Workshop „Current Developements in Electrosynthesis and Electrocatalysis”
Rostock, Germany, 04.08.2021

(3) 54th Jahrestreffen Deutscher Katalytiker
Weimar, Germany, Online event, 16.03.–19.03.2021

(2) 71th Annual Meeting of the International Society of Electrochemistry
Belgrade Online, 31.08.–04.09.2020

(1) ICASEC Summer School 2019, Electrochemical Approaches to Chemical Synthesis
Germany, Göttingen, 06.09.–09.09.2019

Talk

(1) **N. Mohebbati**
Electrochemical Generation of Hypervalent Bromine(III) compounds.
(Virtual LIKAT Workshop, Rostock, Germany, 04.08.2021)

Poster

(3) **Mohebbati, N.**, Prudlik, A., Francke, R.
Polymediators in Electrosynthesis – Influence of the Molecular Weight Distribution on the Electrocatalytic Properties
(54th Jahrestreffen Deutscher Katalytiker, Weimar, Germany)

(2) **Mohebbati, N.**, Francke, R.
Polymediators and Polyelectrolytes in Organic Electrosynthesis
(71th Annual Meeting of the International Society of Electrochemistry, Belgrade-Online)

(1) **Mohebbati, N.**; Schille, B., Francke, R.
Polymediators and Polyelectrolytes in Organic Electrosynthesis
(ICASEC Summer School 2019, Göttingen, Germany)

Declaration of the doctoral candidate according to § 4 (1) letters g and h
Of the doctoral degree regulations
Of the Faculty of Mathematics and Natural Sciences
of the University of Rostock

Name: Mohebbati, Nayereh

Address: Albrechtstraße 27, 65185, Wiesbaden, Hessen

I intend to elaborate a dissertation on the topic

Mechanistic Analysis of Electrochemical Reactions involving Mediators and Electro-generated Reagents

at the Faculty of Mathematics and Natural Sciences at the University of Rostock. My supervisor is Mr/Ms

Prof. Dr. Robert Francke

I, herewith, declare the following:

1. The opportunity for this PhD project was not communicated to me commercially. In particular, I have not engaged any organisation that for money seeks supervisors for the drawing up of dissertations or that performs entirely or partially on my behalf the duties incumbent upon me regarding the examinations.
2. I hereby declare under oath that I have completed the work submitted here independently and have composed it without outside assistance. Furthermore, I have not used anything other than the resources and sources stated and where I have taken sections from these works in terms of content or text, I have identified this appropriately.

..... this ....

(Place) (Signature)